GEO 225 Week 4 Lecture #3

Earthquakes & Earth Structure

Press-Siever-Grotzinger-Jordan Chapter 21

Judson & Richardson Ch. 9 ~~Press & Siever~~ Chs. 18–19

Seismology: the study of earthquakes and the (seismic) waves emitted by them — the latter are the principal means of (remotely) sensing or imaging the ⊕'s interior.

A seismic model of the ⊕ consists of three parameters

1. density = mass / unit volume
   kg / m³

	density (kg/m³) at STP	
granite	2700	don't give these
basalt	2900	
peridotite	3300	
mean ⊕	5517	
Fe	7900	

2. incompressibility — measures how easy or hard it is to squeeze something

   κ (kappa) (units force / unit area or N/m² — called a Pascal — abbreviated Pa)

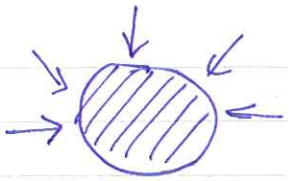

sample under pressure P
volume V

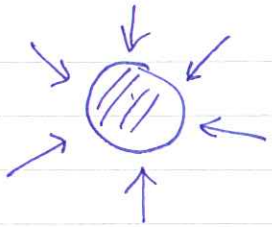

augment pressure

$P \rightarrow P + dP$
$V \rightarrow V + dV$

↑ negative (sample is compressed)

fractional change in volume

$$dP = -\kappa \left(\frac{dV}{V}\right)$$

↑ makes $\kappa > 0$

	κ (Pa) at STP
water	$0.2 \cdot 10^{10}$
granite	$5.5 \cdot 10^{10}$
basalt	$7.5 \cdot 10^{10}$
peridotite	13 ~~10~~ $\cdot 10^{10}$
steel	$17 \cdot 10^{10}$
air (STP)	$1.4 \cdot 10^{5}$

$M = \times 10^6$
$G = \times 10^9$

Just give air, water peridotite

peridotite 130 GPa
water 2 GPa
air 0.14 MPa

In general the denser a solid or liquid material, the greater its incompressibility

All the above substances are generally considered to be ~~incompressible~~ hard to compress

For comparison : $\kappa_{air} = 1.4 \cdot 10^5$ Pa
at STP

Take a marble-sized piece of any of the above materials.

Squeeze as hard as you can in your fist using only your muscles.

A strong person can exert

$$dP \approx 1 \text{ atmosphere} = 10^5 \text{ Pa}$$

Thus $\left(\frac{dV}{V}\right)_{granite} \approx \frac{10^5}{0.2 \cdot 10^{10}} \approx 2 \cdot 10^{-5}$

water $5 \cdot 10^{-5}$

not very much

0.0002% change

0.005%

use water & air as examples

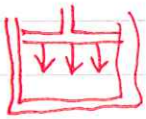

In contrast

$$\left(\frac{dV}{V}\right)_{air} \approx \frac{10^5}{1.4 \cdot 10^5} \approx 0.7$$

70% — air is easily compressed

3. rigidity : μ (also Pa) — measure of ability to withstand shear

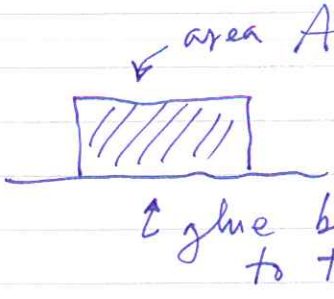

$F/A = 2\mu\theta$ ← angle of shear

note: rigidity also positive

	μ (Pa) at STP
granite	$2 \cdot 10^{10}$
basalt	$4 \cdot 10^{10}$
peridotite	$8 \cdot 10^{10}$ ← give only this so GPa

The rigidity of a fluid (liquid or gas) is zero: can't even perform thought experiment of gluing block on table

$\mu = 0$ ← melts, water, air

Above "typical" values at $P = 1$ atm.

In general ρ, κ, μ all increase with increasing pressure — this responsible for much of increase within the ⊕.

Two types of seismic waves can propagate in a solid material

1. compressional or P waves

↑ historically P for primary — since first waves to arrive at a distant station after a 'quake.

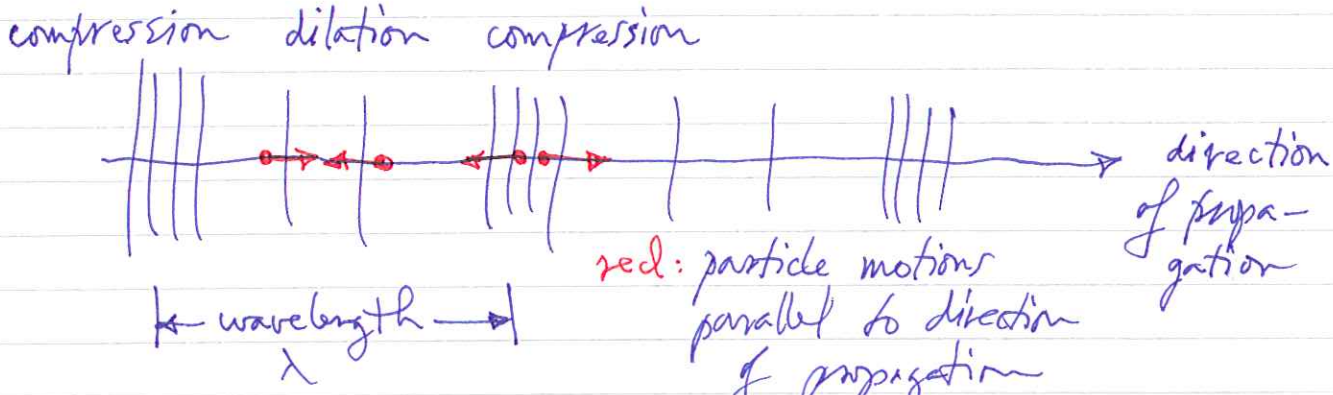

These are sound waves. Their speed is

$$\alpha = \sqrt{\frac{\kappa + \frac{4}{3}\mu}{\rho}}$$

P waves can propagate in a fluid such as air or water

$$\alpha_{fluid} = \sqrt{\frac{\kappa}{\rho}} \quad (\text{since } \mu = 0)$$

air: density $\rho = 1.2$ kg/m^3

2. shear or S waves ↑ secondary

$$\alpha = \sqrt{\frac{1.4 \cdot 10^5}{1.2}} = 340 \frac{m}{sec}$$

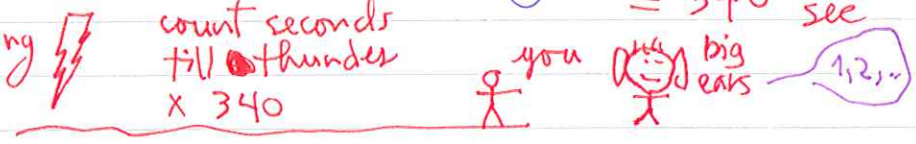

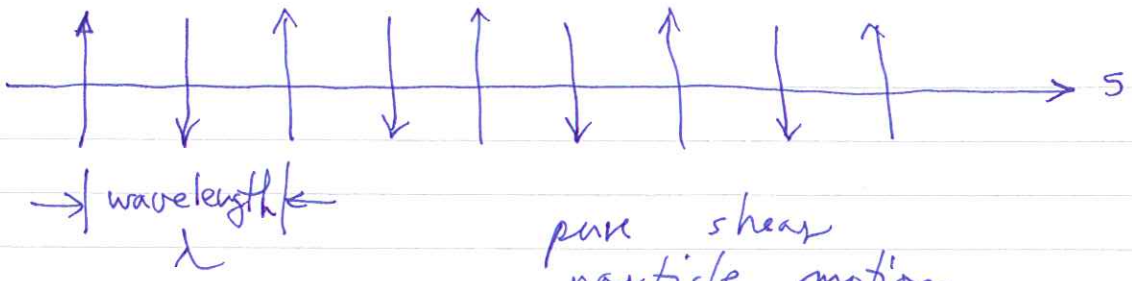

pure shear
particle motion
perpendicular to
direction of propagation

Speed $\beta = \sqrt{\frac{\mu}{\rho}}$ — cannot propagate in a fluid

	α (km/s)	β (km/s) (at STP)
air	0.34	—
water	1.5	—
granite	6.0	3.6
basalt	7.0	3.8
peridotite	8.0	4.6 ← give only these

In general in a solid $\alpha \approx \sqrt{3}\,\beta$

$K \approx \frac{5}{3}\mu$ $\approx 1.7\,\beta$

PREM model of ⊕ : note $\beta = 0$ in fluid outer core ; also α decreases from 13.7 km/s to 5.0 km/s at CMB

Differences between 1066A & 1066B illustrate current level of uncertainty — greatest in upper mantle phase transition zone and inner core

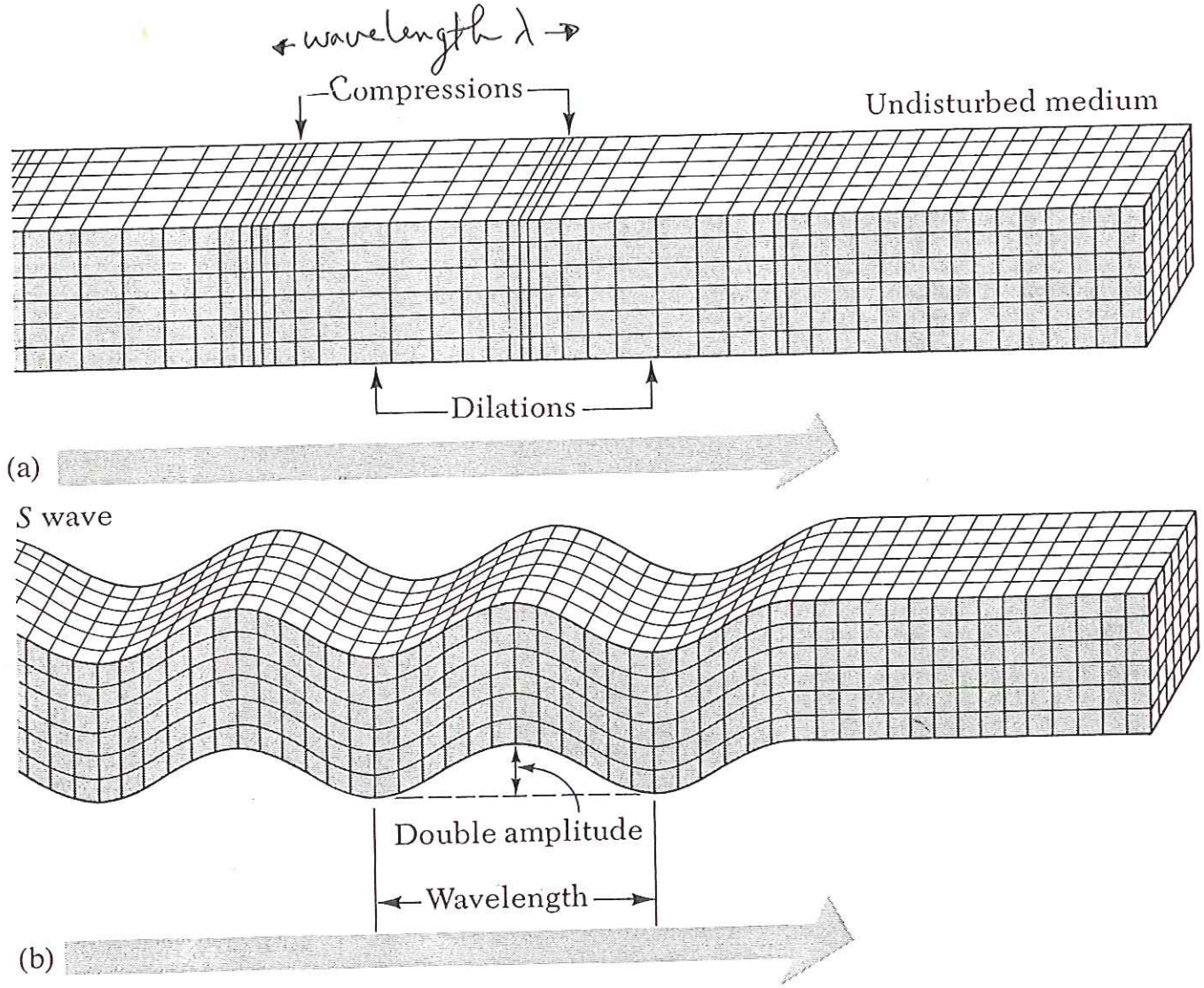

Figure 2.1 The two types of body waves. [From Bruce A. Bolt, *Nuclear Explosions and Earthquakes*. W. H. Freeman and Company. Copyright © 1976.]

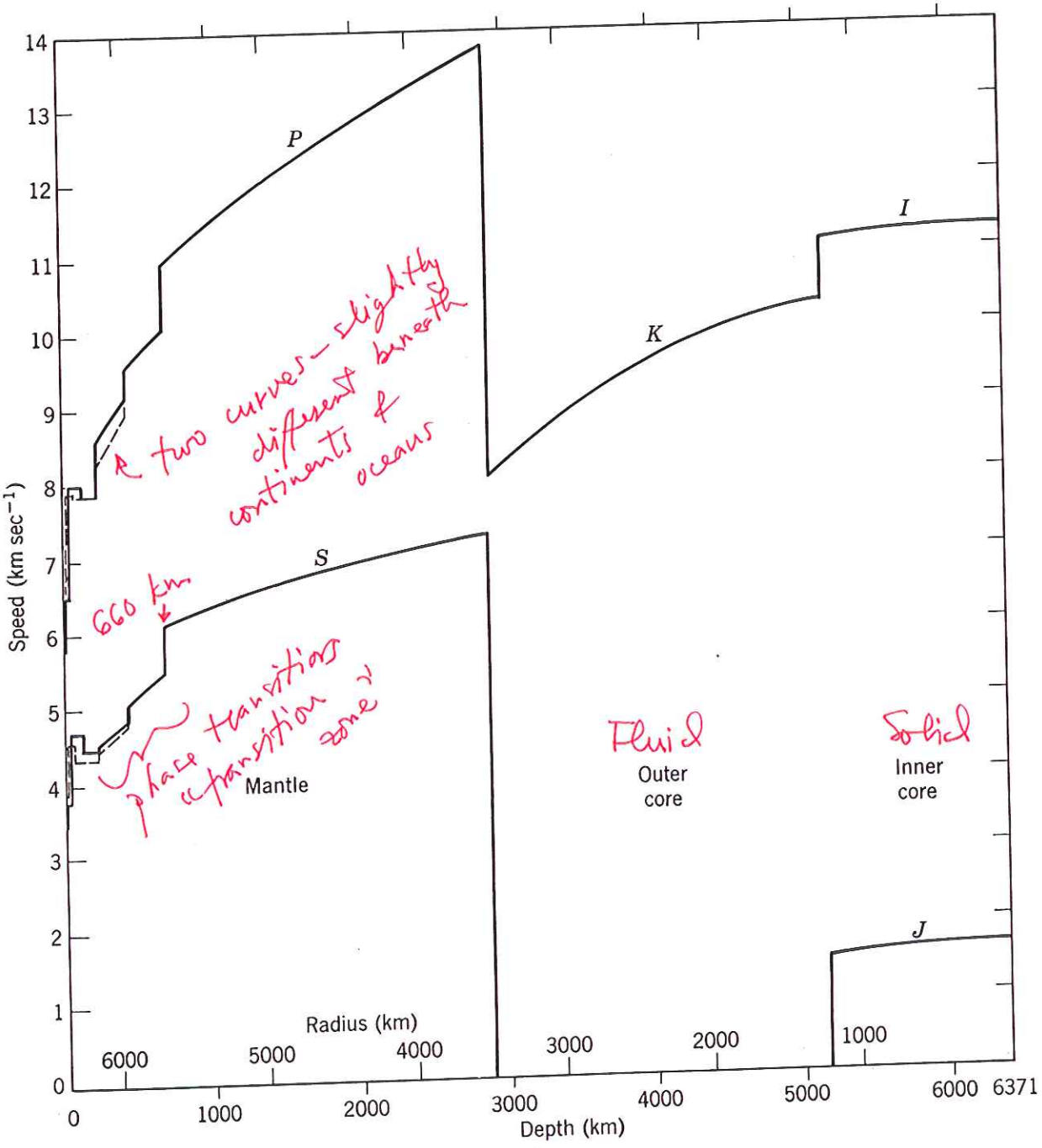

Figure 6.14. Velocities of body waves (P and S) within the Earth. Data for the earth model by Dziewonski et al. (1975)—see Appendix G.

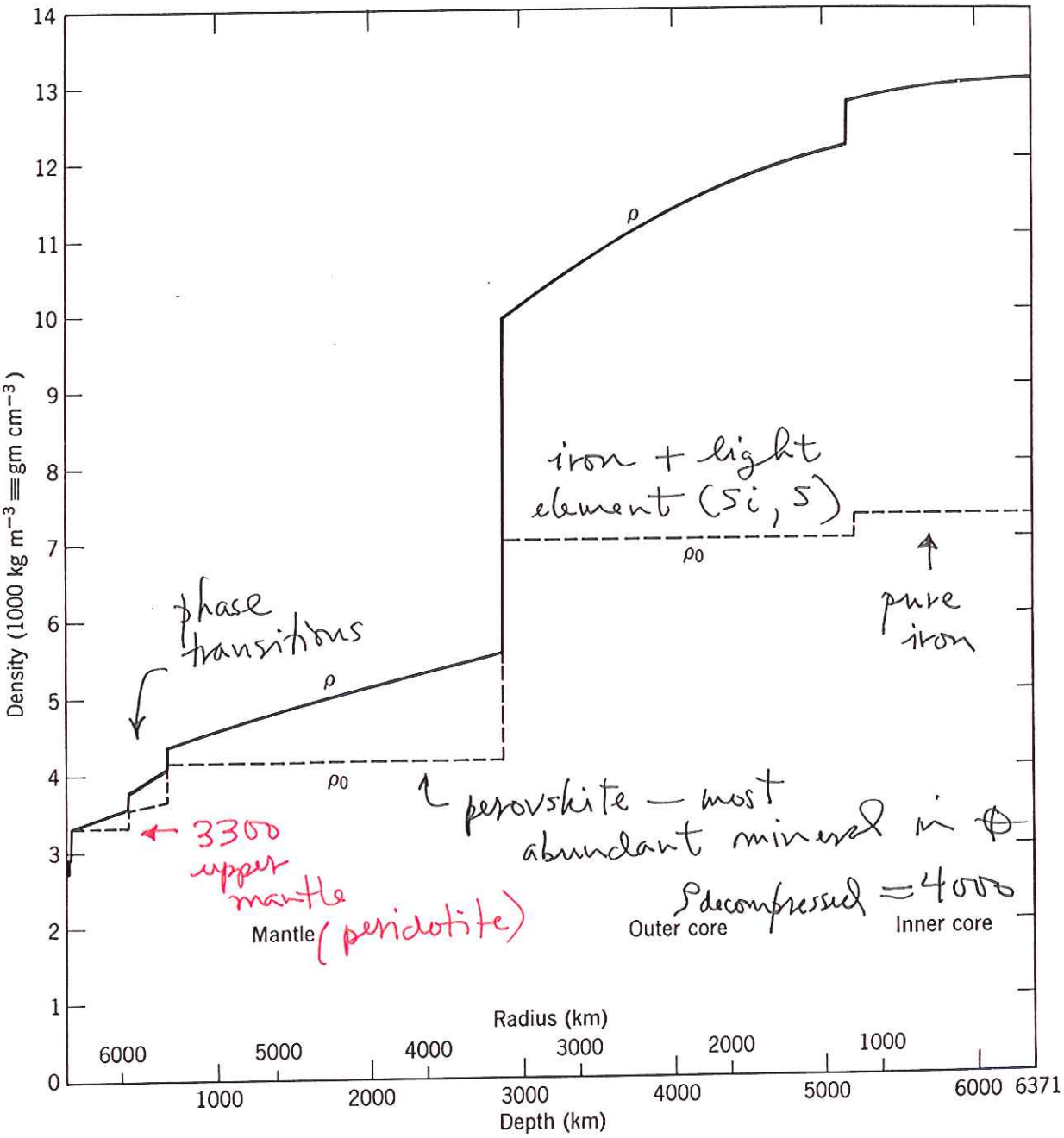

Figure 6.17. Density profile of Earth model by Dziewonski et al. (1975) (solid line) with corresponding extrapolated zero pressure (and room temperature) density (broken line).

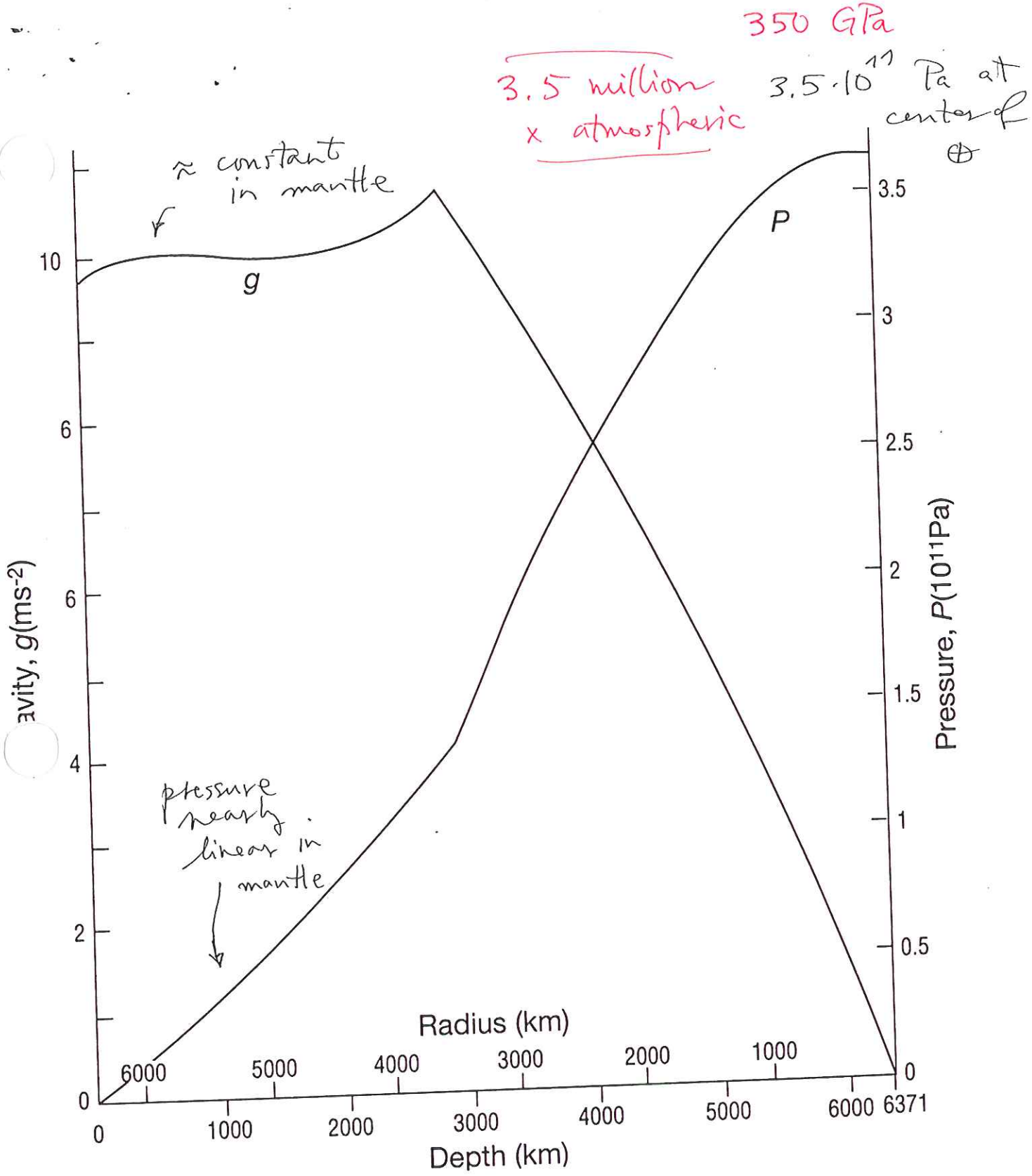

Figure 5.19(b). Profiles of gravity, g, and pressure, P, corresponding to the density profile in Fig. 5.19(a).

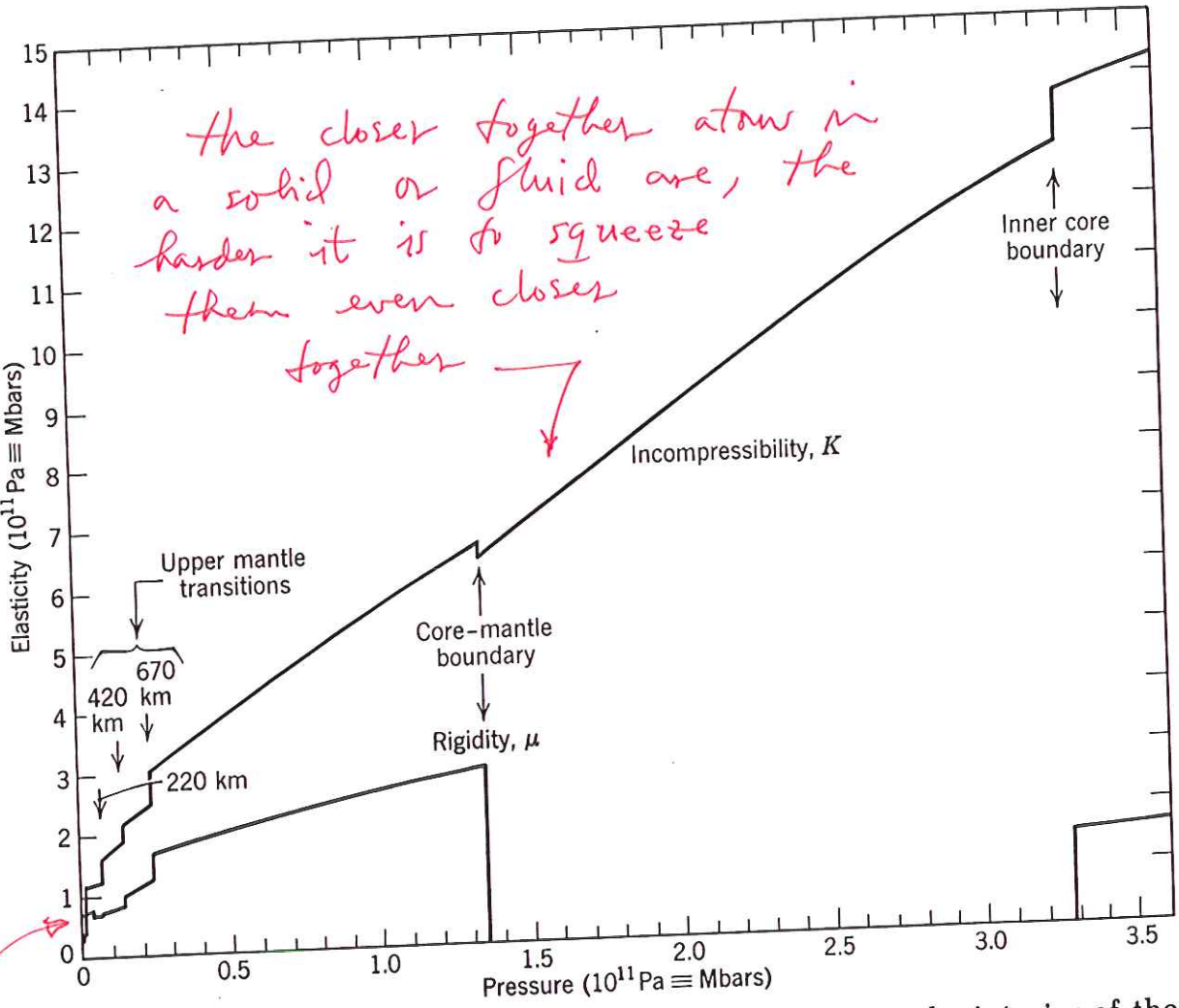

Figure 6.18. Variations of elastic constants with pressure in the interior of the Earth (model data by Dziewonski et al. 1975—Appendix G).

the closer together atoms in a solid or fluid are, the harder it is to squeeze them even closer together →

note: pressure — not depth

0.8 · 10^11 Pa here — as in our table

The variation in time t and space s of particle displacement in a wave is of the form

$$A \cos 2\pi \left(\frac{t}{T} - \frac{s}{\lambda} \right)$$

A = amplitude

T = period

λ = wavelength

s = distance measured along ray

t = time

Speed v (either α or β) $= \frac{\lambda}{T}$ ← wavelength / ← period

Consider the waves excited by an earthquake (regarded for the moment as a point source)

Thought experiment — homogeneous medium

radius $s = vt$

spherical wavefronts propagate outward at speed v

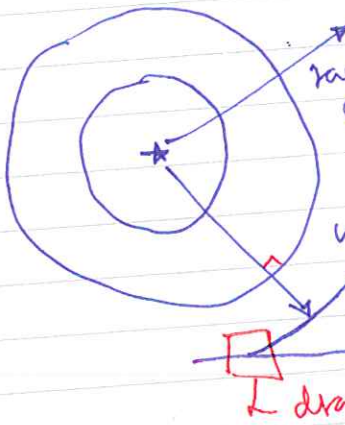

Can think of wave as travelling along straight rays

← draw blowup of this

What happens when a wave encounters a boundary between two materials?

Drill sergeant gives 2 orders:
(1) one step every second (analogue of fixed T)
(2) keep abreast of persons next to you

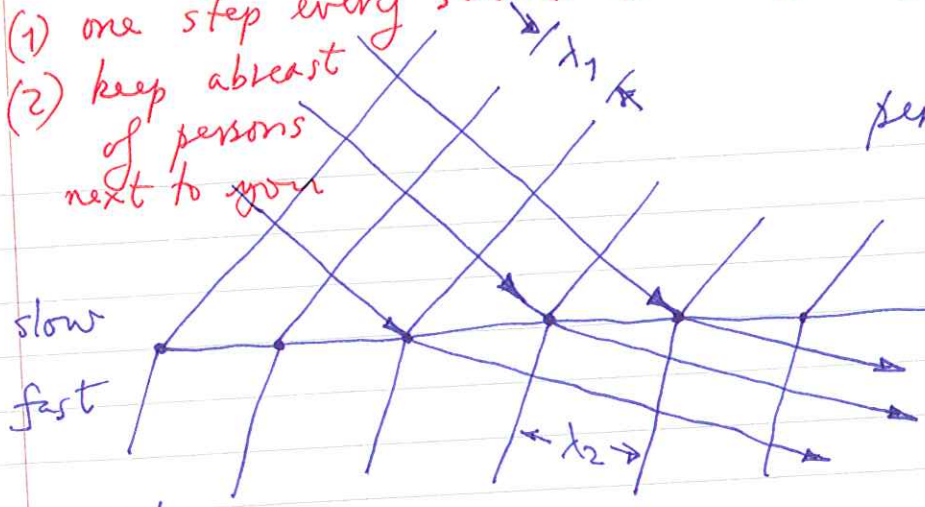

period T of wave is fixed

speed v_1

speed $v_2 > v_1$

Wave is refracted upward upon entering a faster medium

Analogy — think of lines of troops leaving a swamp and entering a blacktop parking lot

one step per second — small steps in swamp & big in parking lot

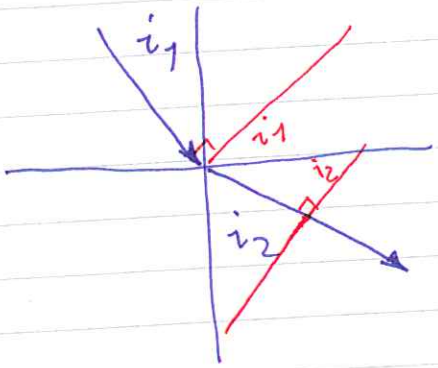

$$\frac{\sin i_1}{v_1} = \frac{\sin i_2}{v_2}$$

Snell's law of refraction

Derivation:

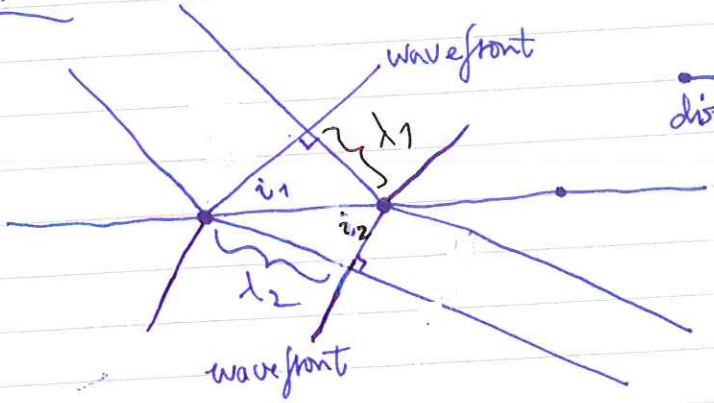

$$\frac{\text{distance}}{\sin i_1} = \frac{\lambda_1}{\sin i_1} = \frac{\lambda_2}{\sin}$$

$$\frac{\sin i_1}{v_1 T} = \frac{\sin}{v_2}$$

same

The velocity within the Earth's mantle increases gradually with depth.

Can regard this as many fine layers

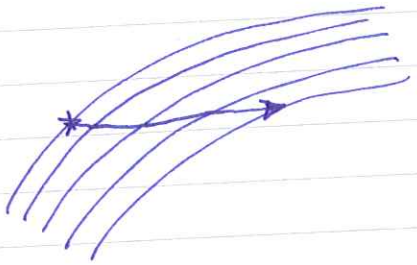

ray is refracted upward in each one

As a result seismic rays are curved within the Earth.

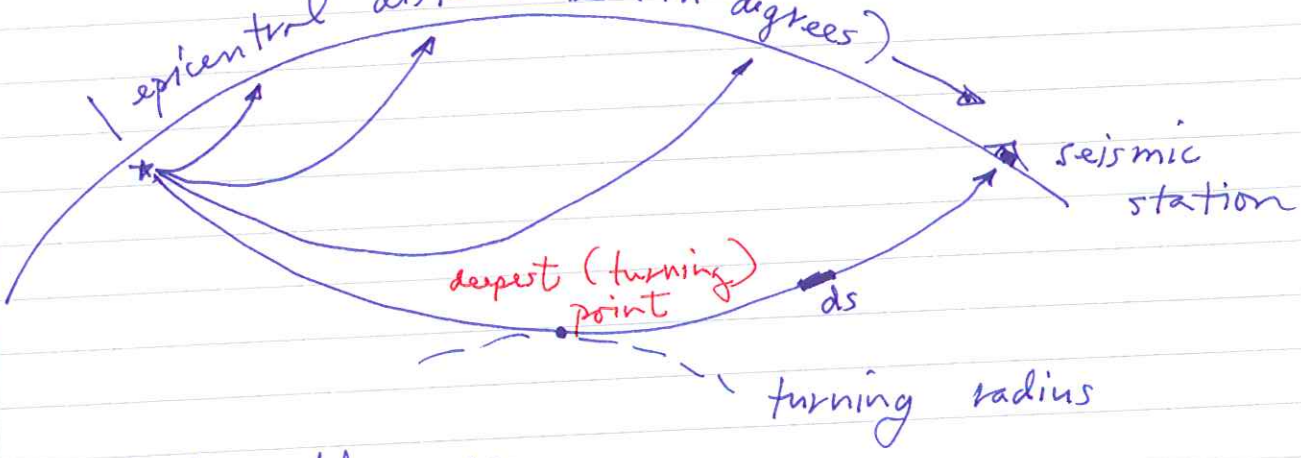

Eventually the ray turns and comes back up

After a sizeable ($M > 4$) earthquake both P and S waves arrive at all stations

Given the wavespeed v as a function of radius r, can find the travel-time curve

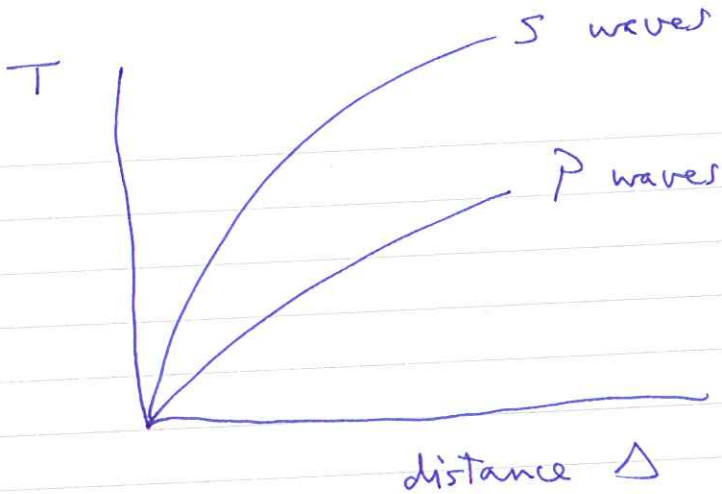

In any little layer $dT = \frac{ds}{v}$ ← distance traveled

Total time: $T = \int \frac{ds}{v}$

$T = \Sigma dT = \Sigma \frac{ds}{v}$

$= \int \frac{ds}{v}$

say the integral adds up all the dT's.

make each Σ look more like $\int$

"that's all there is to integration"

Below the CMB at 2900 km depth S waves can no longer propagate. Furthermore P waves are refracted deep down into the core because of the decrease in α from 13.7 to 8.0 km/s

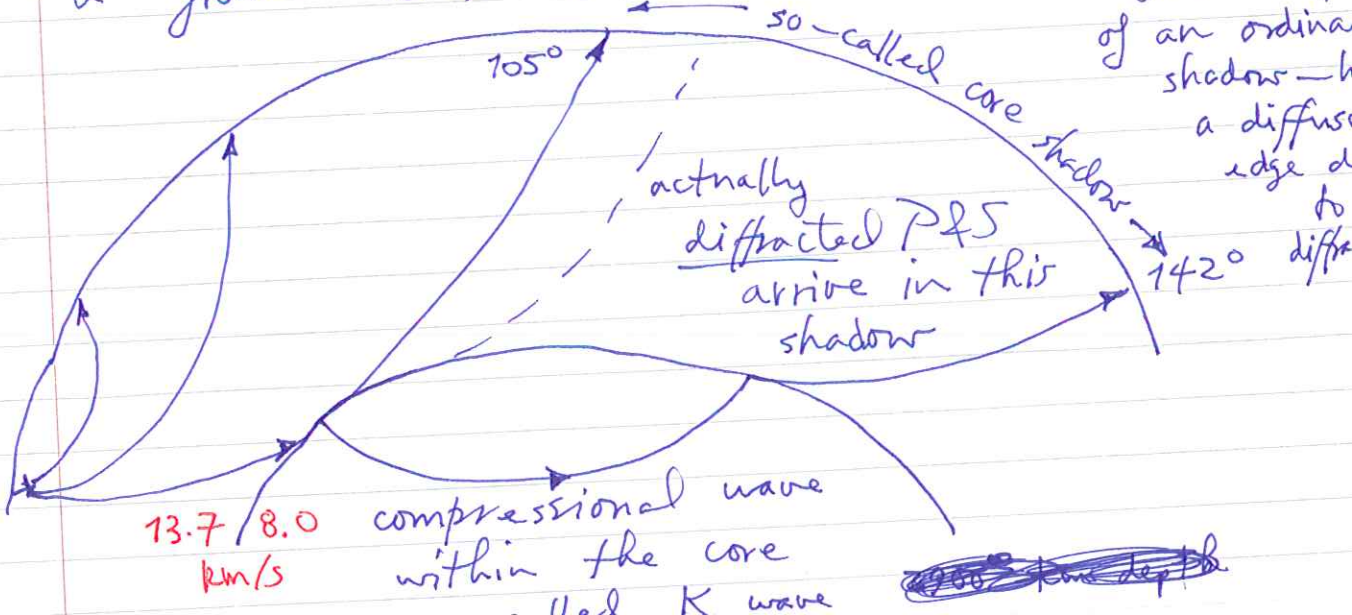

Wave energy can also reflect off of the CMB.

Snell's law governs reflections also

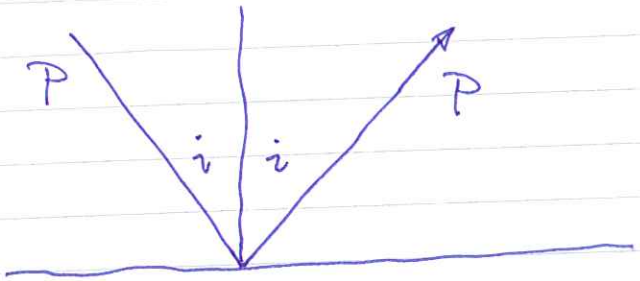

Angle of incidence = angle of reflection for a like-type wave.

But an incoming P also generates a reflected S and vice-versa

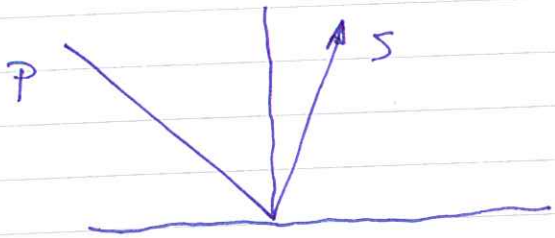

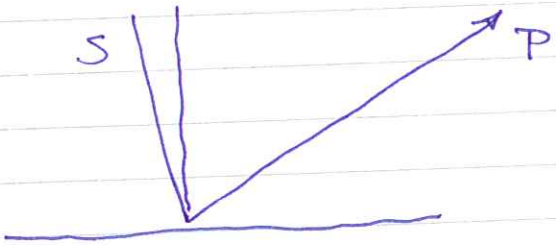

$$\frac{\sin i_{inc}}{\alpha} = \frac{\sin i_{refl}}{\beta}$$

incident P

$$\frac{\sin i_{inc}}{\beta} = \frac{\sin i_{refl}}{\alpha}$$

incident S

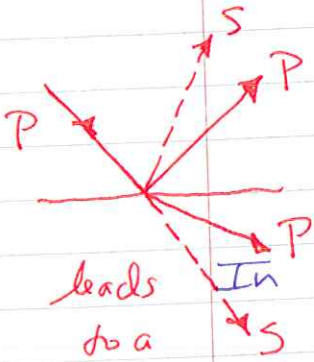

leads to a myriad of possible ray arrivals after an earthquake

In general: $\frac{\sin i_1}{v_1} = \frac{\sin i_2}{v_2}$ Snell's law

Reflected wave nomenclature:

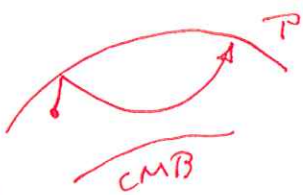

pP leaves a deep quake going up
ditto sS

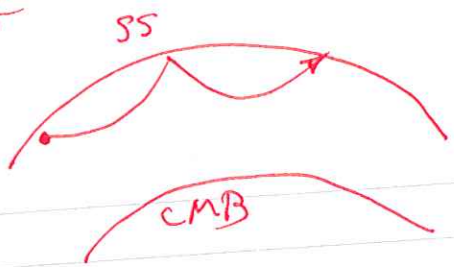

c : CMB reflection
i : ICB reflection

also:

K: P wave in fluid core
I: P wave in solid inner core

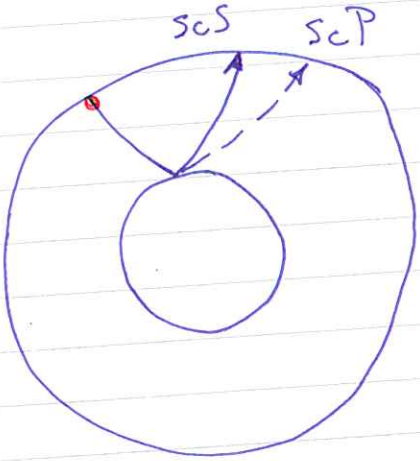

Names are concatenated in the obvious manner

e.g. multiple surface reflections

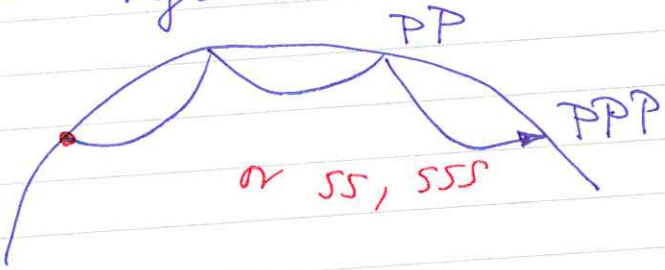

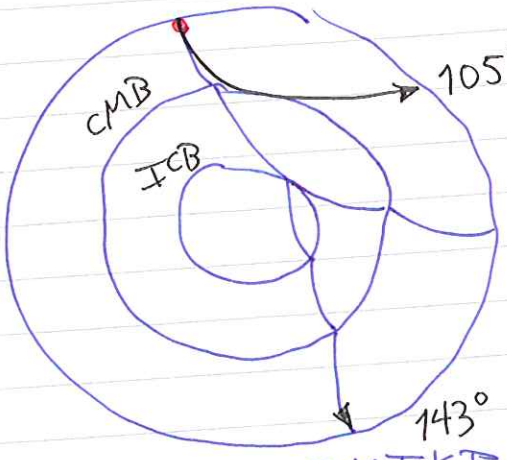

PKiKP arrives in core shadow — first observed by Danish seismologist Inge Lehman in (1936)

Careful analysis and culling of seismograms reveals many of these multiply reflected and converted phases.

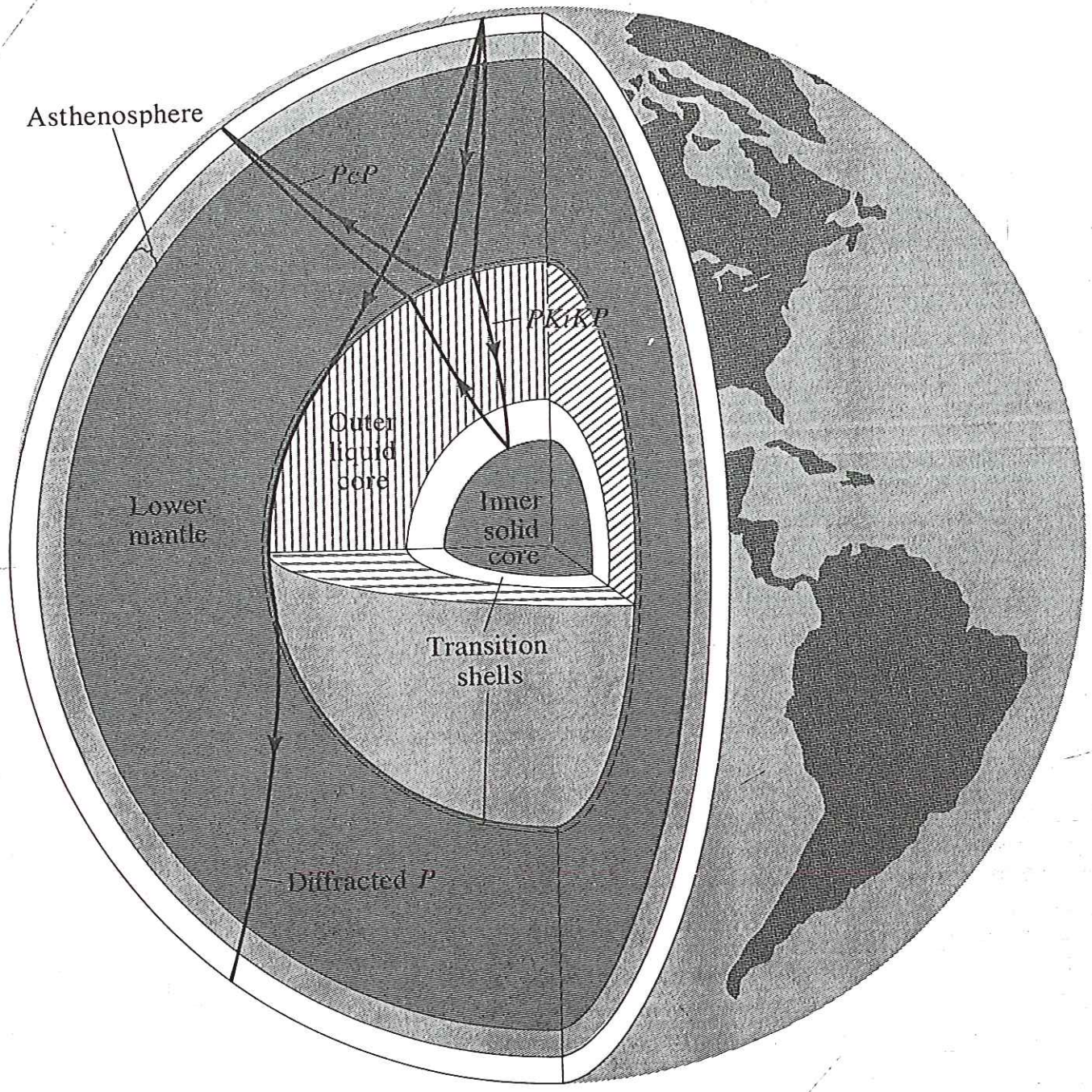

Figure 1.3 A cross section of the Earth based on the most recent seismological evidence. The outer shell consists of a rocky mantle that has structural discontinuities in its upper part and at its lower boundary that are capable of reflecting or modifying earthquake waves. Below the mantle an outer fluid core surrounds a solid kernel at the Earth's center; between the two is a transition shell. The paths taken by three major kinds of earthquake waves are shown. The waves reflected from the outer liquid core are designated *PcP;* the waves reflected from the inner solid core are *PKiKP;* and the waves that creep around the liquid core are diffracted *P*. [From Bruce A. Bolt, "The Fine Structure of the Earth's Interior." Copyright © 1973 by Scientific American, Inc. All rights reserved.]

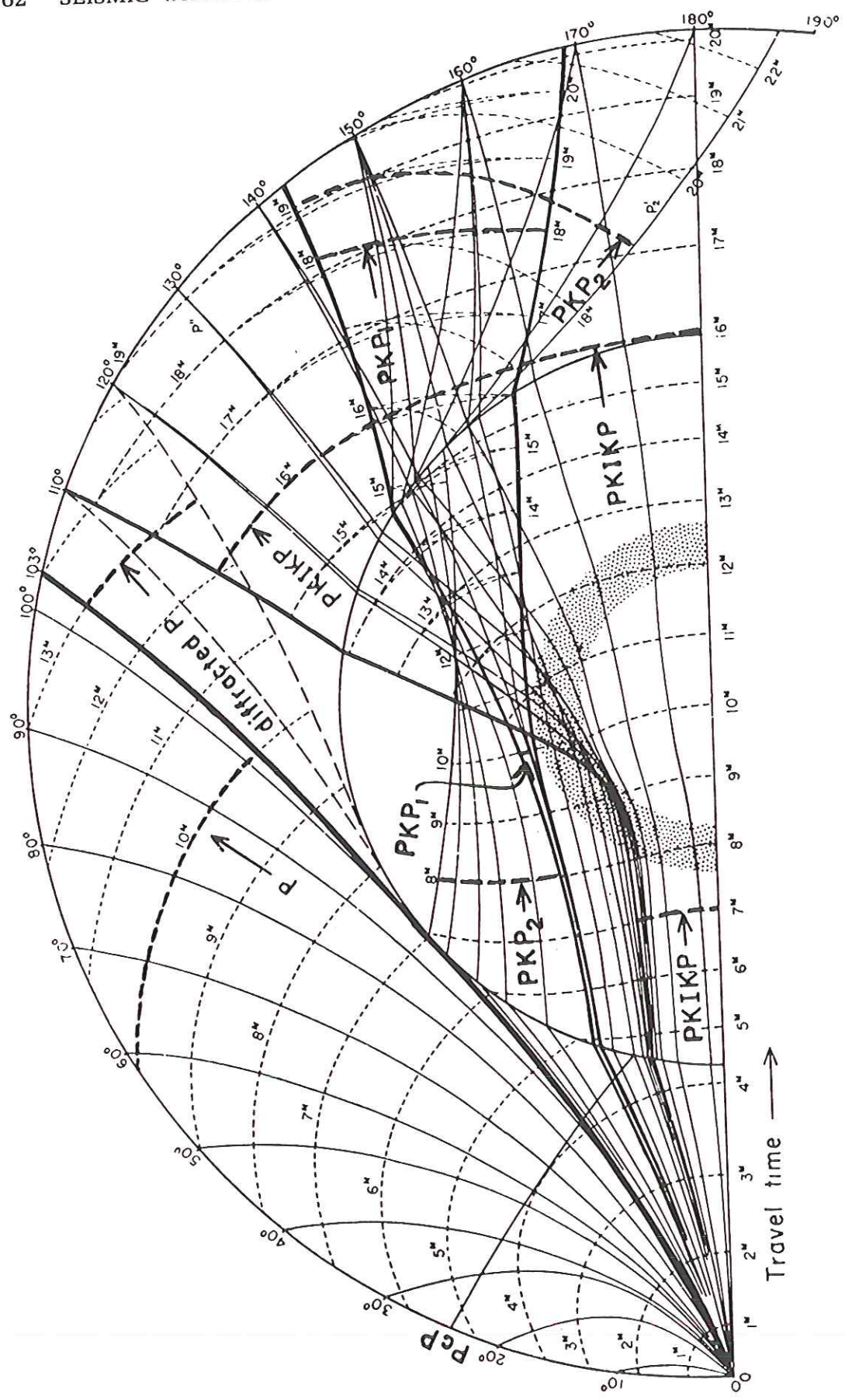

Figure 6.13. Rays and wavefronts for compressional waves in the Earth. Reproduced, by permission, from Gutenberg (1959). (Copyright Academic Press.)

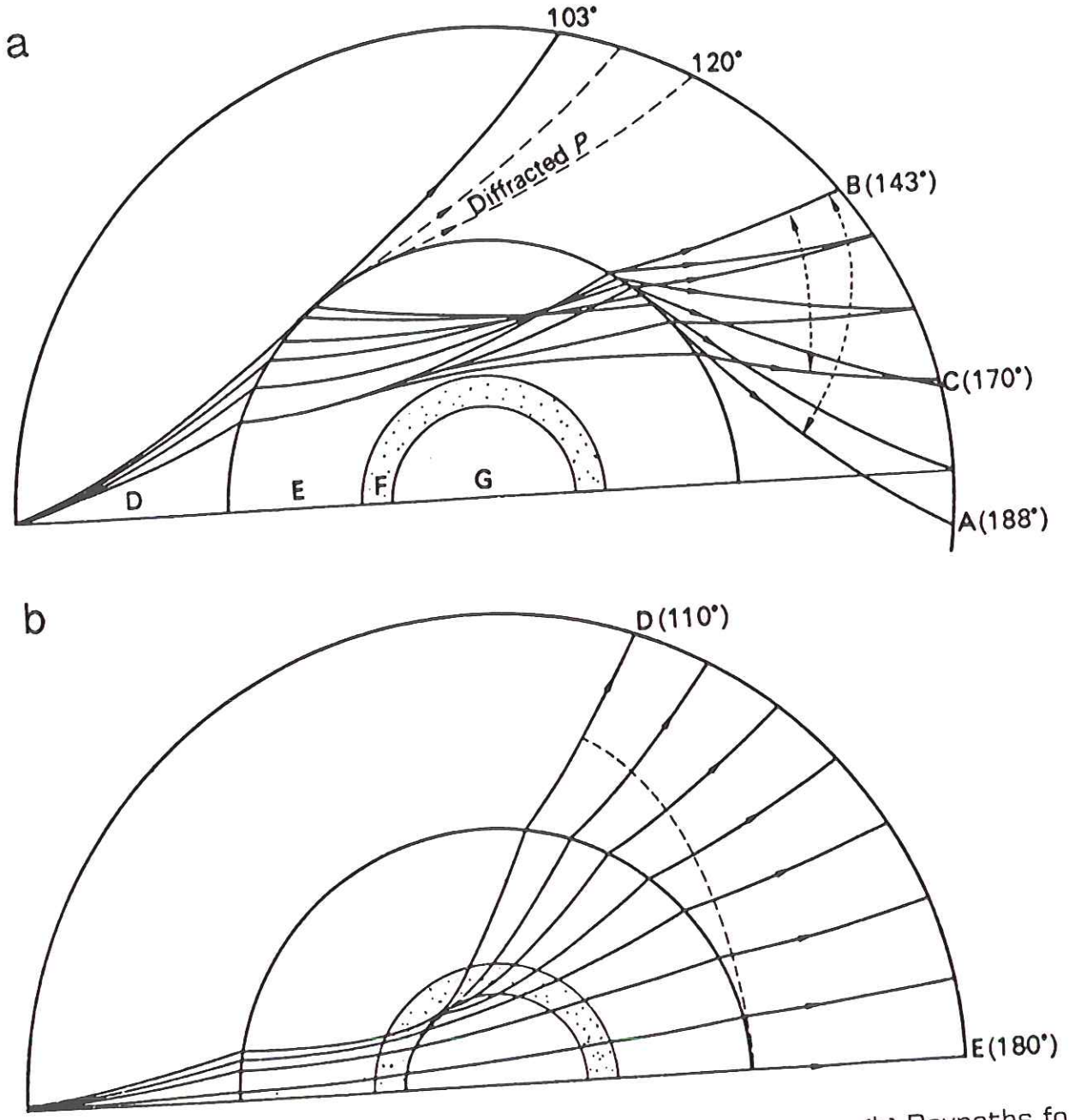

FIGURE 7.52 (a) Raypaths for *PKP* waves traversing the outer core. (b) Raypaths for *PKIKP* waves. (After B. Gutenburg.)

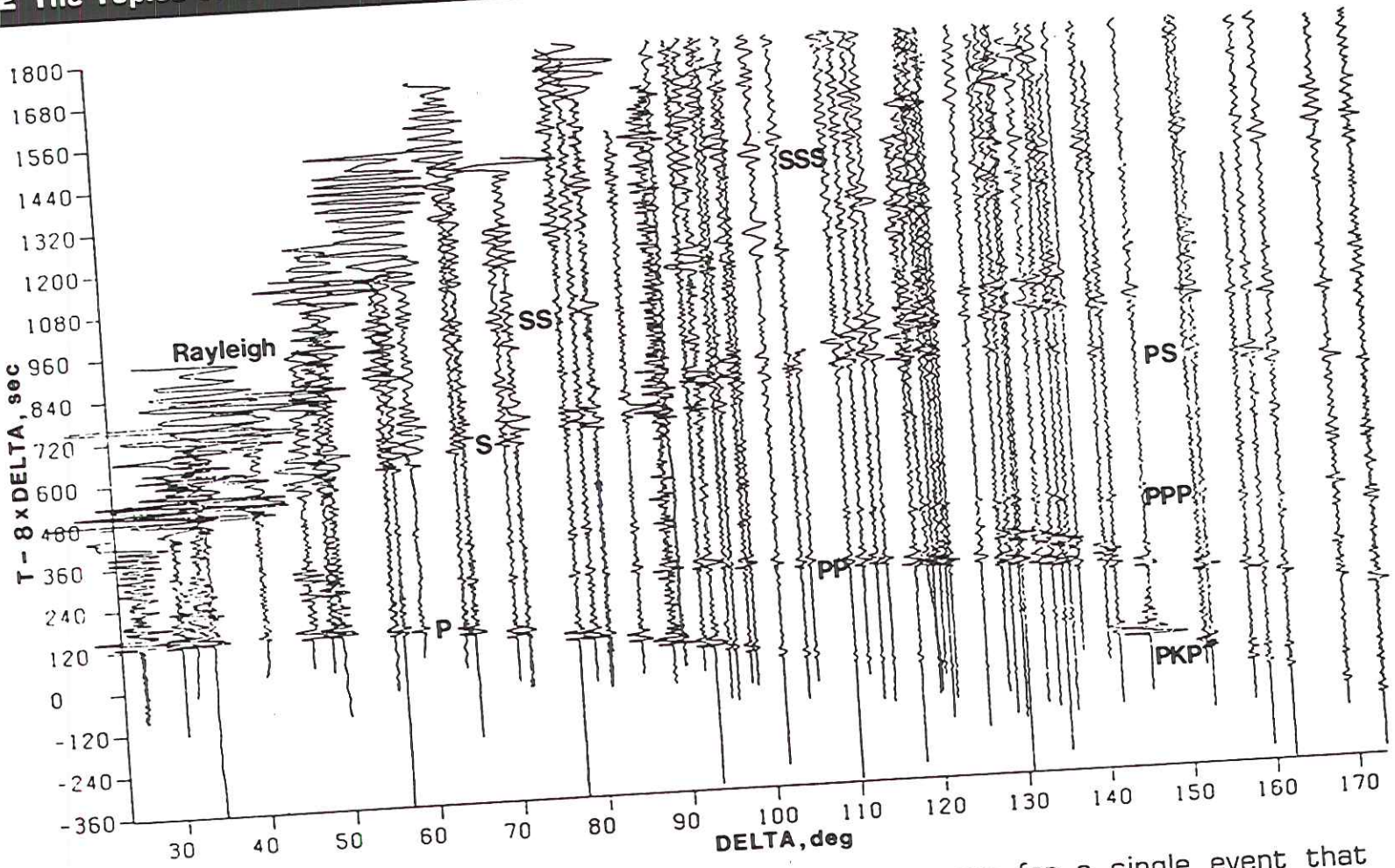

FIGURE 1.18 A collection of vertical-component seismograms for a single event that occurred near Sumatra, plotted at the angular distance to each station. The records are from the World Wide Standardized and Canadian Seismic Networks. Upward motion on each trace is toward the left. Note that coherent arrivals can be tracked from trace to trace. These define the travel-time behavior for different paths through the Earth. The start time of each trace has been reduced by a value of 8Δ s, where Δ is the angular distance. Thus, traces on the right begin much later than traces on the left. (Modified from Müller and Kind, [illegible] with permission of the Royal Astronomical Society.)

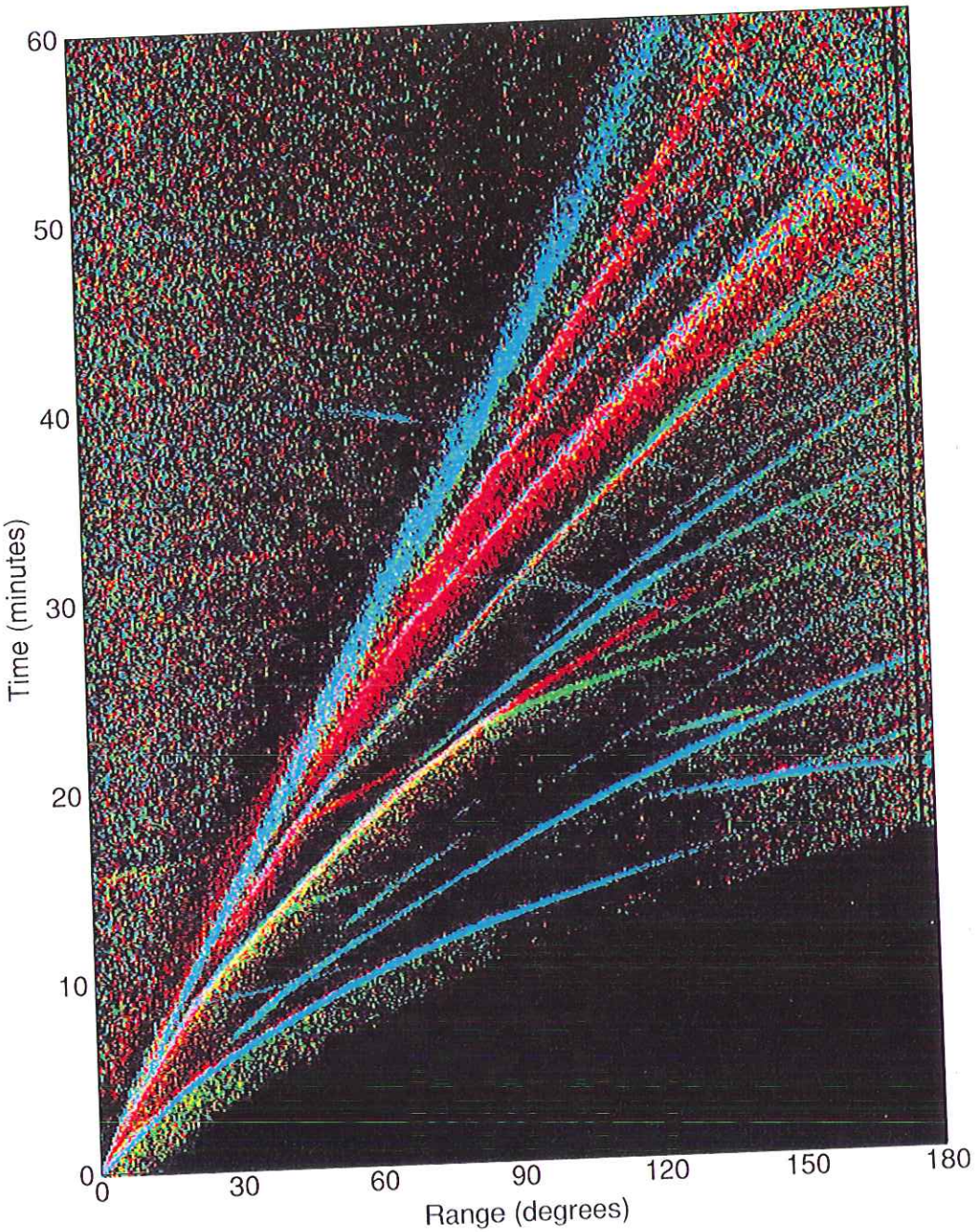
60
50
40
30
20
10
0
Time (minutes)
0
30
60
90
120
150
180
Range (degrees)

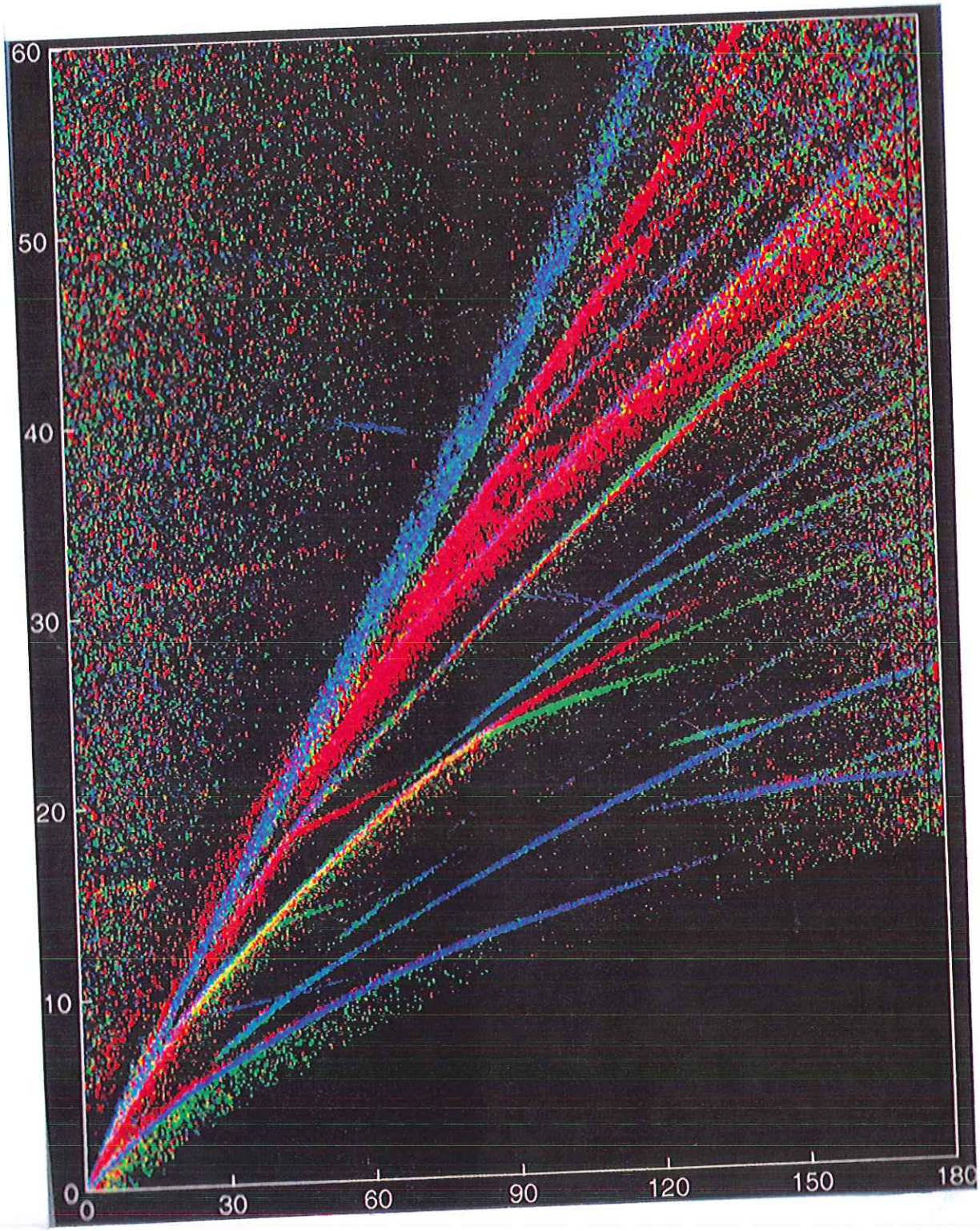
60
50
40
30
20
10
0
0
30
60
90
120
150
180

This is 10's of 1000's of seismograms, all plotted together

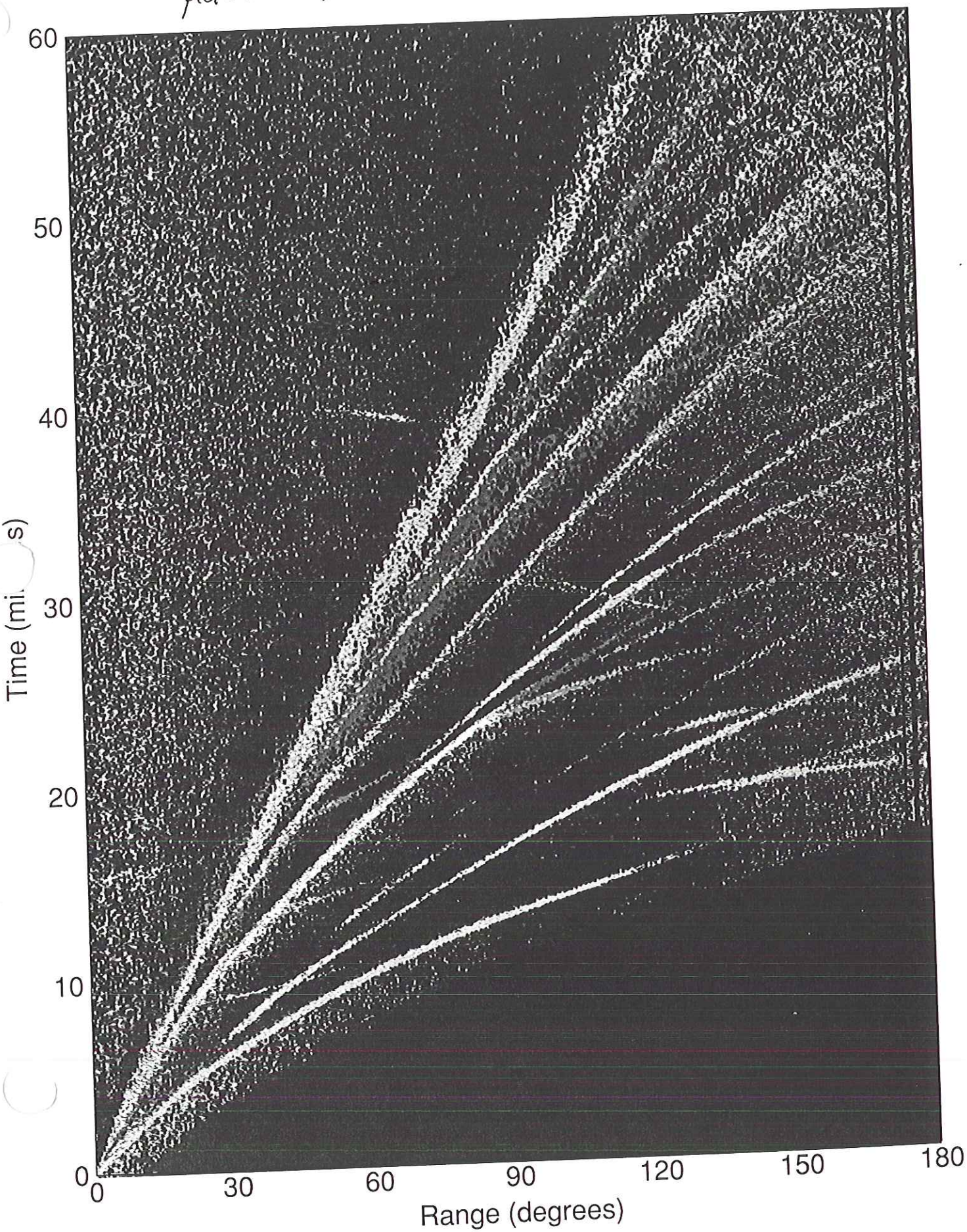

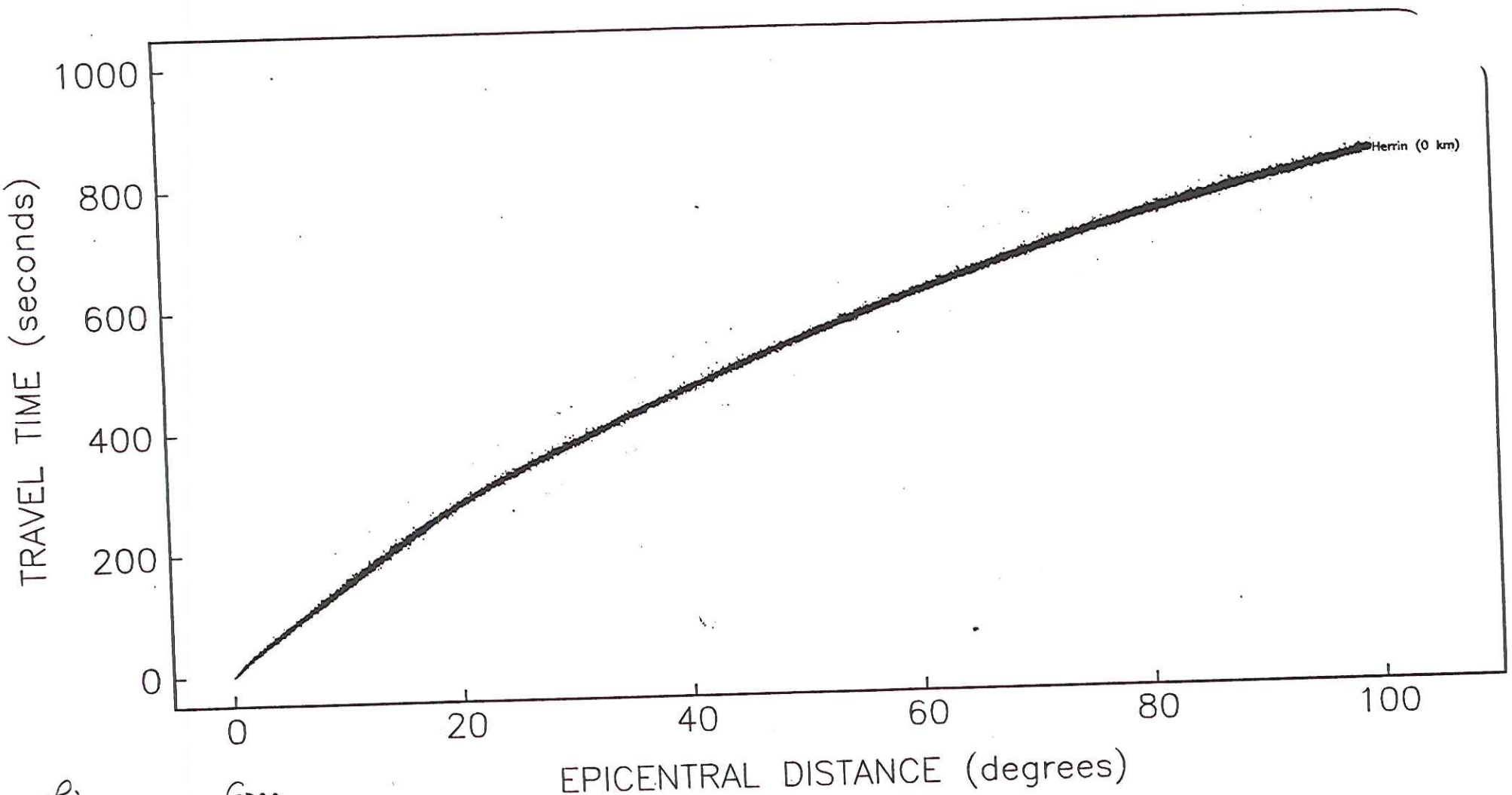

This comes from picking the first arrival

here

Figure 3 - P-wave travel time curve, plotted from the 132,380 P-phases, from the 479 magnitude 6+ events used in the preliminary analysis. (For plotting speed only one of every four points was plotted.) The Herrin (1968) travel time tables were used to correct for source depth and the surface focus travel time curve is plotted for reference. The "one-minute" P phases can be clearly seen.

Surface events $M > 6$

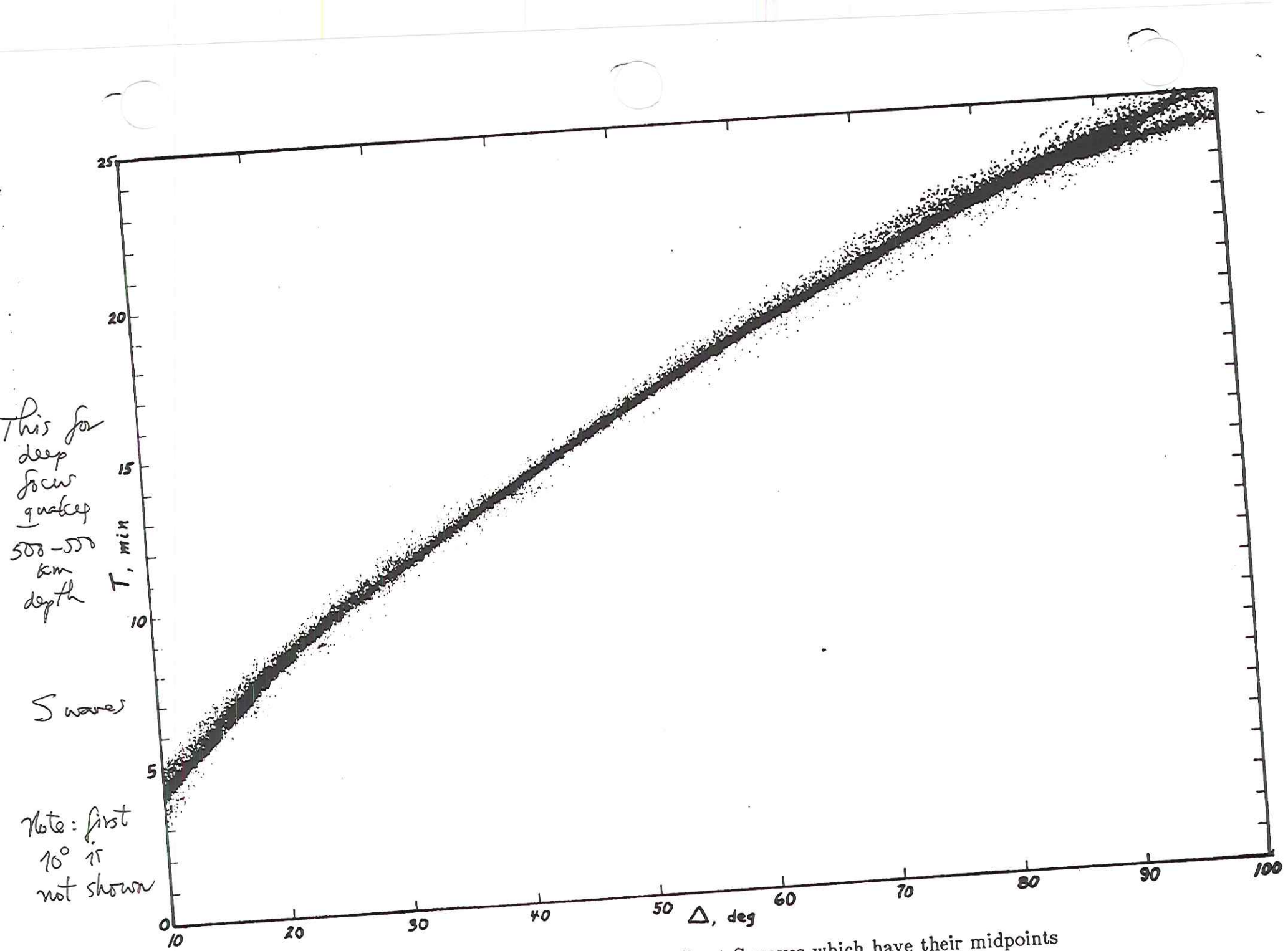

Figure 2. ISC travel time data for the direct S waves which have their midpoints below active continental regions. About 58,000 data points are contained in this

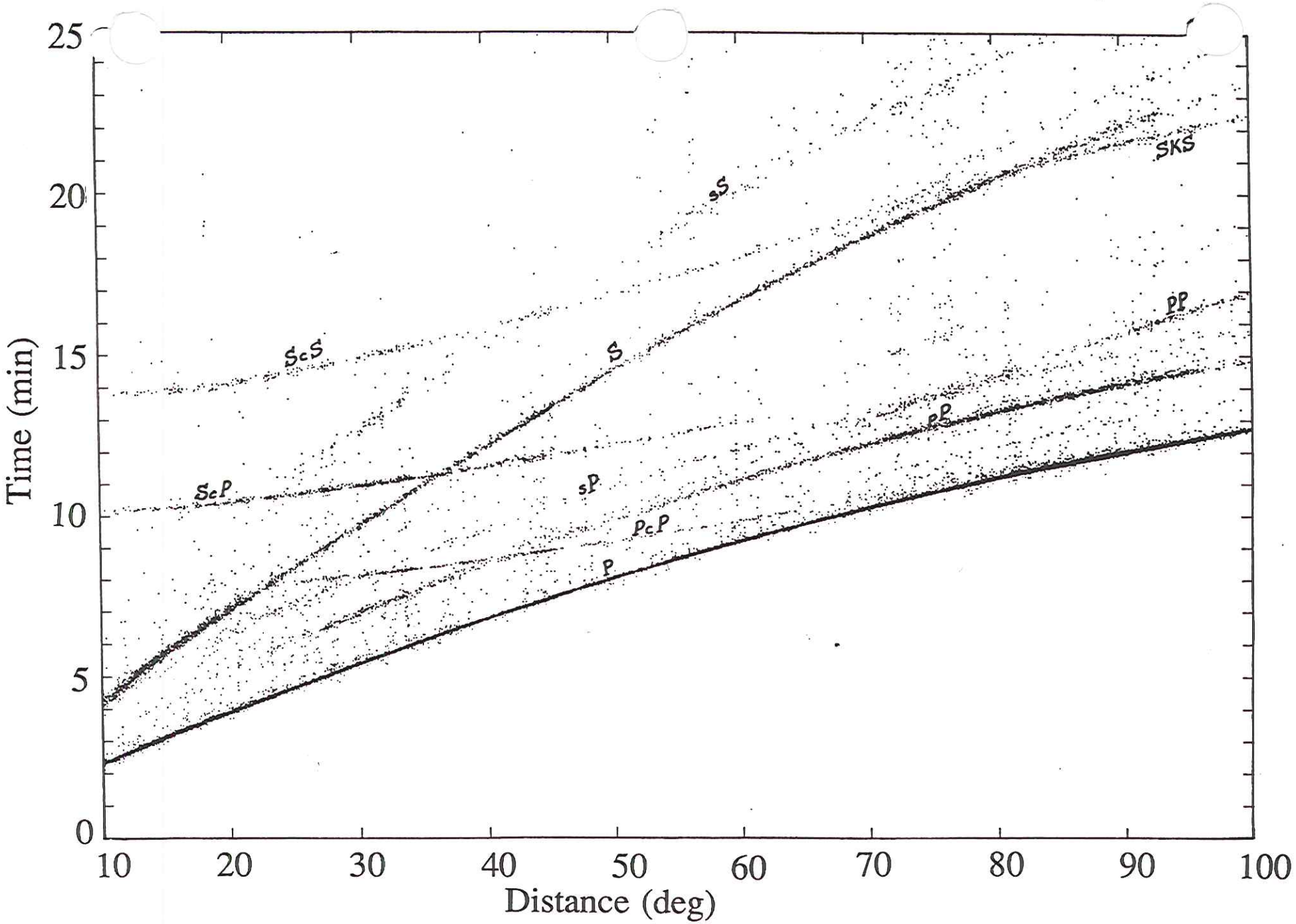

Figure 6. ISC travel time data for earthquakes with focal depths in the interval 500 to 550 km. An approximate depth correction has been applied to place all of the focal depths at 525 km. About 38,000 data points are contained in this plot.

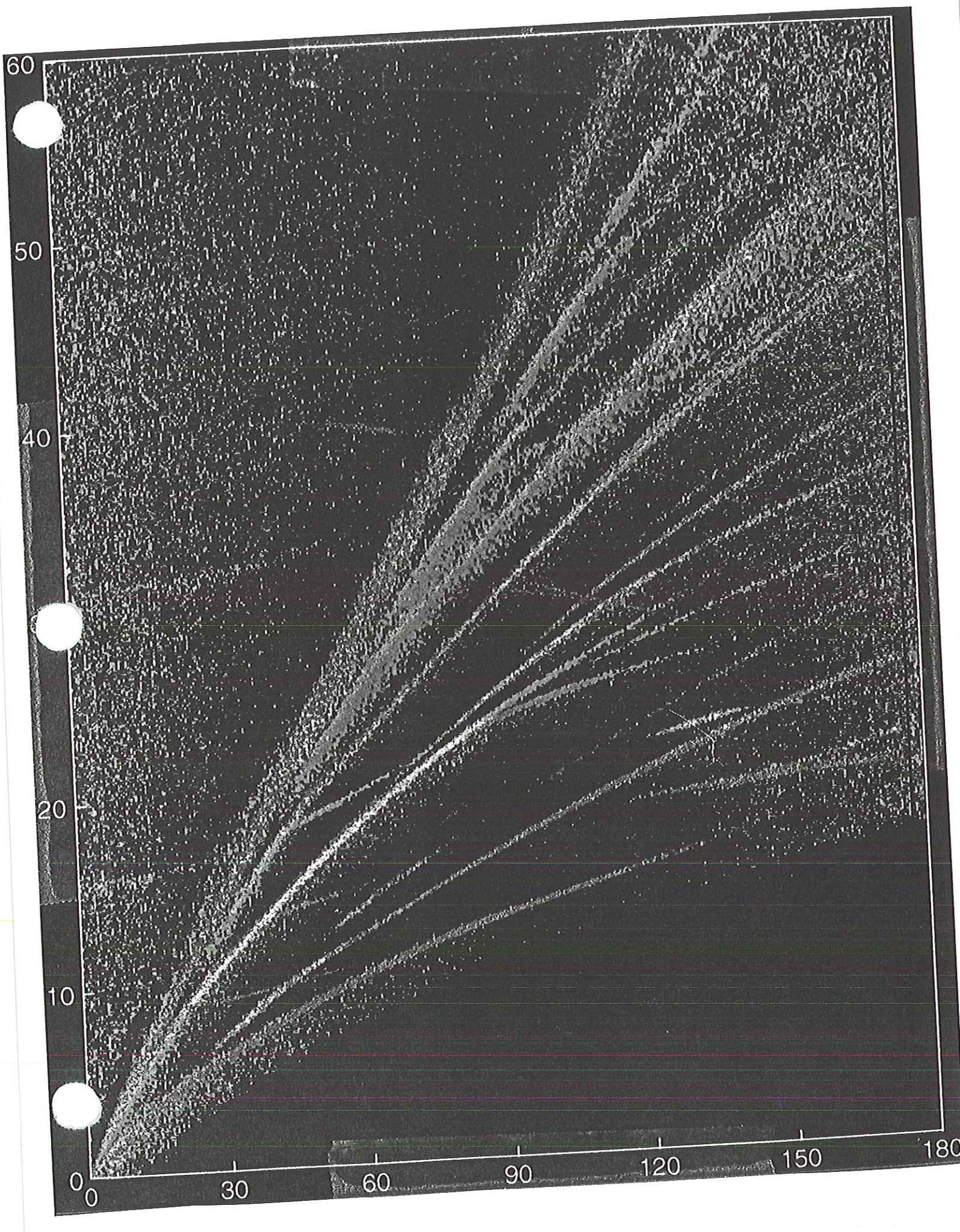
60
50
40
20
10
0
0
30
60
90
120
150
180

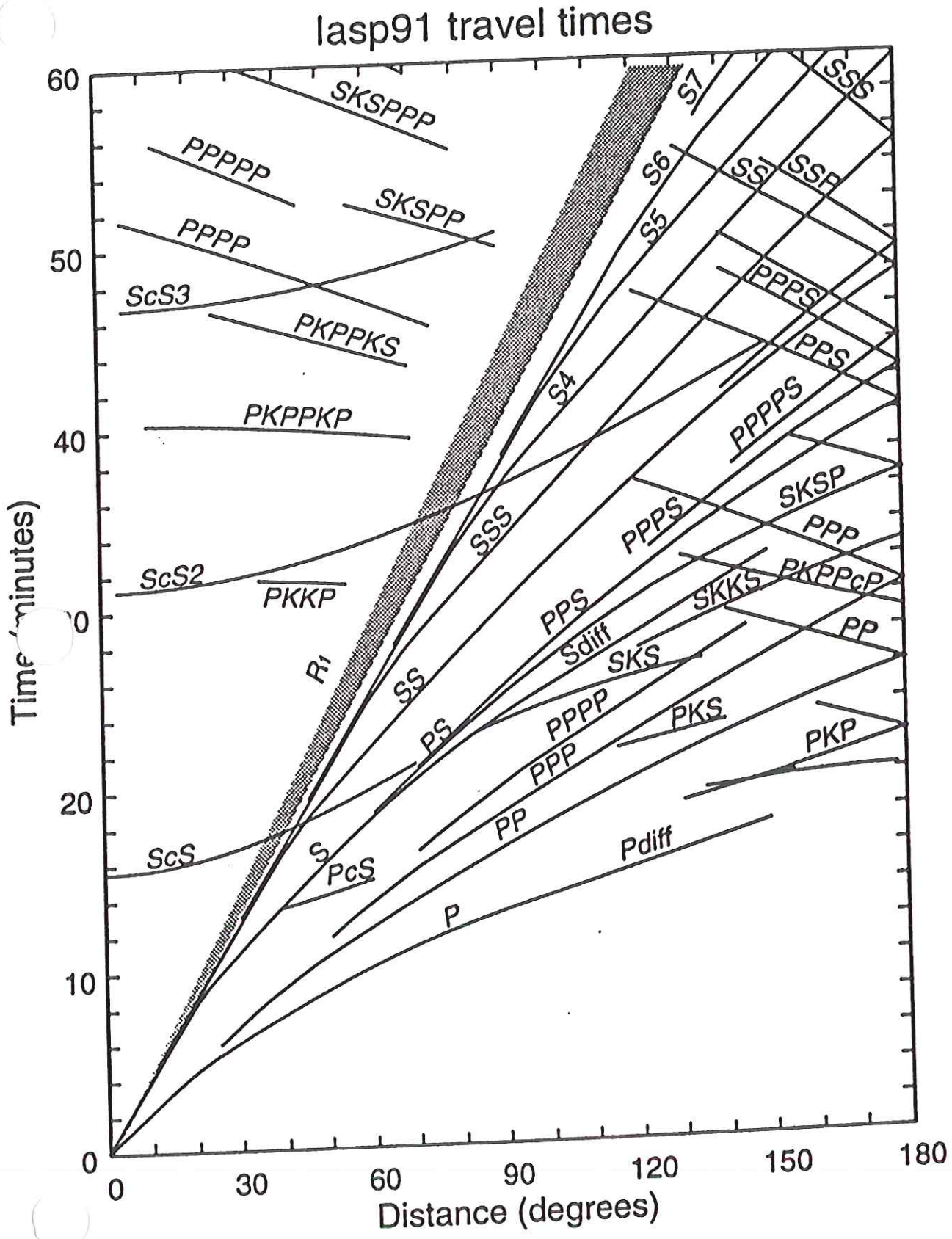
Iasp91 travel times
Time (minutes)
Distance (degrees)
0
10
20
30
40
50
60
0
30
60
90
120
150
180
SKSPPP
PPPPP
SKSPP
PPPP
ScS3
PKPPKS
PKPPKP
ScS2
PKKP
ScS
R1
S
PcS
S7
S6
S5
S4
SSS
SS
PS
SSS
SSP
PPPS
PPS
PPPPS
SKSP
PPP
PKPPcP
PP
SKKS
Sdiff
SKS
PPPP
PKS
PKP
PPP
PP
Pdiff
P

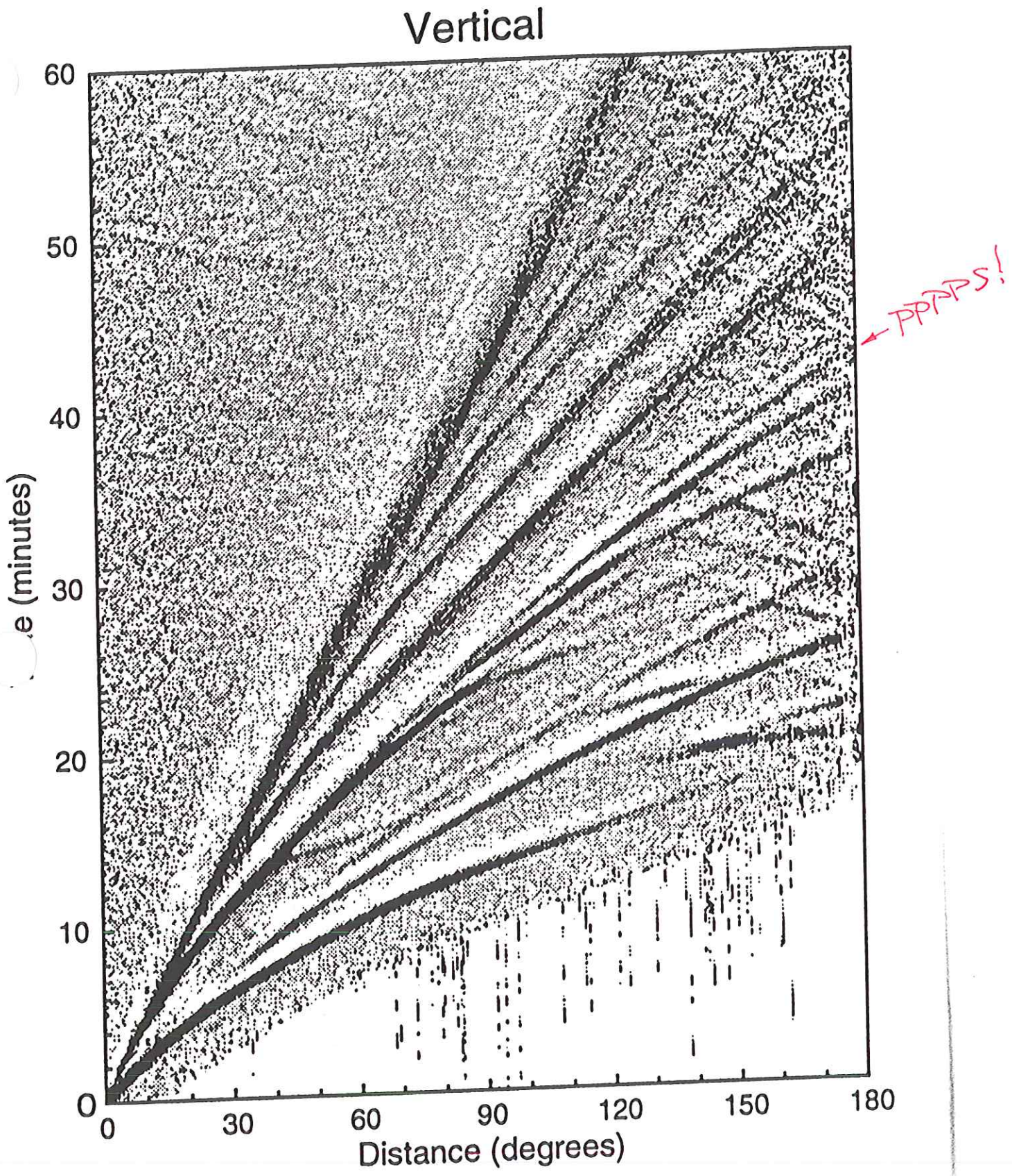
Vertical
60
50
40
30
20
10
0
e (minutes)
0
30
60
90
120
150
180
Distance (degrees)
PPPPS!

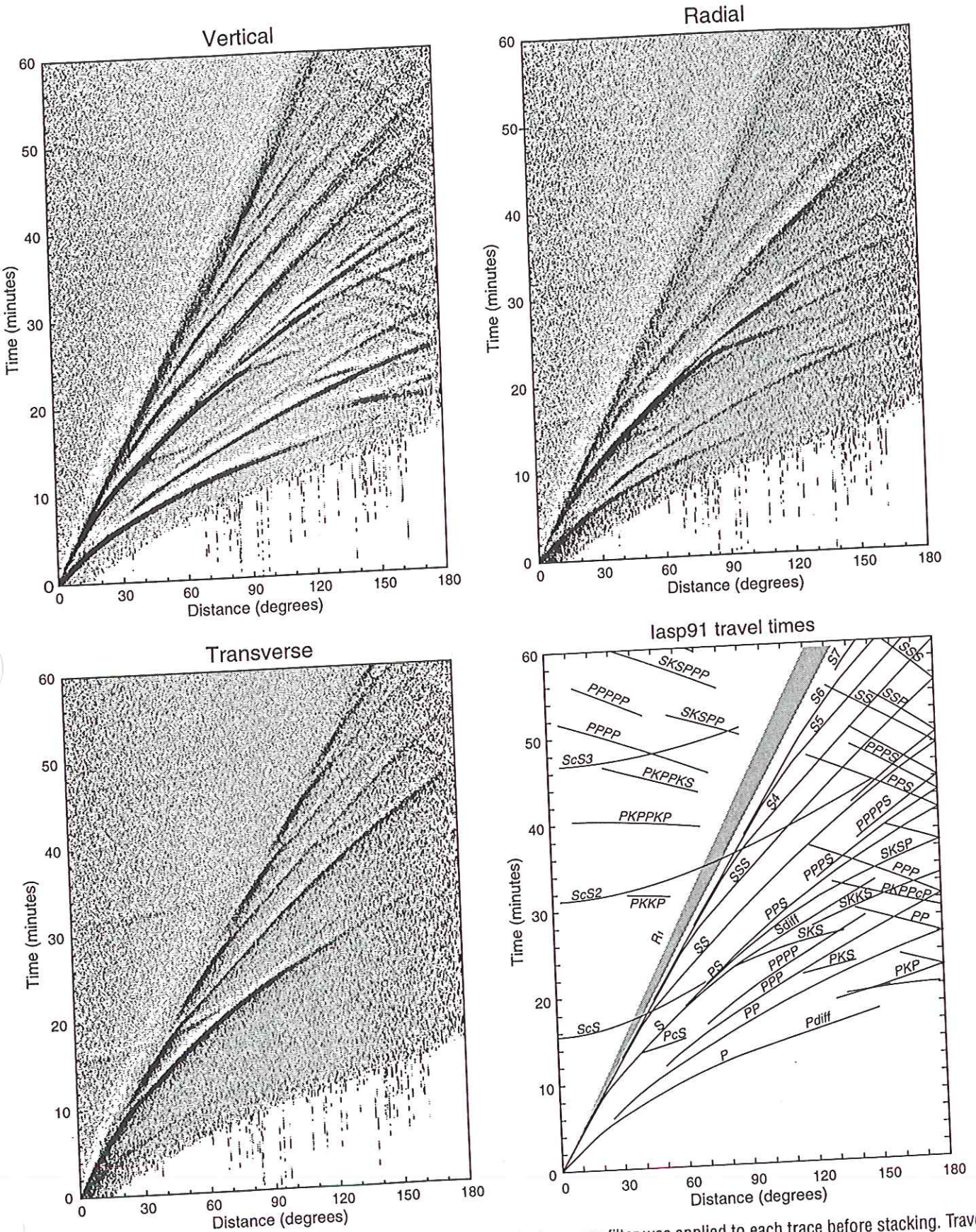

▲ **Figure 7.** Vertical, radial, and transverse stacks resulting after a 30 s low-pass filter was applied to each trace before stacking. Travel times calculated for the *iasp*91 model for the visible seismic phases in these stacks are shown in the lower right.

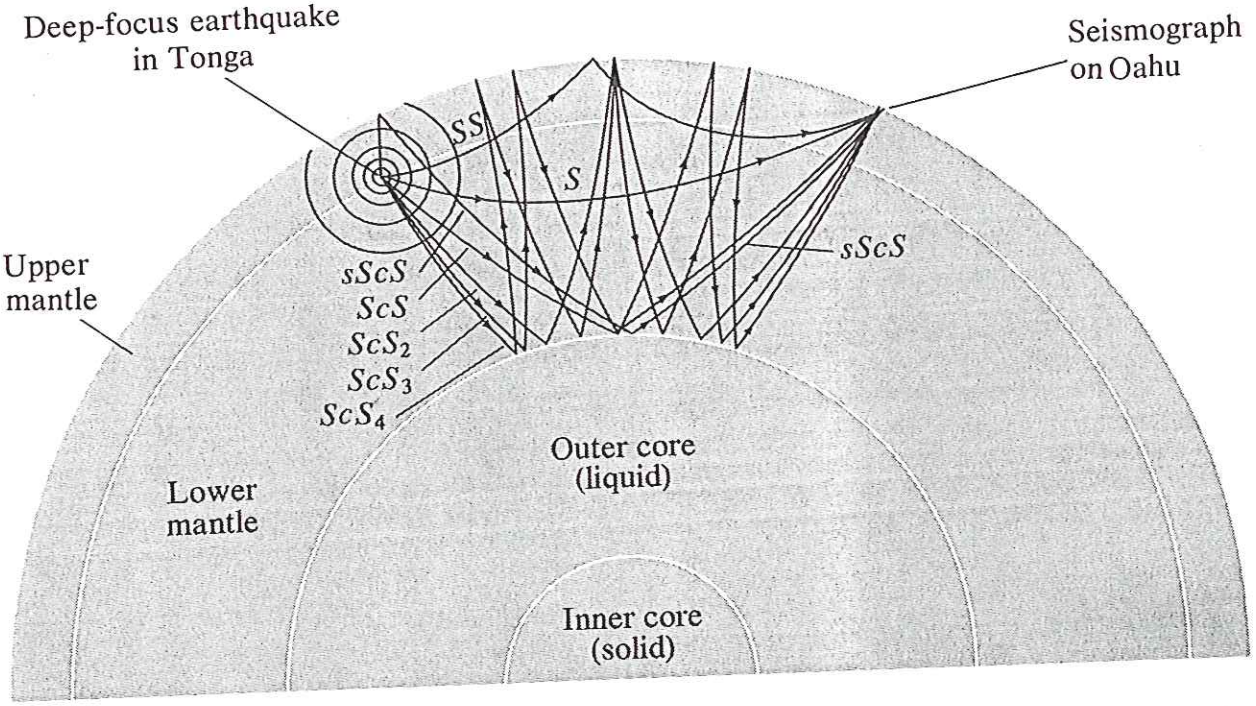

(a)

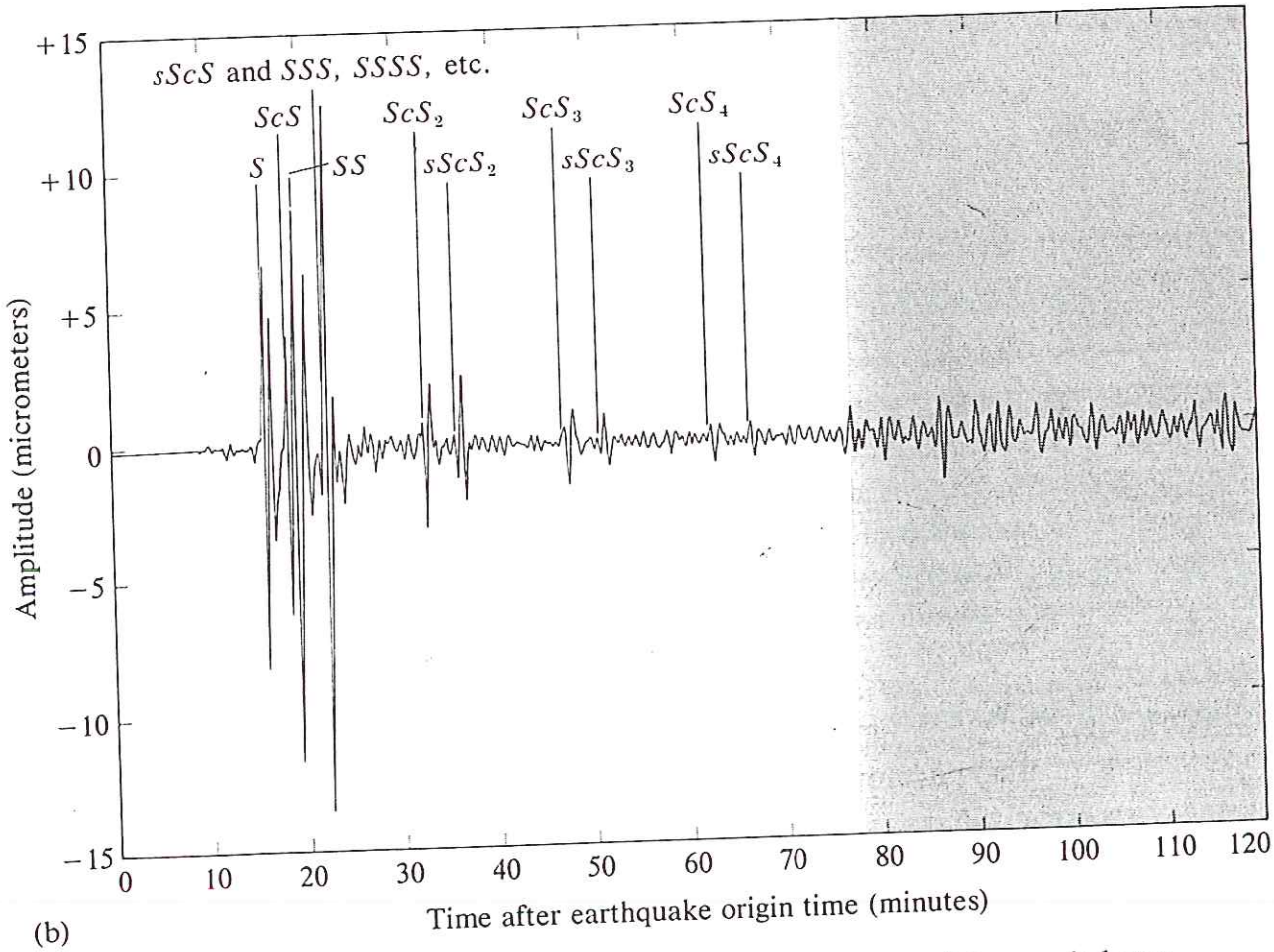

(b)

Figure 5.3 Multiple surface reflections (a) and seismogram (b) recorded at a seismographic station at Oahu, Hawaii. These waves followed a deep-focus earthquake near the South Pacific island of Tonga in October 1974. [From Thomas H. Jordan, "The Deep Structure of the Continents." Copyright © 1978 by Scientific American, Inc. All rights reserved.]

Box 1.4 The Seismological Discovery of the Earth's Inner Core

P′

By I. Lehmann

An explanation of the P_3' wave is required, since now it can hardly be considered probable that it is due to diffraction. A hypothesis will here be suggested which seems to hold some probability, although it cannot be proved from the data at hand.

We take it that, as before, the earth consists of a core and a mantle, but that inside the core there is an inner core in which the velocity is larger than in the outer one. The radius of the inner core is taken to be $r_1 = \frac{8}{10} r_0$ sine $16° = 0.2205\ r_0$, so that the ray whose angle of incidence at the surface of the earth is 16° just touches the inner core.

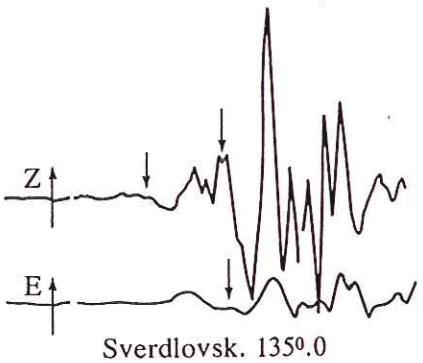

Sverdlovsk. 135⁰.0

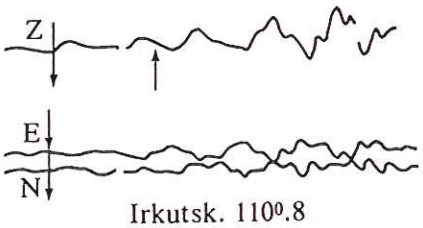

Irkutsk. 110⁰.8

June 16, 1929, P_3' records

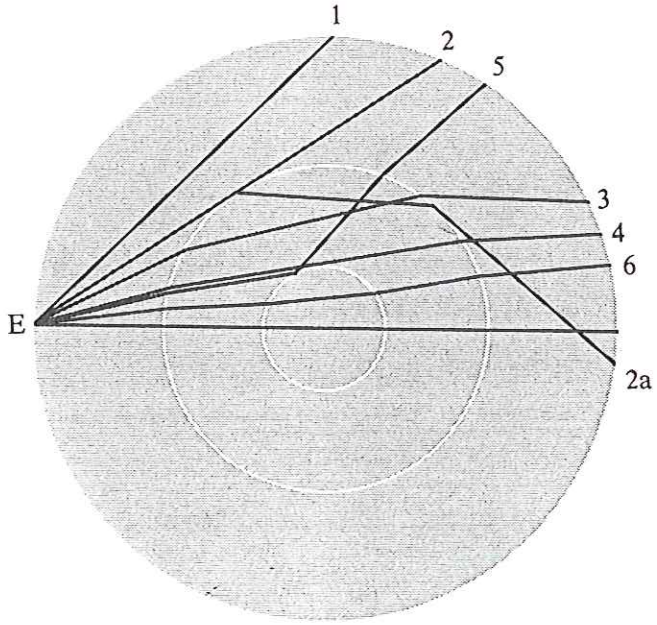

Paths through the Earth with inner and outer cores. [From Lehmann, 1936.]

From I. Lehmann, "*P′*," Bureau Central Seismologique International, Series A, *Travaux Scientifique, 14,* 88, 1936.

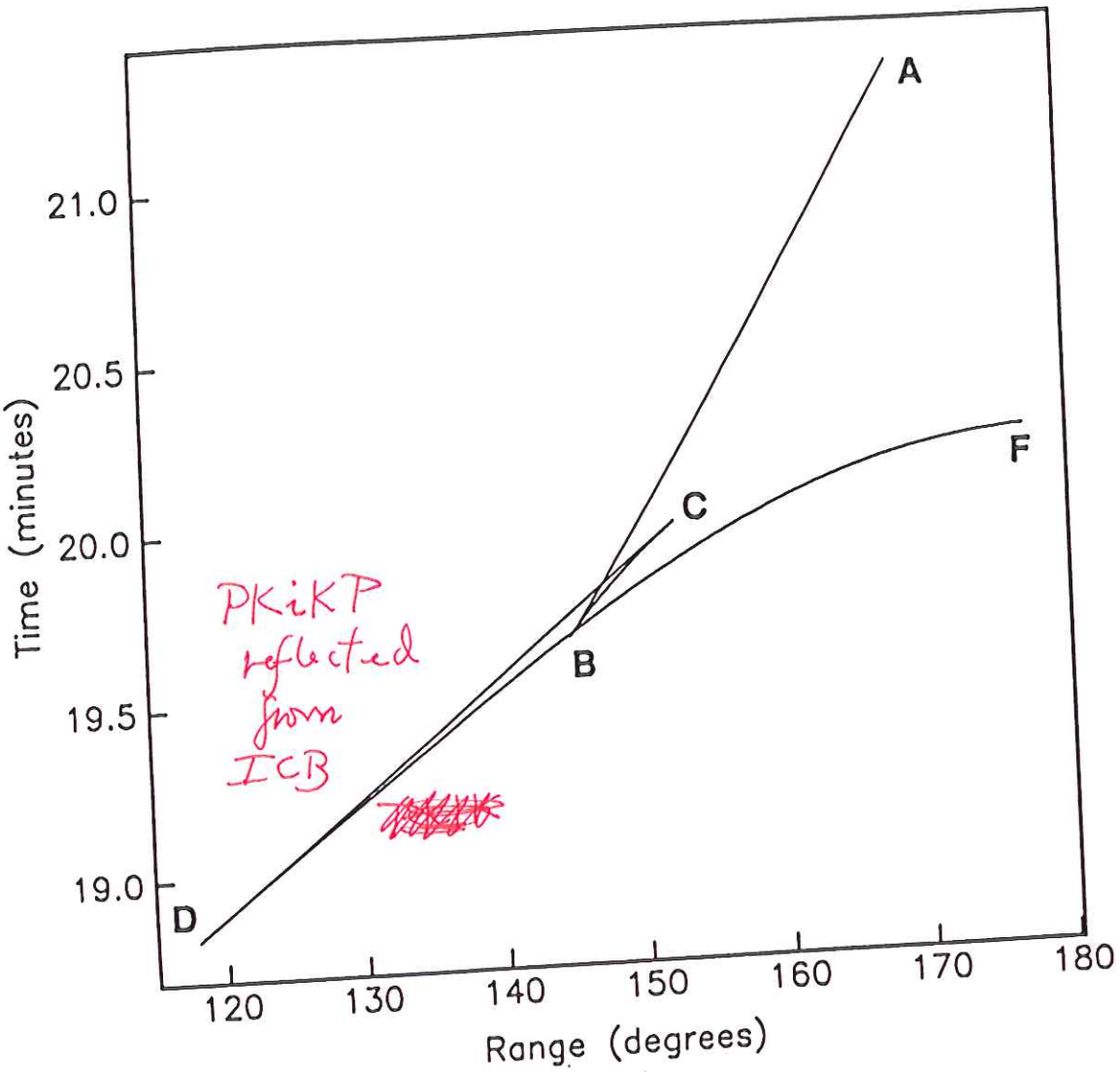

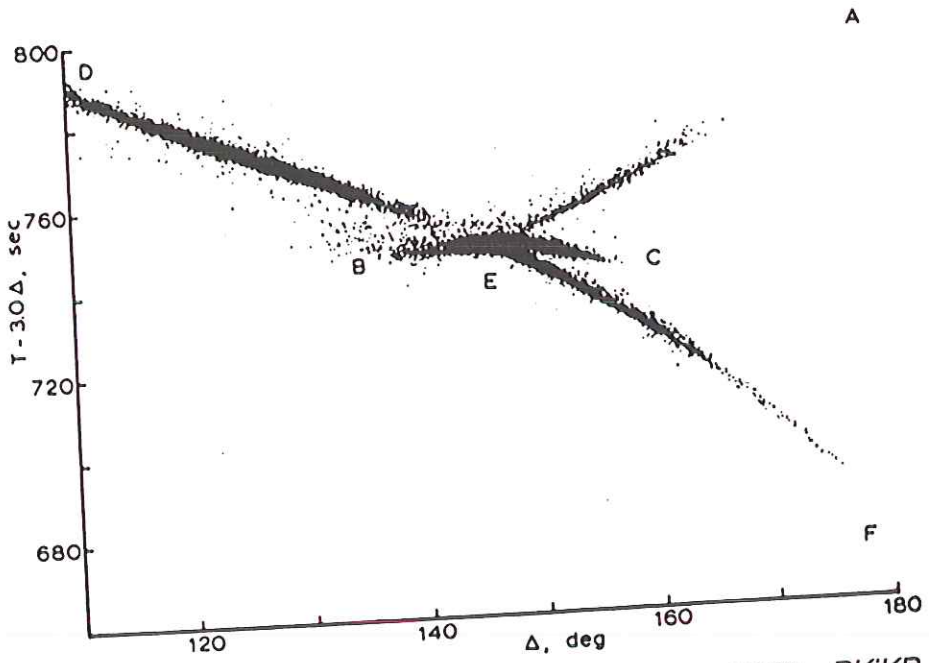

FIGURE 7.53 (Top) Theoretical travel-time curves for *PKP* (*ABC*), *PKiKP* (*CD*), and *PKIKP* (*DF*) branches for PREM. (Bottom) Reduced travel times of about 60,000 *P* waves in the core showing the various branches of the core phases. (Top from Shearer and Toy, 1991; *J. Geophys. Res.* **96**, 2233–2247, 1991; © copyright by the American Geophysical Union. Bottom from Johnson and Lee, 1985.)

Examples :

(1) multiple ScS and sScS from 1994 Bolivian earthquake June 9, 1994 670 km deep — largest deep-focus event ever recorded ← Tonga event in Oahu better

(2) PP KP

(3) Shearer upper-mantle reflections

Inverse problem of determining $\alpha(r)$ and $\beta(r)$ from measured T versus Δ of the various arrivals is well-understood.

As a result the seismic velocities within the ⊕ are very well determined.

This has been done for one other solar system body — the Moon. The ~~Apollo~~ Apollo ~~astronauts~~ astronauts placed seismometers on all missions.

Moonquakes & meteorite impacts provided seismic sources.

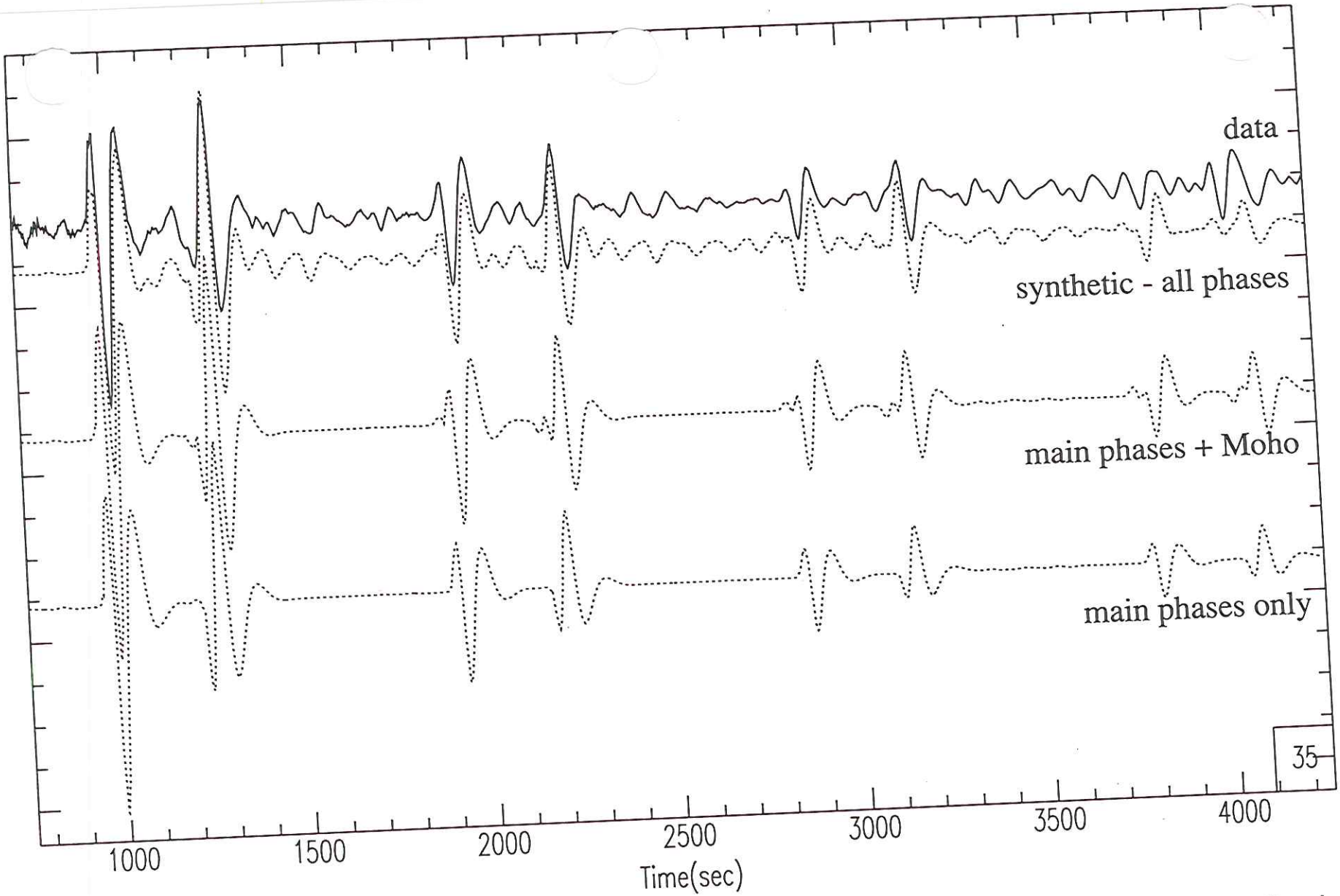

Example of radial component seismogram (low-passed at 100s) from the most western station in Bolivia (STO1), and comparison with synthetics. Traces are (from bottom): - CORE synthetic with main phases only. CORE synthetic with Moho phases included (note that Moho precursors alter the shape of sScS pulses, thus constraining the Moho depth). CORE synthetic with all discontinuities included. Additional phases seen are boundary interaction phases from D400, D600 and D230. Note that most of these phases are also seen in the data (top trace), allowing us

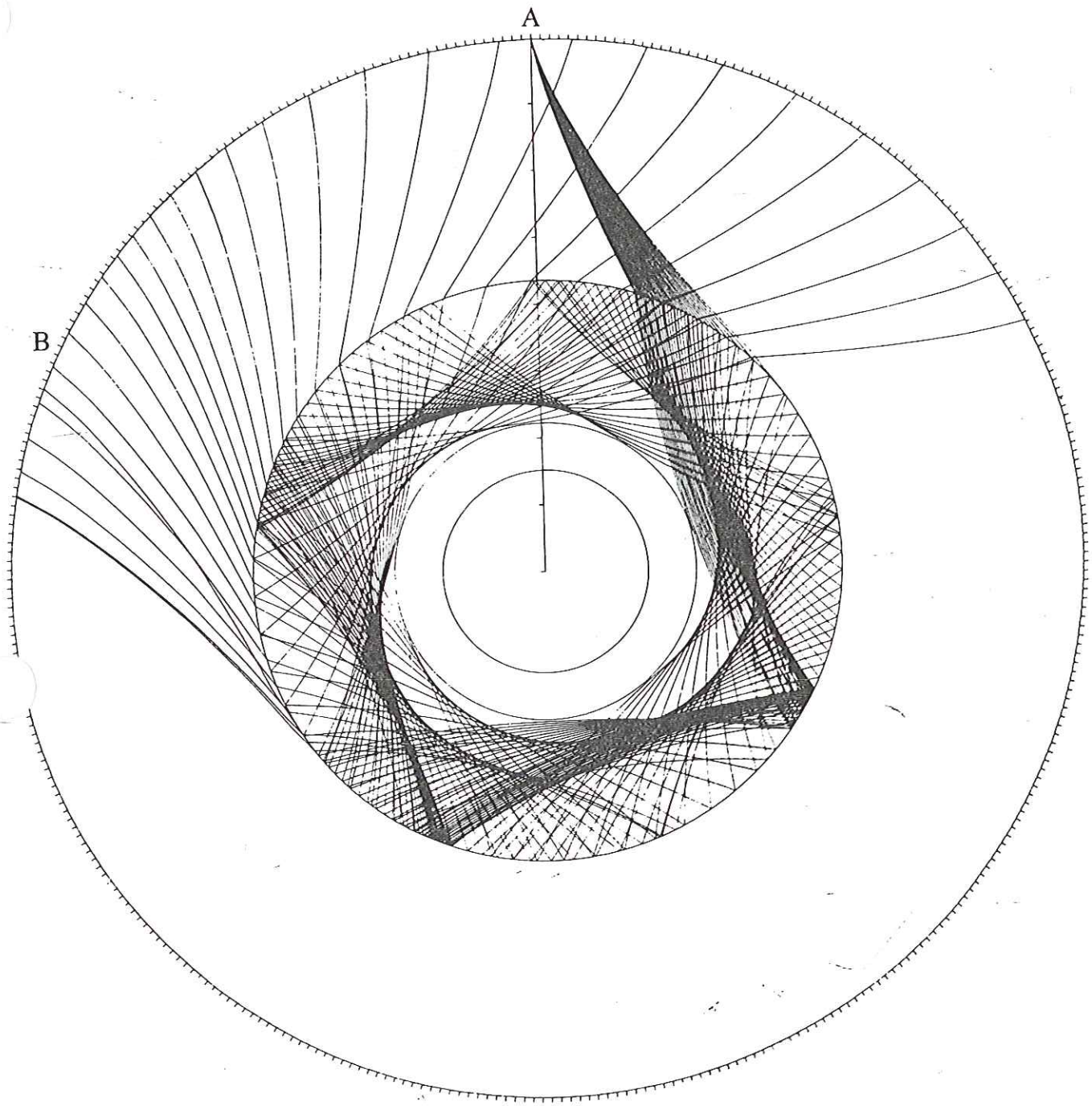

Figure 4.5 Multiple reflections from *P* waves trapped inside the Earth's liquid outer core. This computer plot depicts the paths of waves, generated by a seismic event at A, that have bounced inside the core seven times before reaching the surface, for example, at Station B. The computer program that produced the ray paths was devised by C. Chapman.

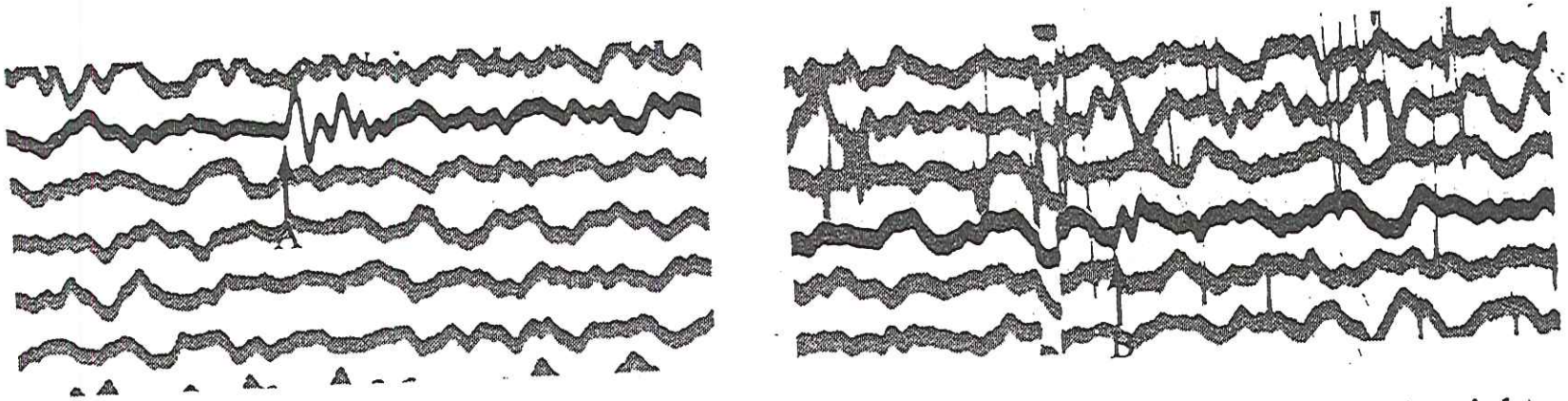

Figure 4.6 *P4KP* and *P7KP*. The faint pulse of a *P7KP* echo can be seen at the right (B) in this seismogram made at Jamestown of an underground explosion on Novaya Zemlya in 1970. The stronger *P4KP* pulse, labeled A at the left, was recorded about 20 minutes earlier. [From Bruce A. Bolt, "The Fine Structure of the Earth's Interior."]

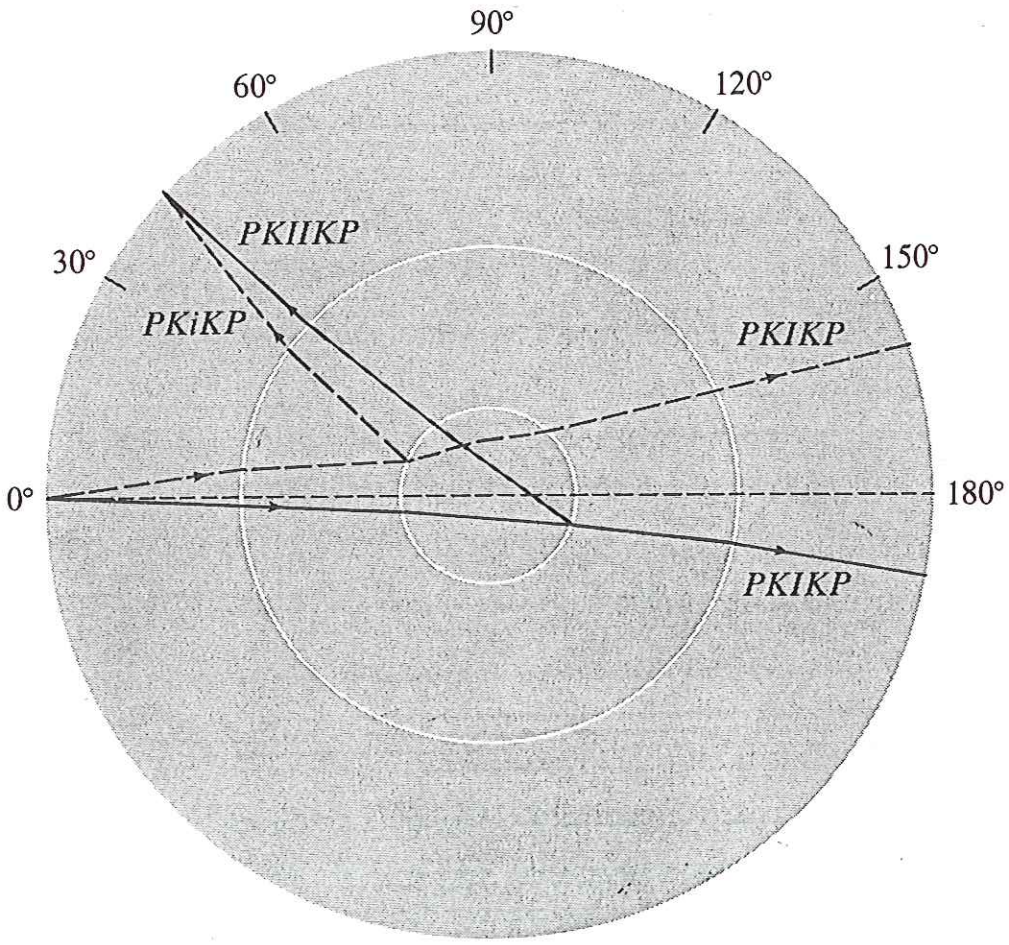

Figure 4.8 Rays corresponding to seismic waves traveling through the Earth's interior from a source at the point marked 0 and reflecting at the outside and inside of the inner core. These reflected waves are called *PKiKP* and *PKIIKP*, respectively.

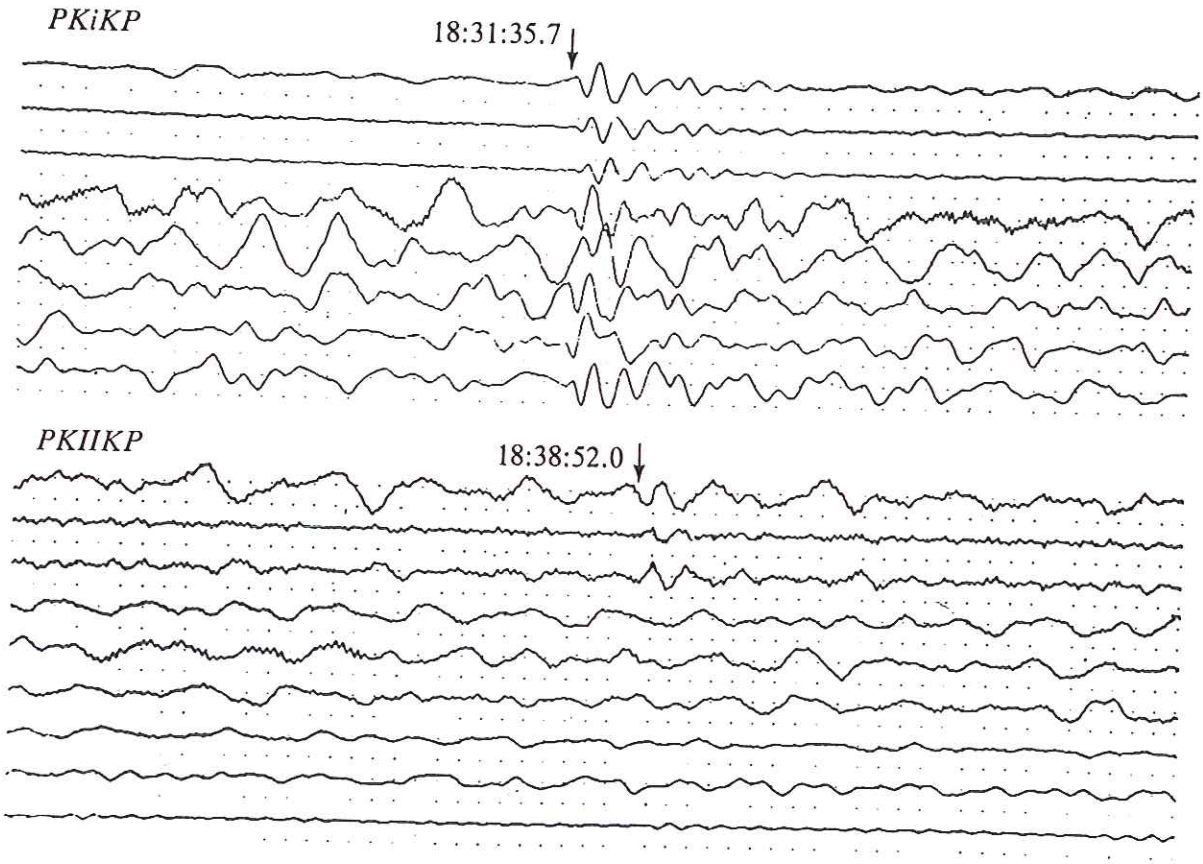

Figure 4.9 Seismograms of *PKiKP* and *PKIIKP* from the LASA seismic array in Montana. The time ticks are 1 second apart. The top three traces for both *PKiKP* and *PKIIKP* show the "beam" of LASA recorded signals that have been filtered at velocities and frequencies most appropriate for detecting a core wave. The remaining traces below are the seismic waves recorded by various smaller sets of seismometers. The arrows show the arrival times of the onsets of the *PKiKP* and *PKIIKP* waves in hours, minutes, and seconds.

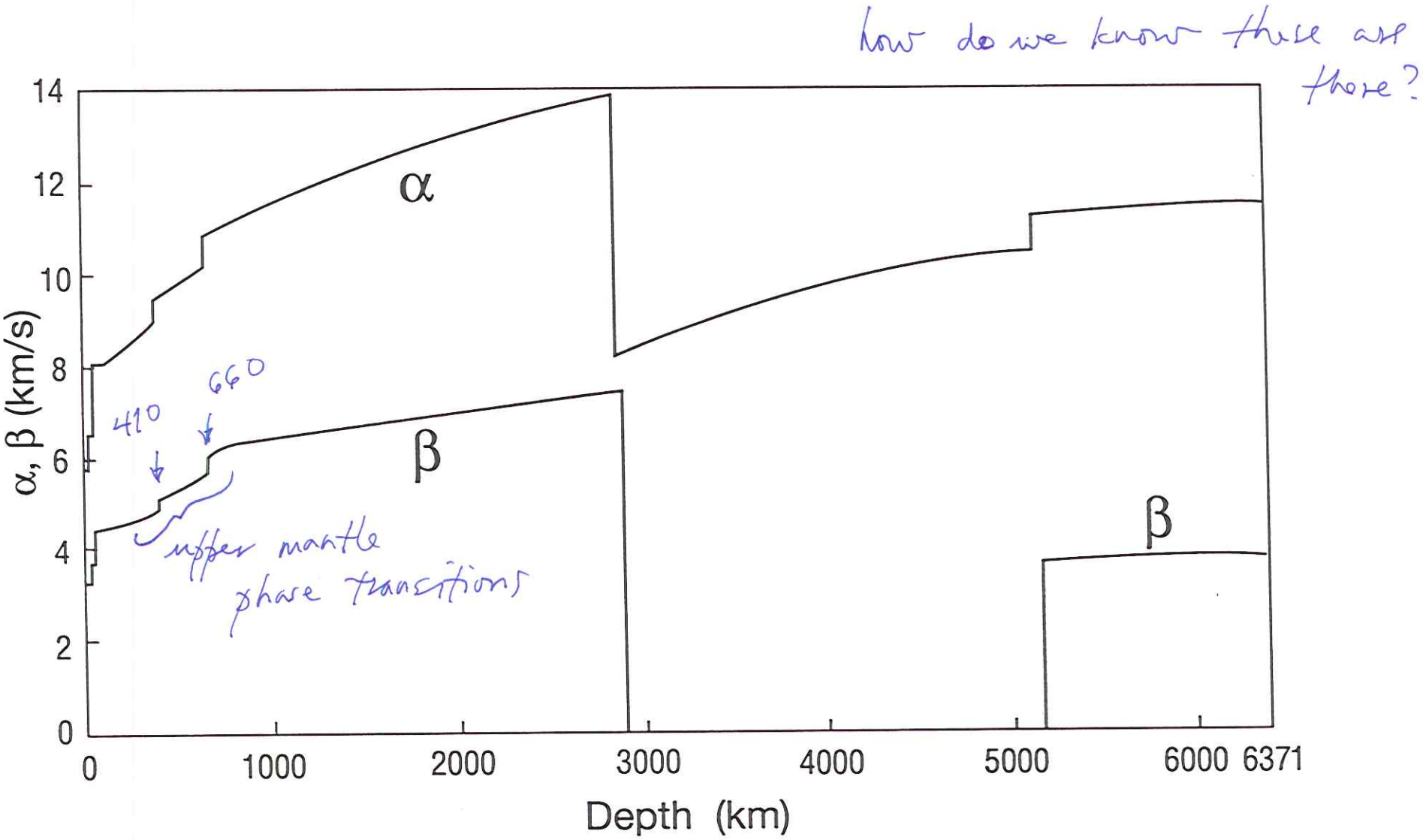

Figure 5.17 P and S wave speeds, α and β, in the iasp91 model of the Earth developed from body wave travel times (Kennett and Engdahl, 1991). Like several other recent Earth models, iasp91 is parameterized, in the sense of having wave speeds that are simple polynomial functions of radius over 11 independently fitted depth ranges.

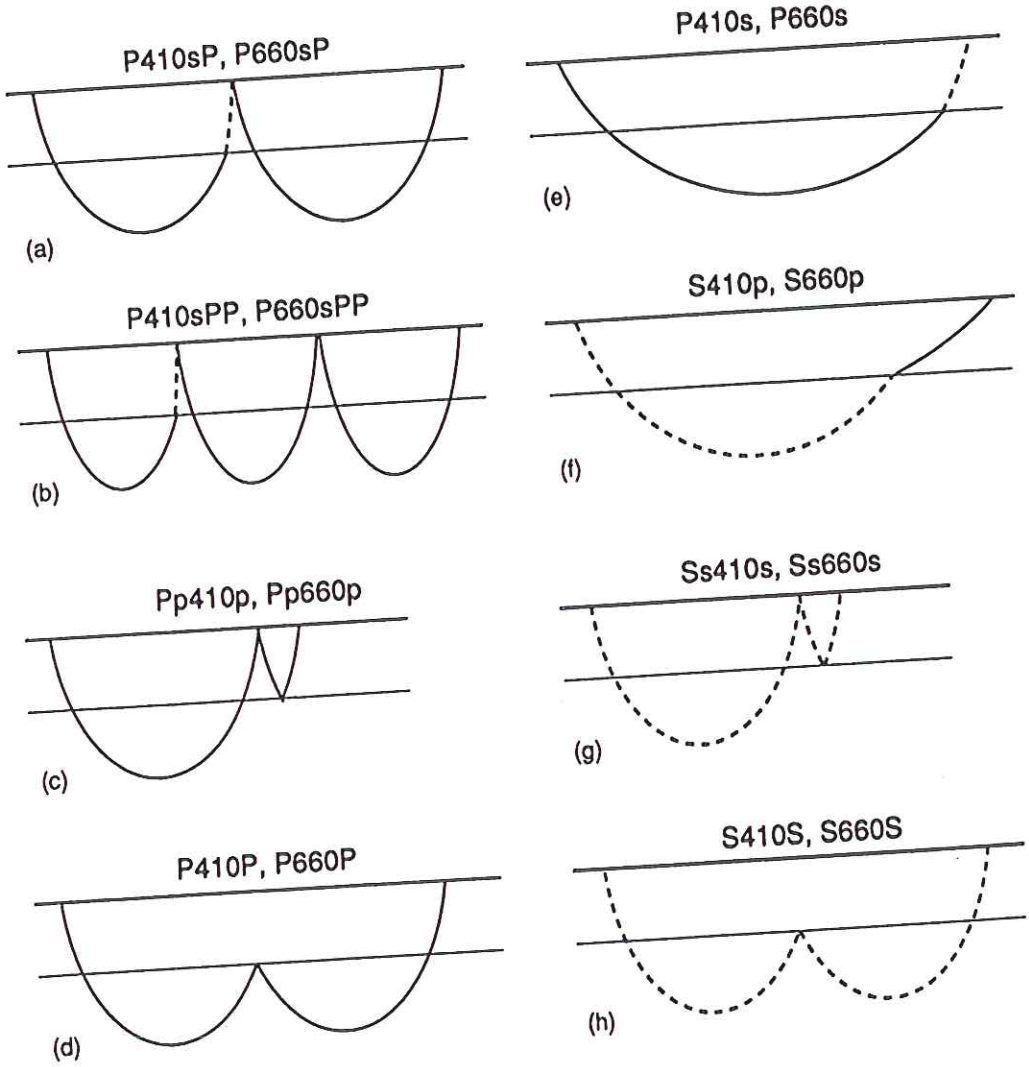
P410sP, P660sP
(a)
P410sPP, P660sPP
(b)
Pp410p, Pp660p
(c)
P410P, P660P
(d)
P410s, P660s
(e)
S410p, S660p
(f)
Ss410s, Ss660s
(g)
S410S, S660S
(h)

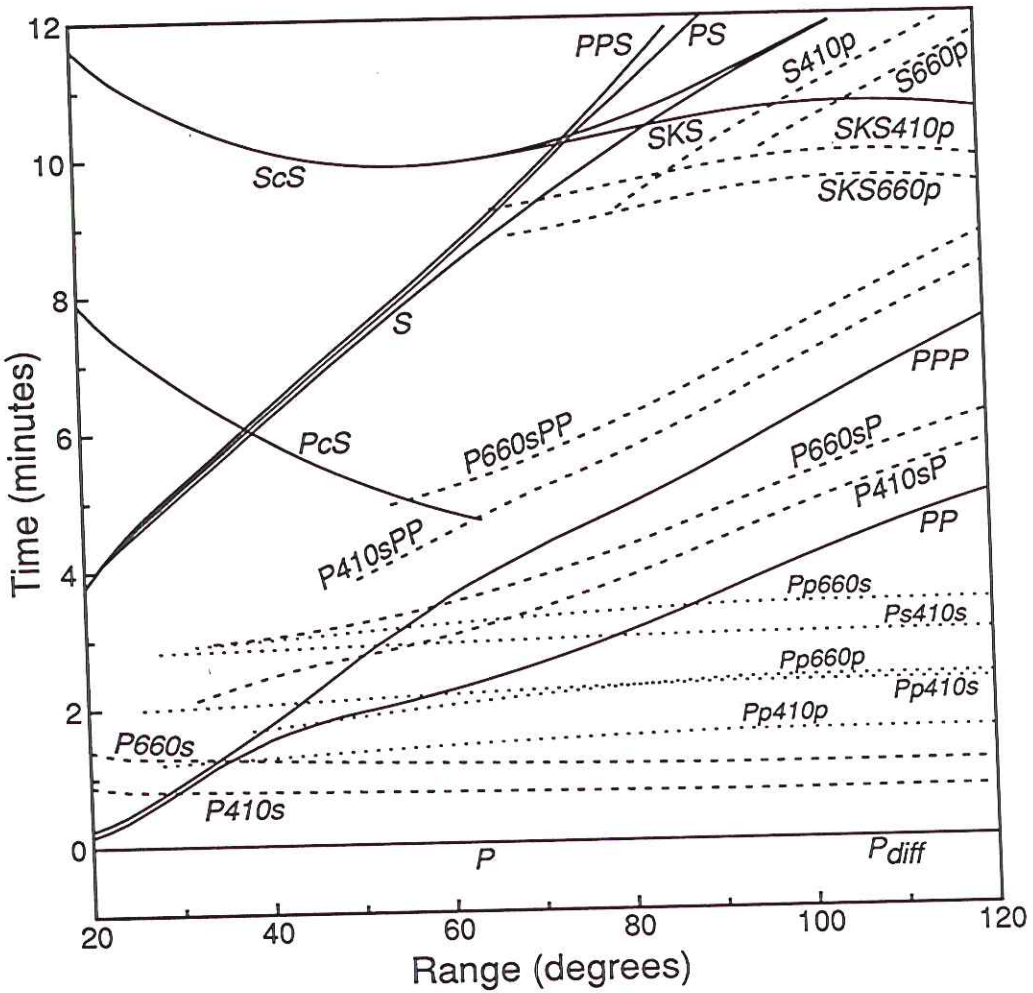

Fig. 6. Travel time curves relative to P for primary seismic phases (solid) and upper mantle discontinuity phases (dashed) for comparison with the stacked image shown in Plate 2. Curves were calculated using PREM, with interfaces assumed at 410-km and 660-km depth.

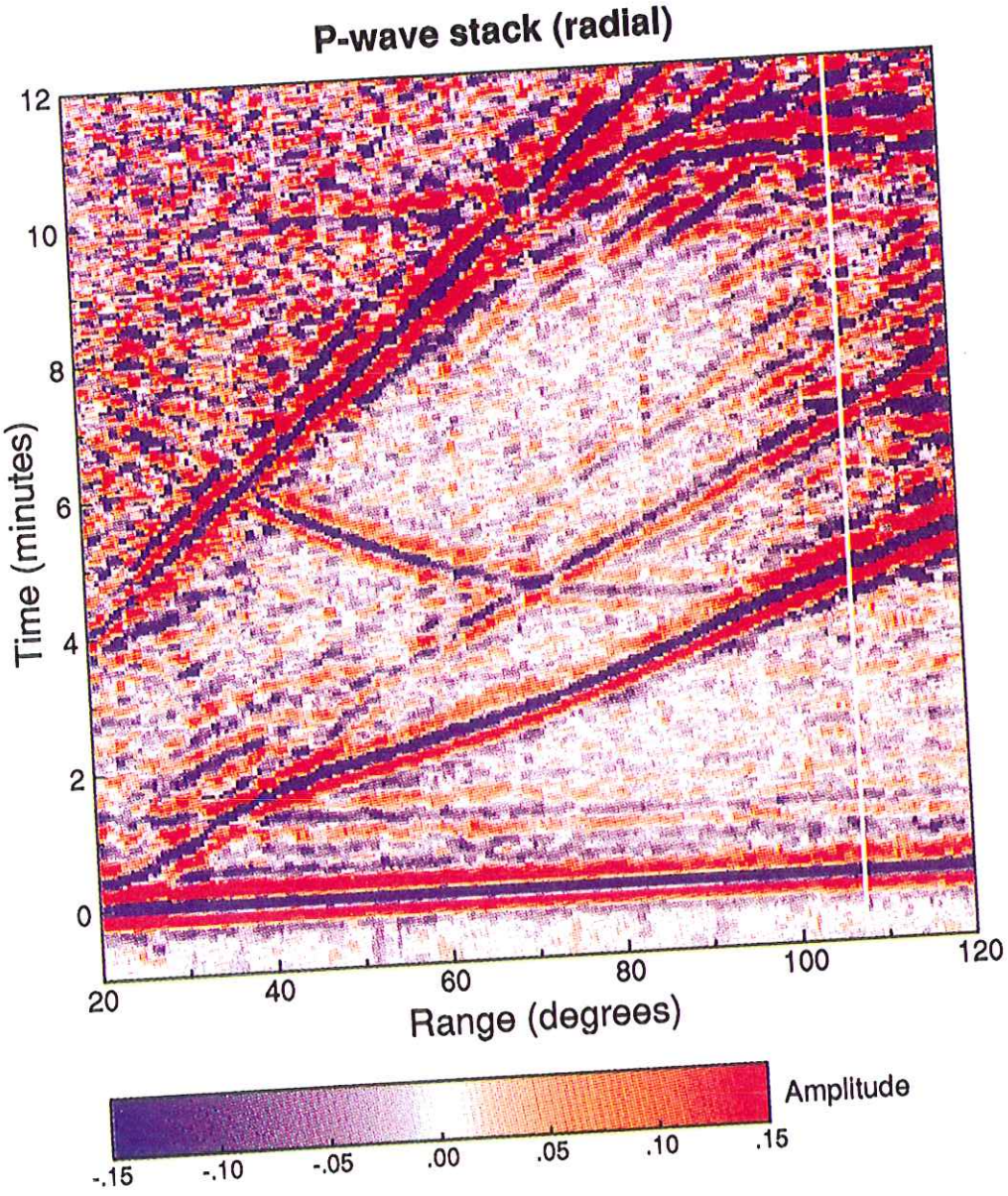
P-wave stack (radial)
Time (minutes)
12
10
8
6
4
2
0
20
40
60
80
100
120
Range (degrees)
Amplitude
-.15
-.10
-.05
.00
.05
.10
.15

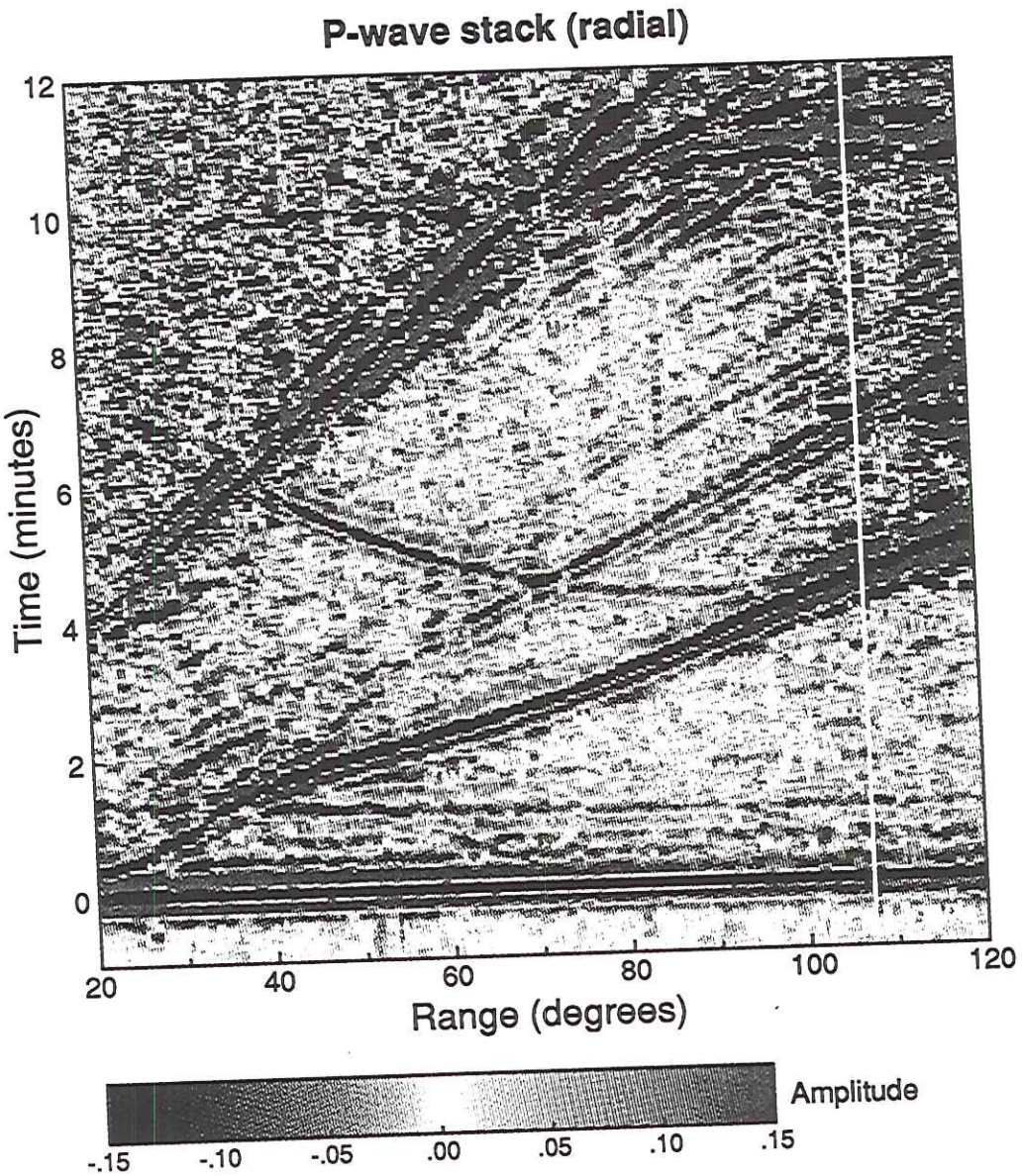

Plate 2. Stacked color image of long-period GDSN data (radial component), aligned on P as a reference phase. Positive amplitudes are shown in red, negative amplitudes in blue, with the scale ranging up to 0.15 of the maximum P wave amplitude. The white vertical streak near 108° is a result of no data falling within this range bin.

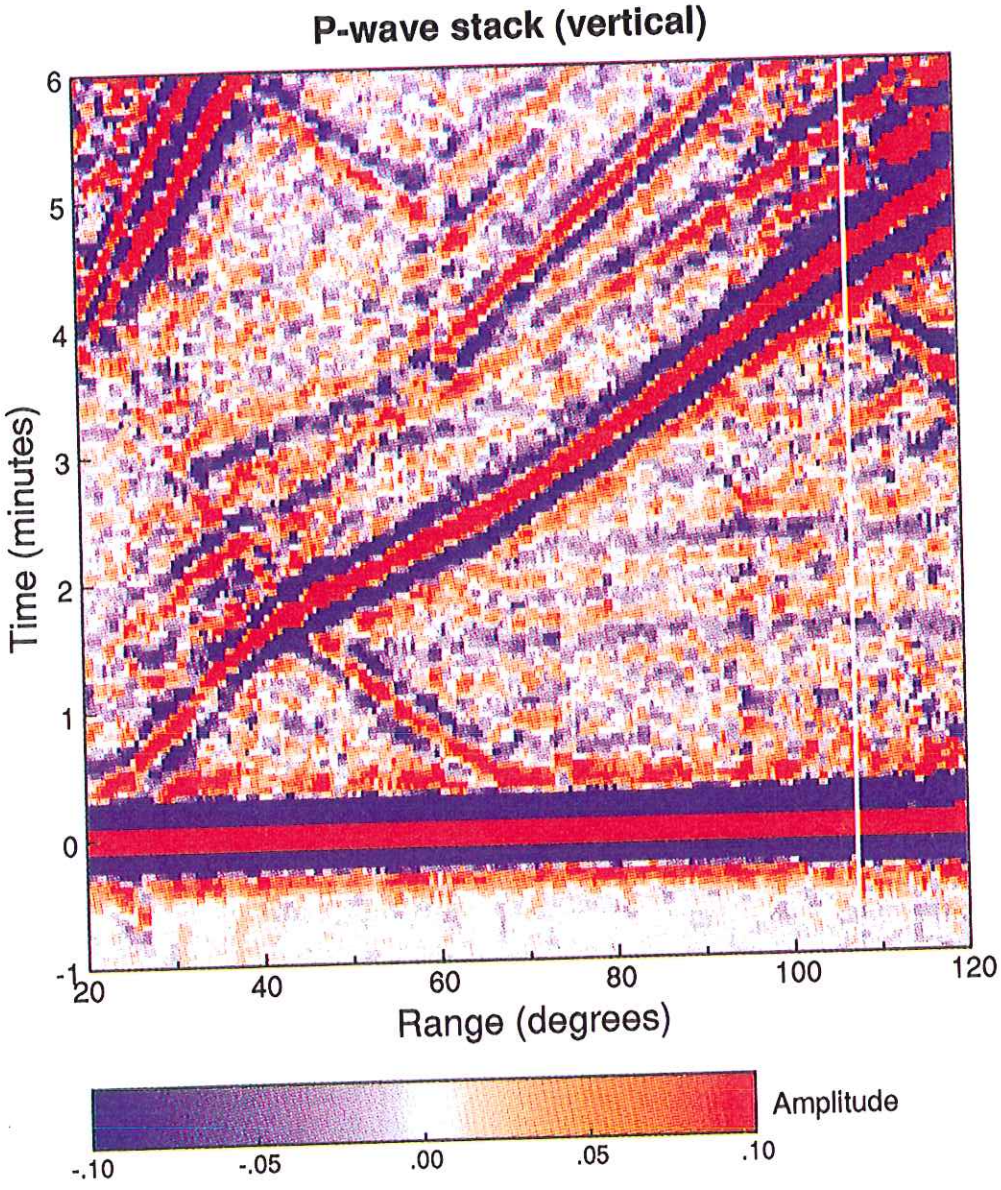
P-wave stack (vertical)
Time (minutes)
6
5
4
3
2
1
0
-1
20
40
60
80
100
120
Range (degrees)
Amplitude
-.10
-.05
.00
.05
.10

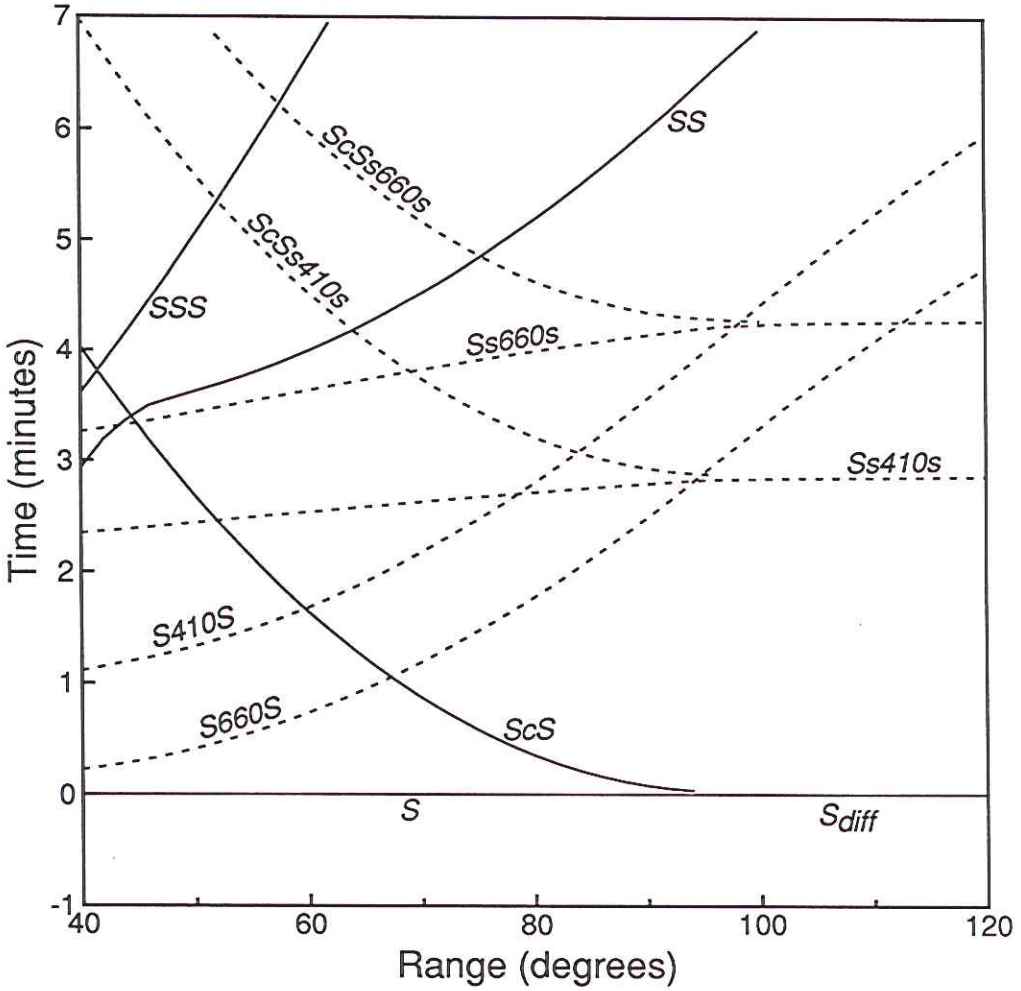

Fig. 7. Travel time curves relative to *S* for primary seismic phases (solid) and upper mantle discontinuity phas for comparison with the stacked image shown in Plate 3. Curves were calculated using PREM, with interfac at 410-km and 660-km depth.

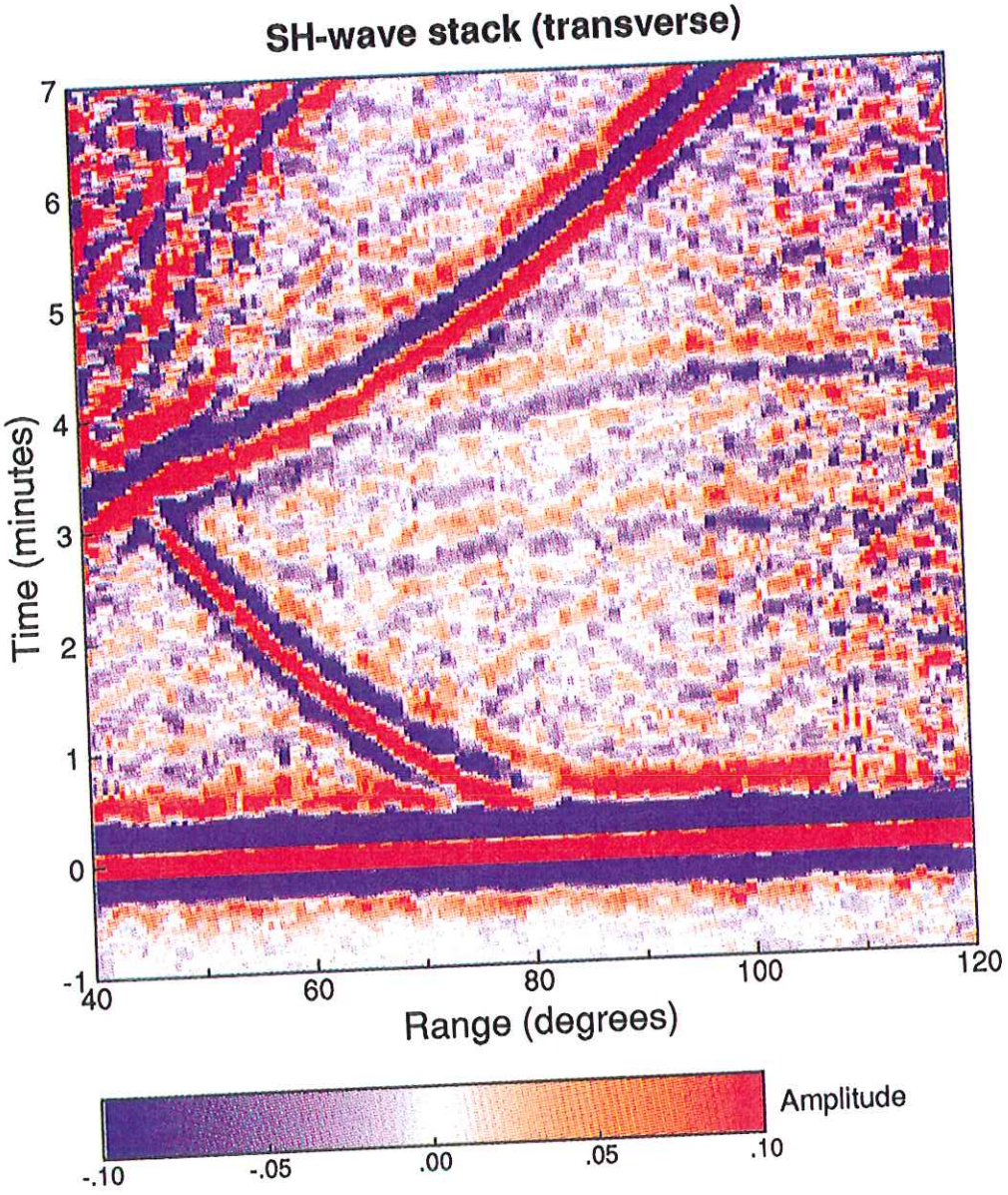
SH-wave stack (transverse)
Time (minutes)
7
6
5
4
3
2
1
0
-1
40
60
80
100
120
Range (degrees)
Amplitude
-.10
-.05
.00
.05
.10

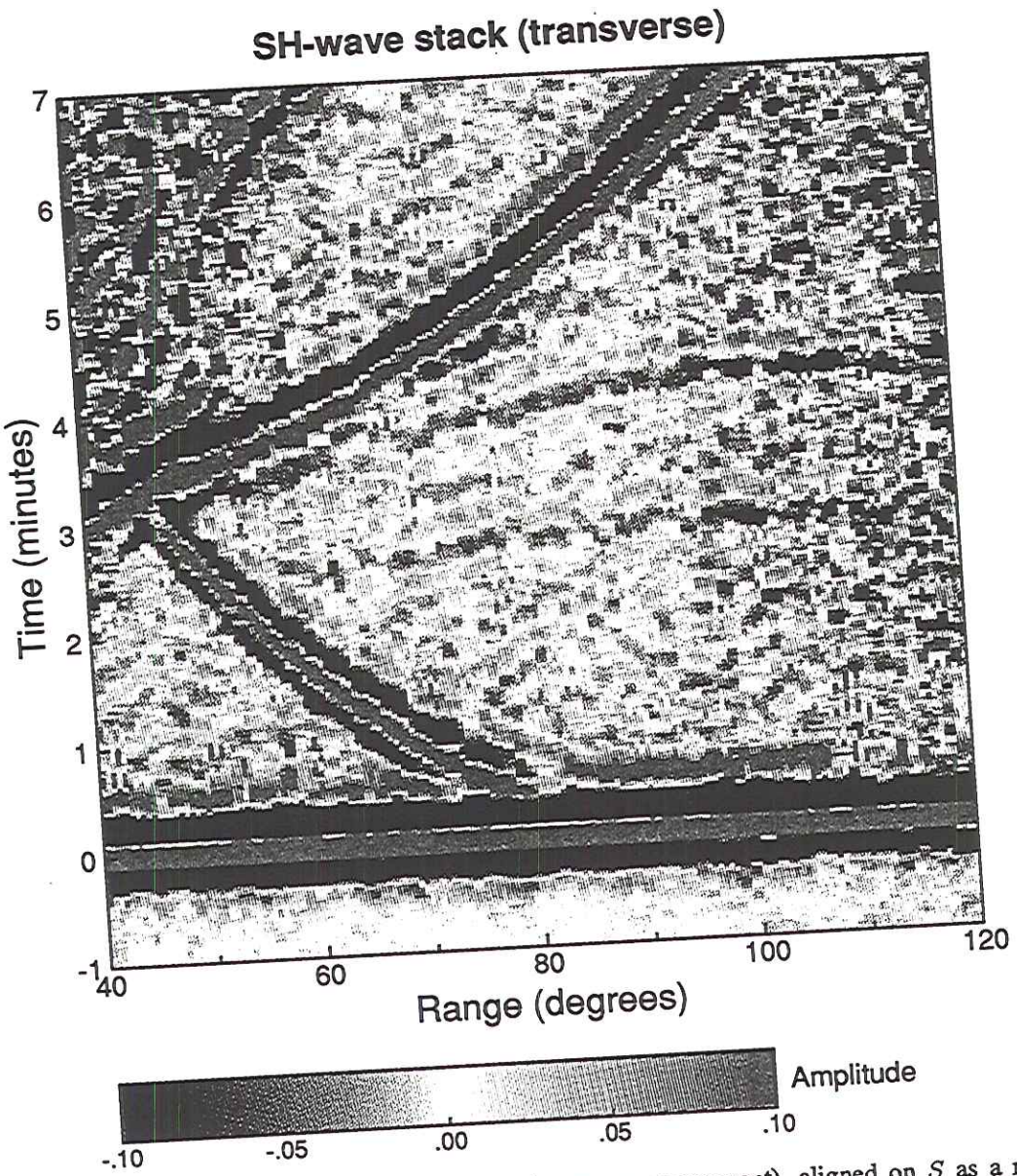

Plate 3. Stacked color image of long-period GDSN data (transverse component), aligned on S as a reference phase. Positive amplitudes are shown in red, negative amplitudes in blue, with the scale ranging up to 0.1 of the maximum S wave amplitude.

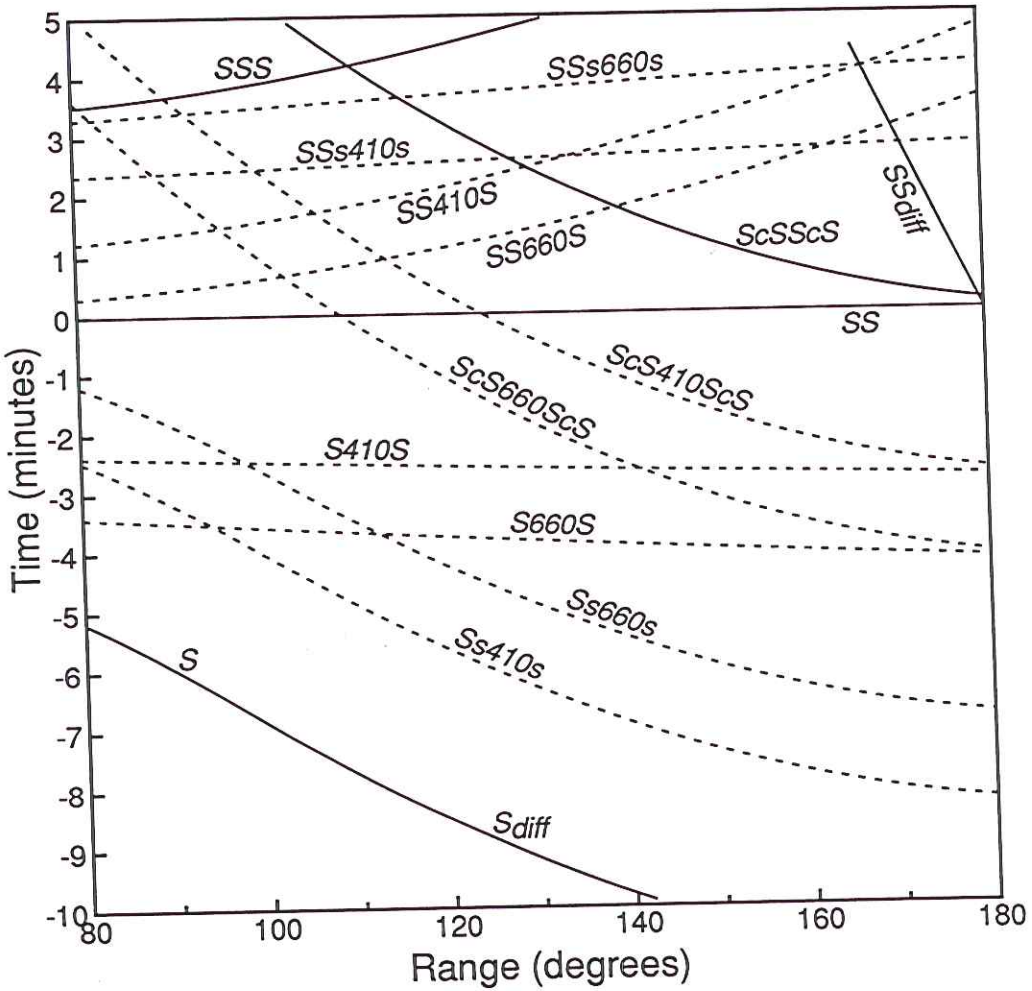

Fig. 8. Travel time curves relative to SS for primary seismic phases (solid) and upper mantle discontinuity phases (dashed) for comparison with the stacked image shown in Plate 4. Curves were calculated using PREM, with interfaces assumed at 410-km and 660-km depth.

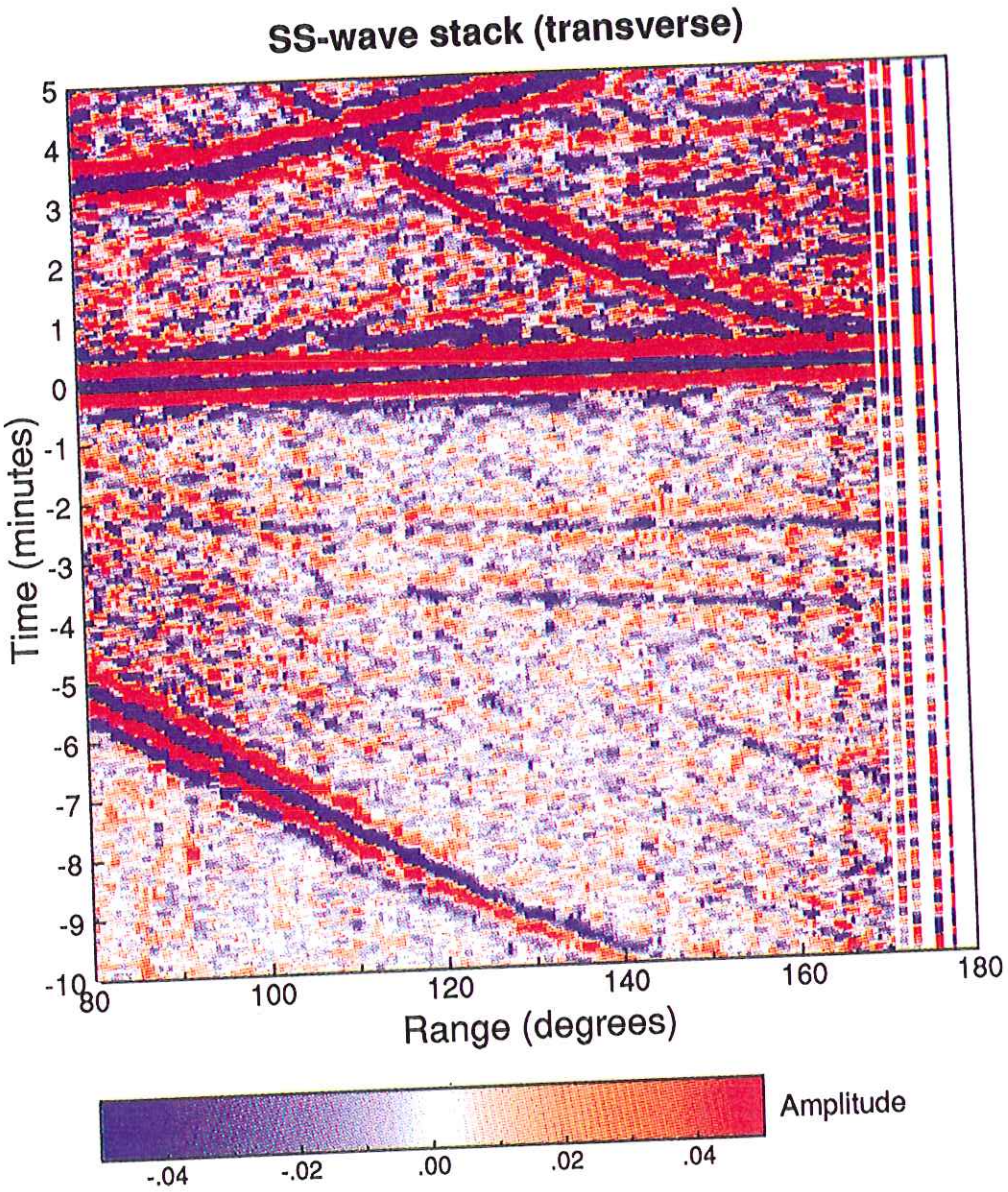
SS-wave stack (transverse)
Time (minutes)
5
4
3
2
1
0
-1
-2
-3
-4
-5
-6
-7
-8
-9
-10
80
100
120
140
160
180
Range (degrees)
Amplitude
-.04
-.02
.00
.02
.04

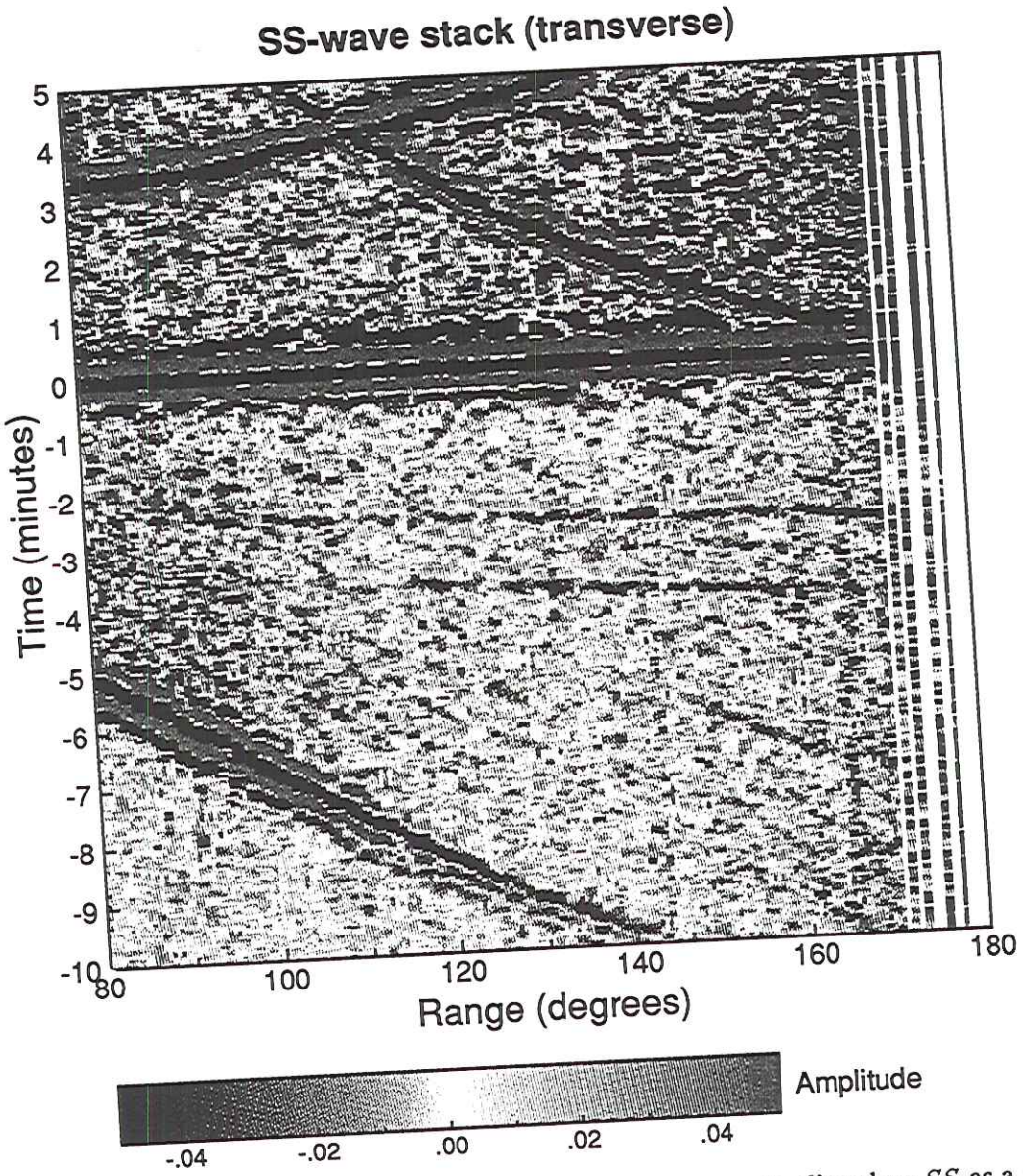

Plate 4. Stacked color image of long-period GDSN data (transverse component), aligned on SS as a reference phase. Positive amplitudes are shown in red, negative amplitudes in blue, with the scale ranging up to 0.05 of the maximum SS wave amplitude.

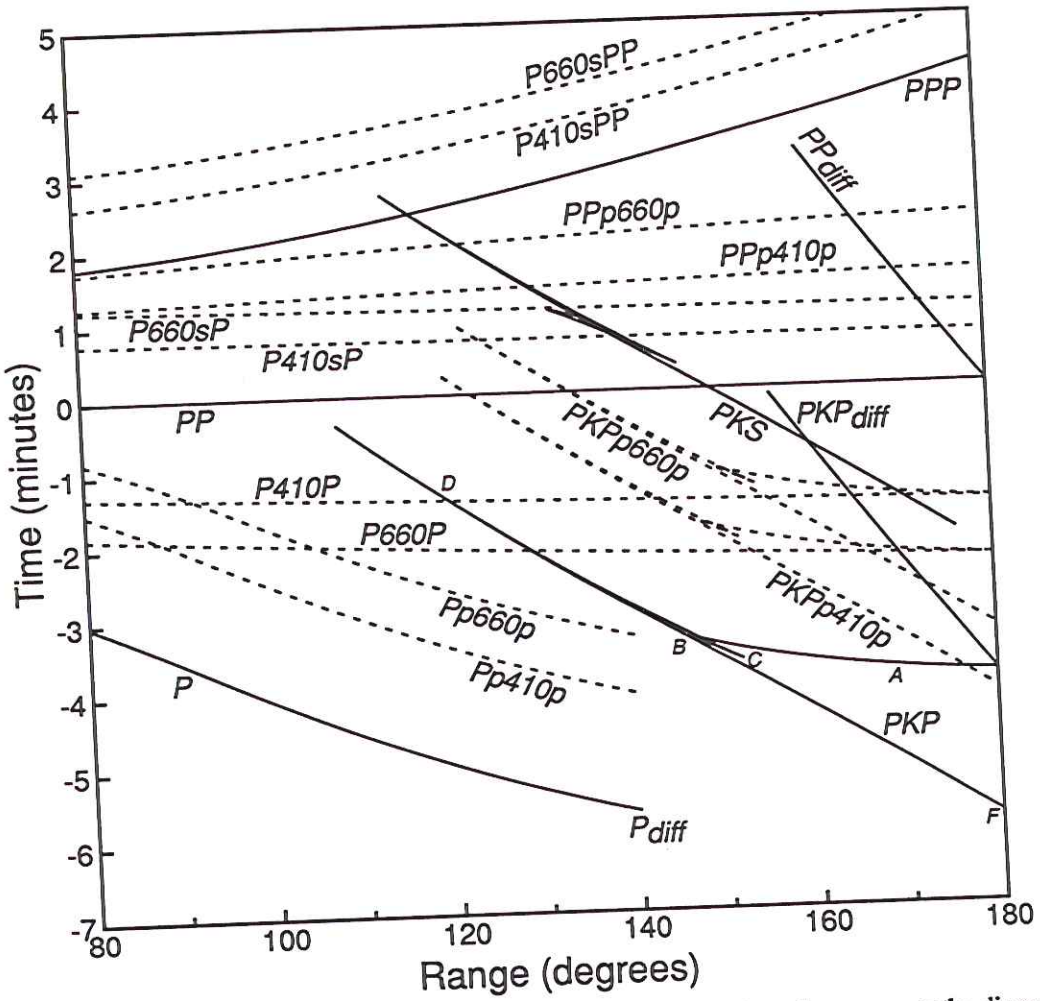

Fig. 9. Travel time curves relative to PP for primary seismic phases (solid) and upper mantle discontinuity phases (dashed) for comparison with the stacked image shown in Plate 5. Curves were calculated using PREM, with interfaces assumed at 410-km and 660-km depth. The various branches of PKP are indicated by letters.

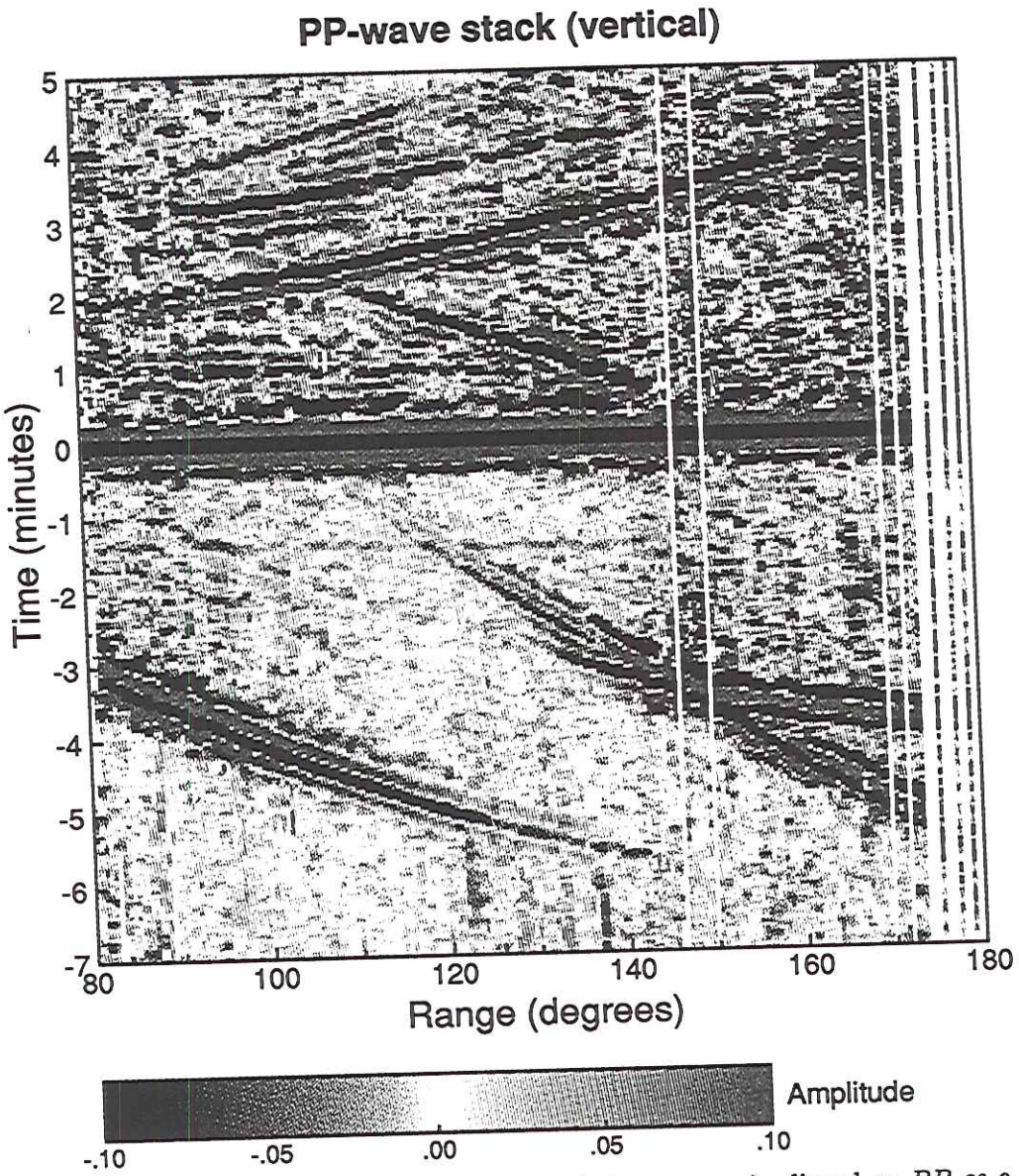

Plate 5. Stacked color image of long-period GDSN data (vertical component), aligned on PP as a reference phase. Positive amplitudes are shown in red, negative amplitudes in blue, with the scale ranging up to 0.1 of the maximum PP wave amplitude.

Both NASA and the European Space Agency (ESA) have plans to land seismometers on Mars in the next few decades.

Soft landings are expensive — likely to be hard. Martian seismometers must be ultra low-power (far from Sun) and very robust (able to withstand drop from World Trade Center) yet be sensitive enough to detect micron displacements — a severe engineering challenge.

Joint French–Russian mission will be launched [redacted] this year (hopefully). ← splash!

Typical hard-landing scenario: cushion with bounce

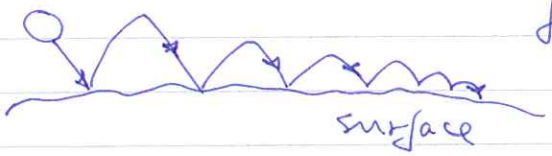

The attention of most [redacted] terrestrial global seismologists is now directed towards the measurement of three-dimensional velocity variations.

Lateral variations in P velocity are ±1% in lower mantle, up to ±4% in upper mantle, also higher just above the CMB.

Observed shear-velocity variations are about twice as large as P velocity variations.

Tomography — Greek tomos = section

Principle:

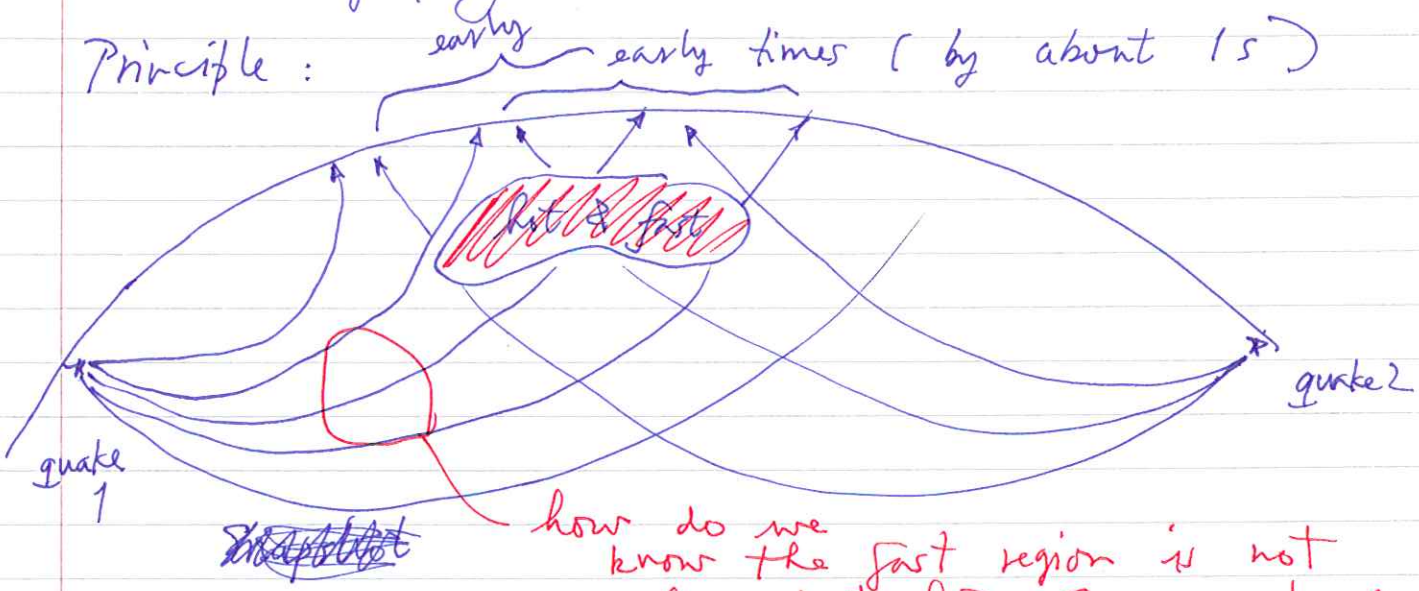

how do we know the fast region is not here instead? Easy — quake 2

By combining observations from many different 'quakes and receiving stations, can image 3-d variations

Example: Su & Dziewonski — 1 million ISC P-wave picks or dont

Ring of cold (subducted?) material around Pacific — hot upwelling in center — snapshot of current state of mantle convection

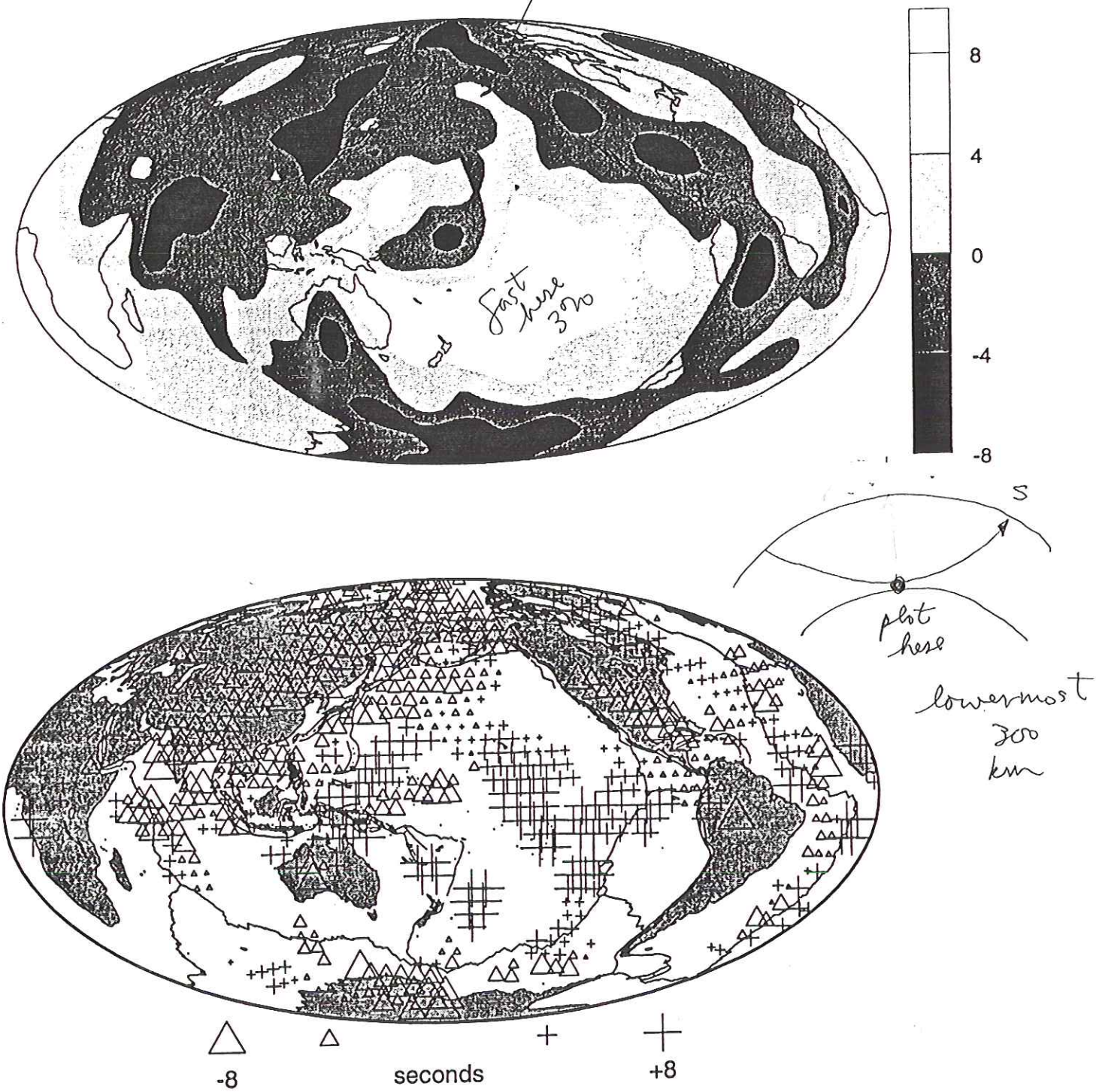

Figure 3. Lower panel: long-period S residuals plotted at the turning point of S for rays which bo[illegible] in the lowermost 300 km of the mantle. The raw data have been lightly smoothed by apply[illegible]ng a running-mean smoothing filter which is a spherical cap of radius 5°. Note the ring of negative residuals (fast velocity) around the Pacific. The upper panel shows a map of the data constructed using spherical splines. The contour levels are in seconds.

Over 2,600 measurements of S-SKS traveltime residuals averaged in 5 degrees spherical caps and their degree-36 expansion in spherical harmonics. Note the distinct pattern of negative anomalies in the Central Pacific and under Africa.

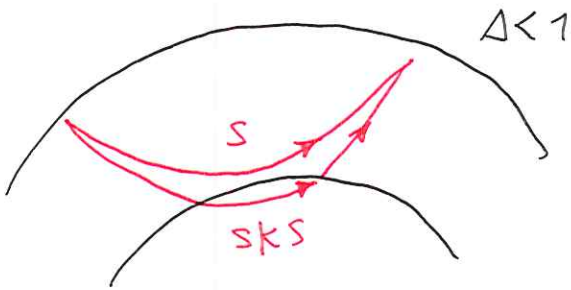

The whole mantle degree - 12 earth model SKS12_WM13 at the depth of 2800 km. The symbols predict S-SKS traveltimes for the measurements in the top map.

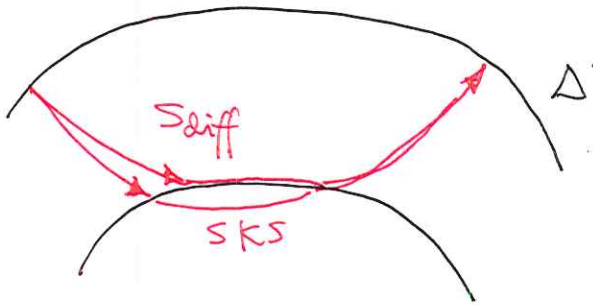

α very uniform in core — signal due to lower mantle — confirms low velocity (blue) donut around rim of Pacific.

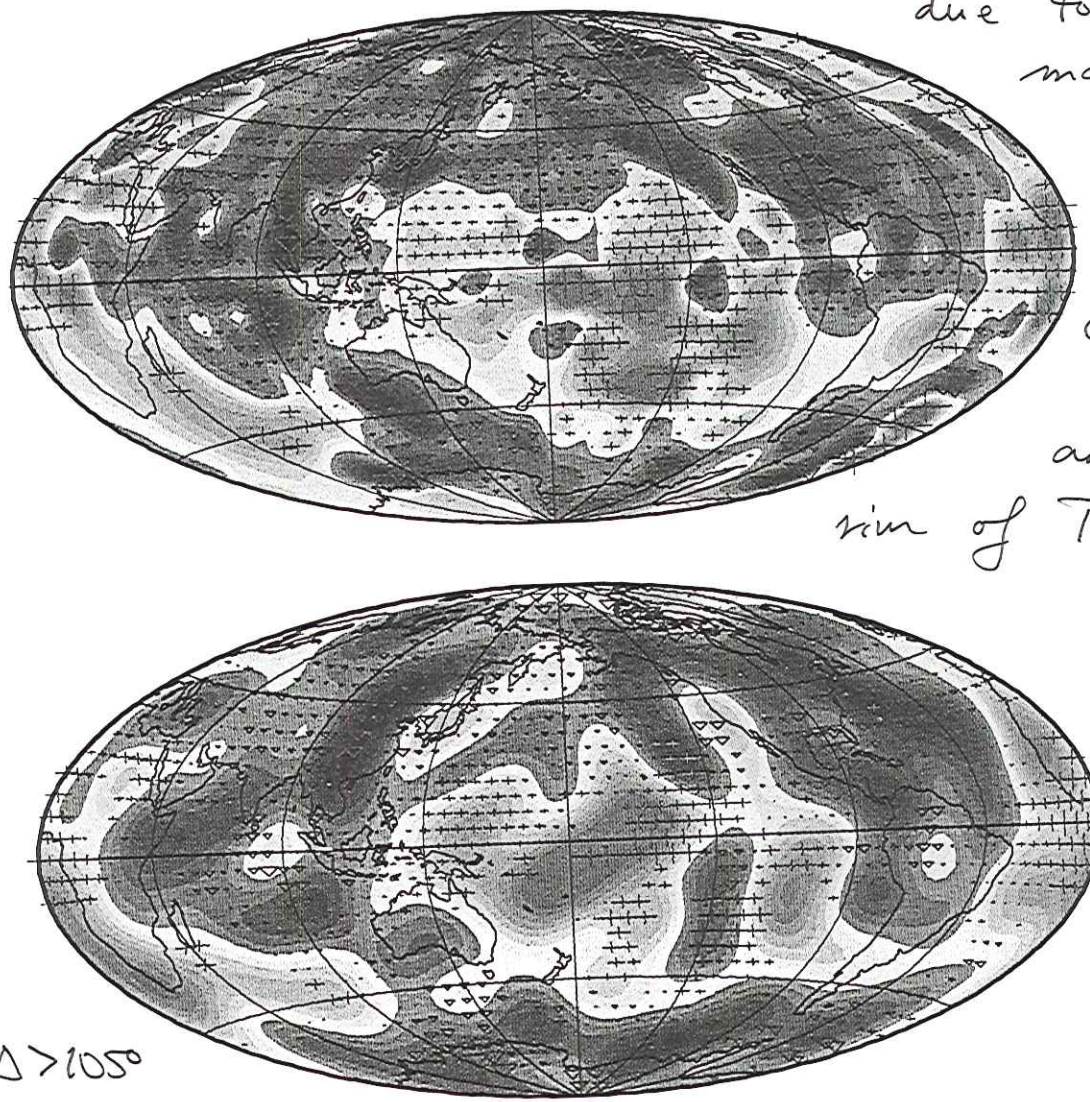

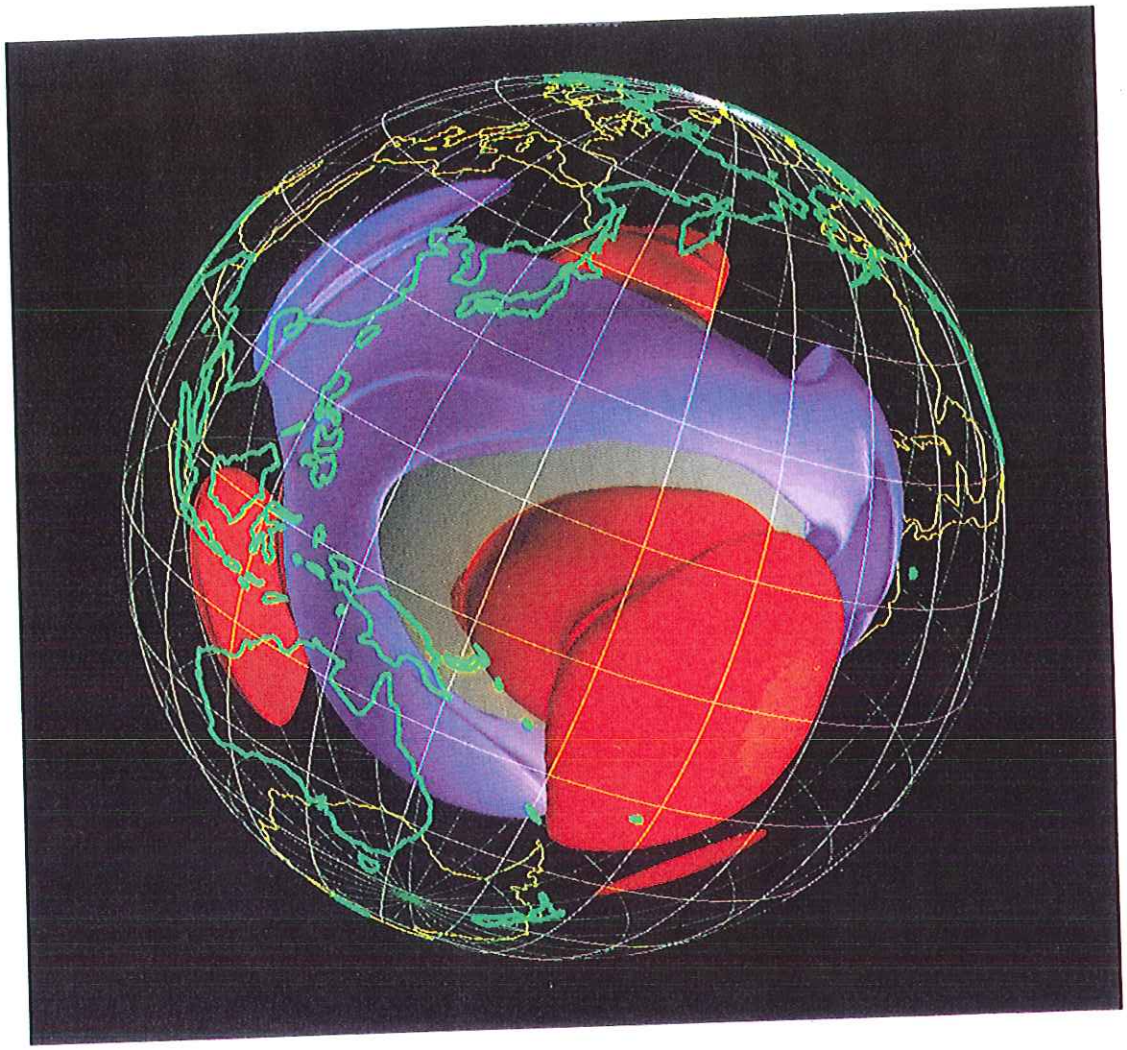

shouldn't think of this as an accurate representation of the ⊕ very low-resolution picture in book views this more from the right

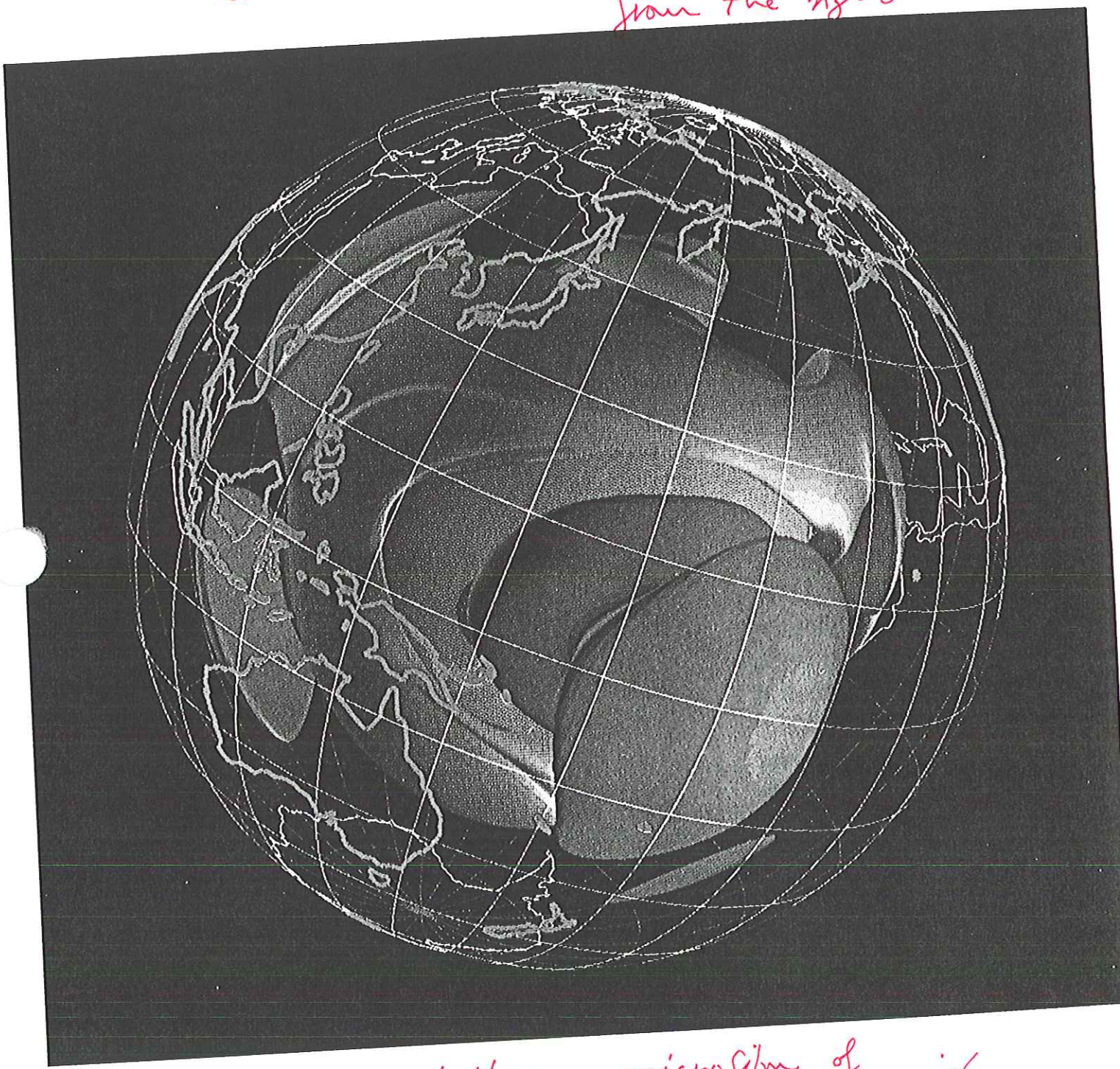

give a metaphor — microfilm of Nassau Hall — maybe a building — yes, it's Nassau Hall — can now see figures — can now read ~~text~~ charter plaque — as tools improve

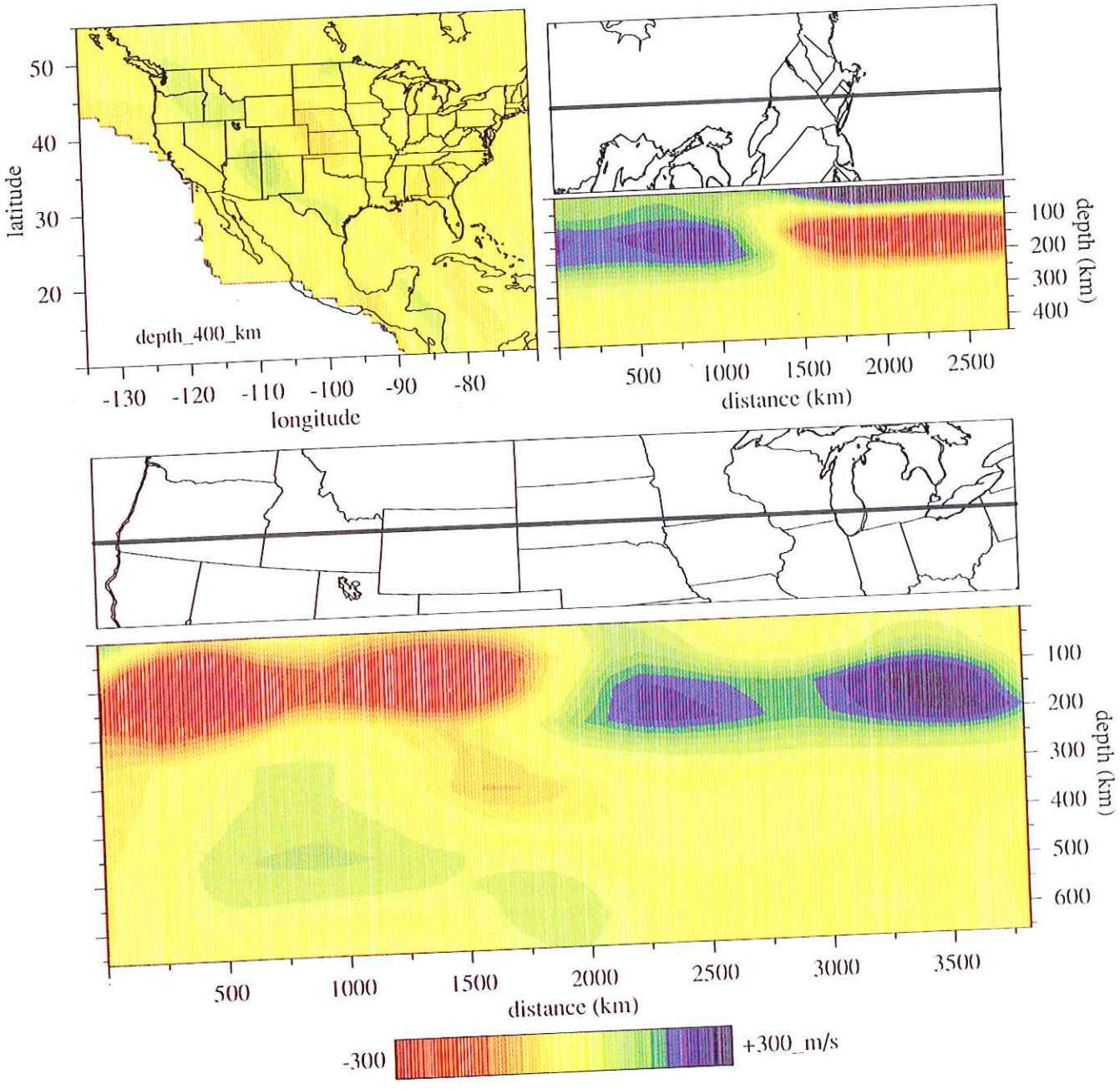
50
40
30
20
latitude
depth_400_km
-130
-120
-110
-100
-90
-80
longitude
500
1000
1500
2000
2500
distance (km)
100
200
300
400
depth (km)
100
200
300
400
500
600
depth (km)
500
1000
1500
2000
2500
3000
3500
distance (km)
-300
+300_m/s

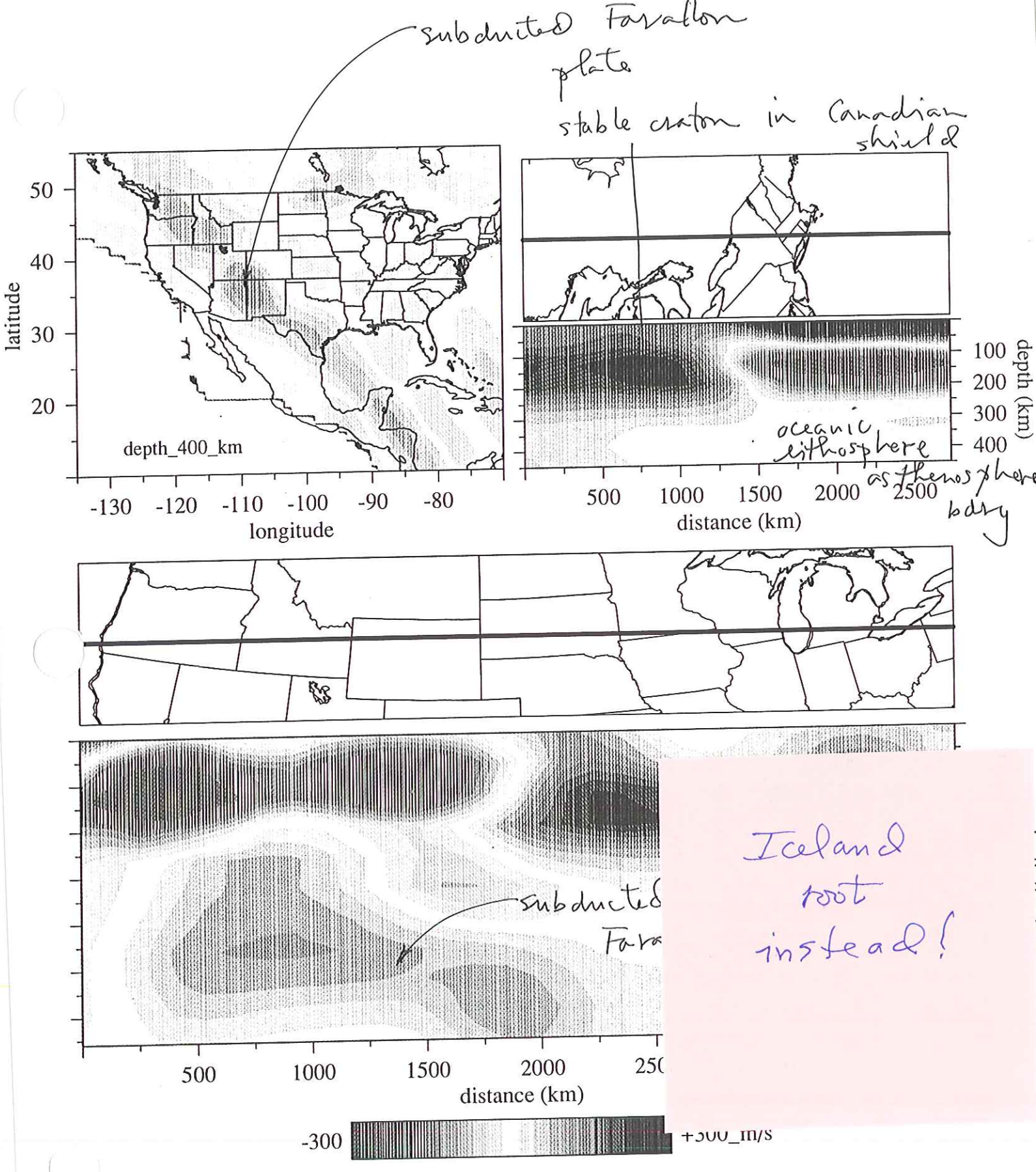

Iceland root instead!

Don't mention Farallon plate in this lecture

Example 2 : inner core anisotropy

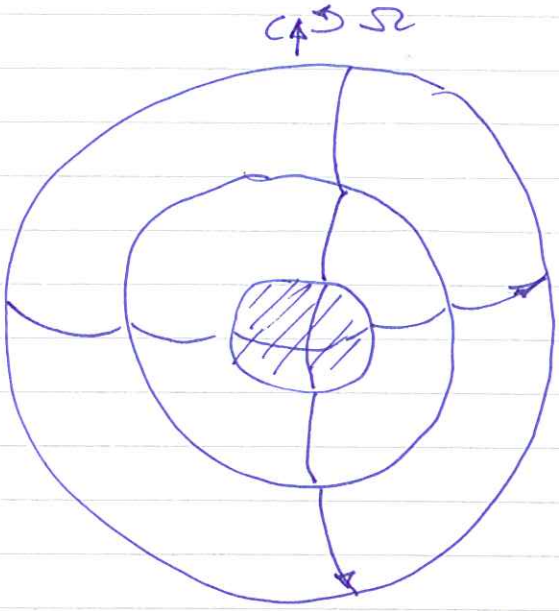

polar paths ≈ 4 seconds faster than equatorial paths

$\Delta \approx 180°$ PKIKP PKP (DF)

The iron xtals in the inner core are preferentially aligned

axis of symmetry tilted by ~ 10° w.r.t. rotation axis

Song & Richards measure Scotia Arc to College, Alaska BC – DF differential times — find convincing evidence for a 1° per year rotation of inner core with respect to mantle. Two possibilities:

(1) hasn't caught up to tidally slowed mantle

(2) more likely — EM torques due to secular variation of $\vec{B}$ field.

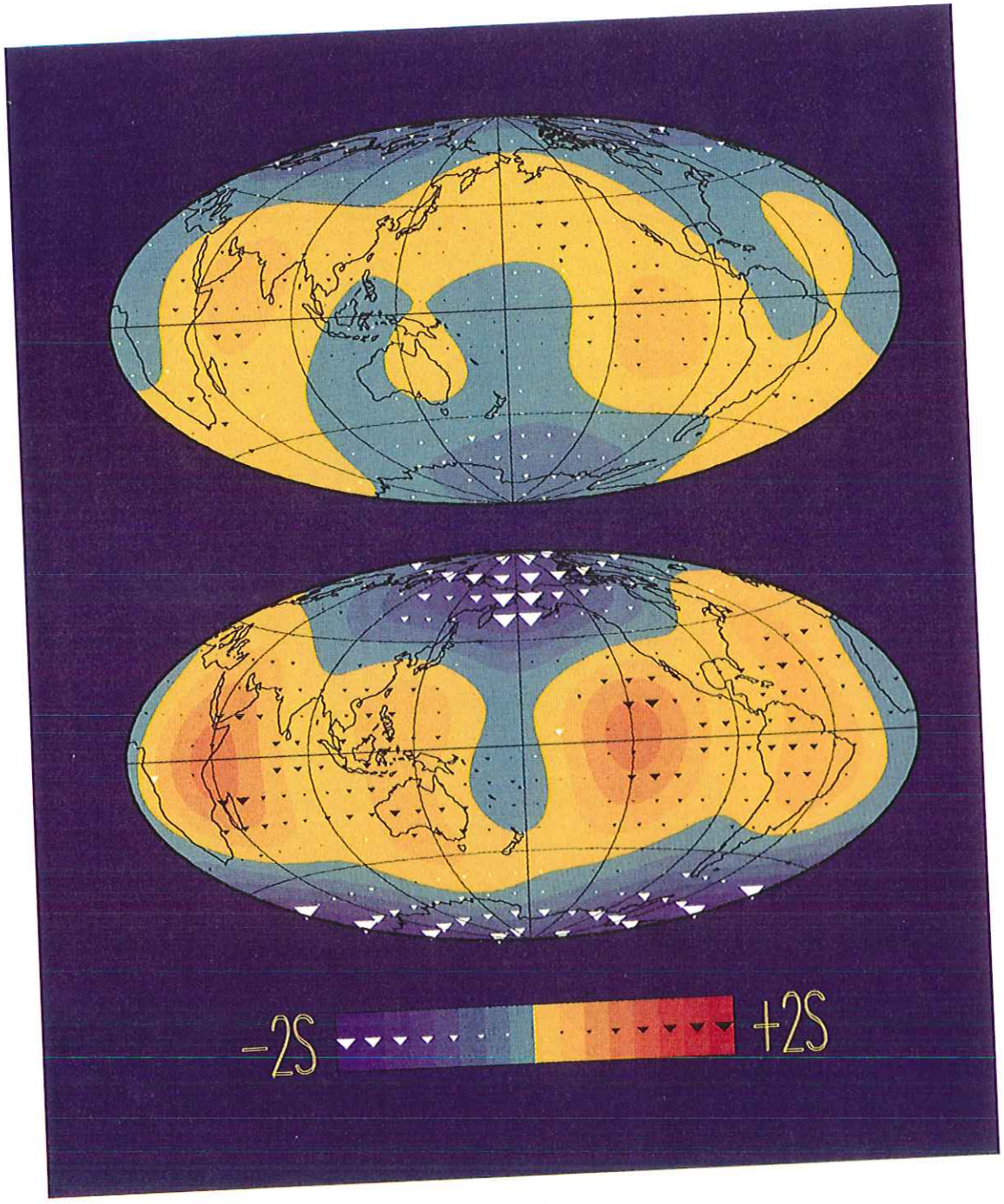
-2S
+2S

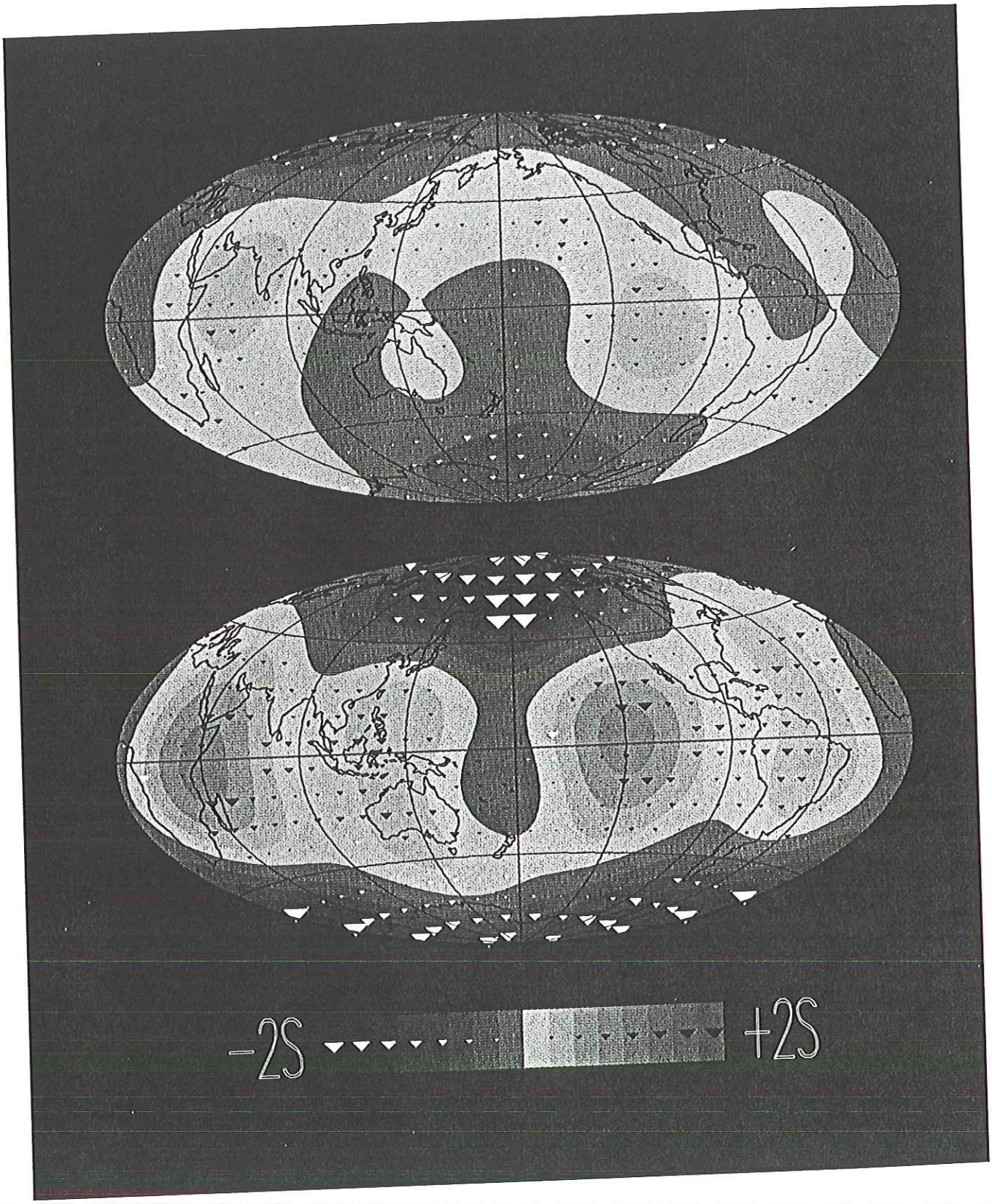
-2S
+2S

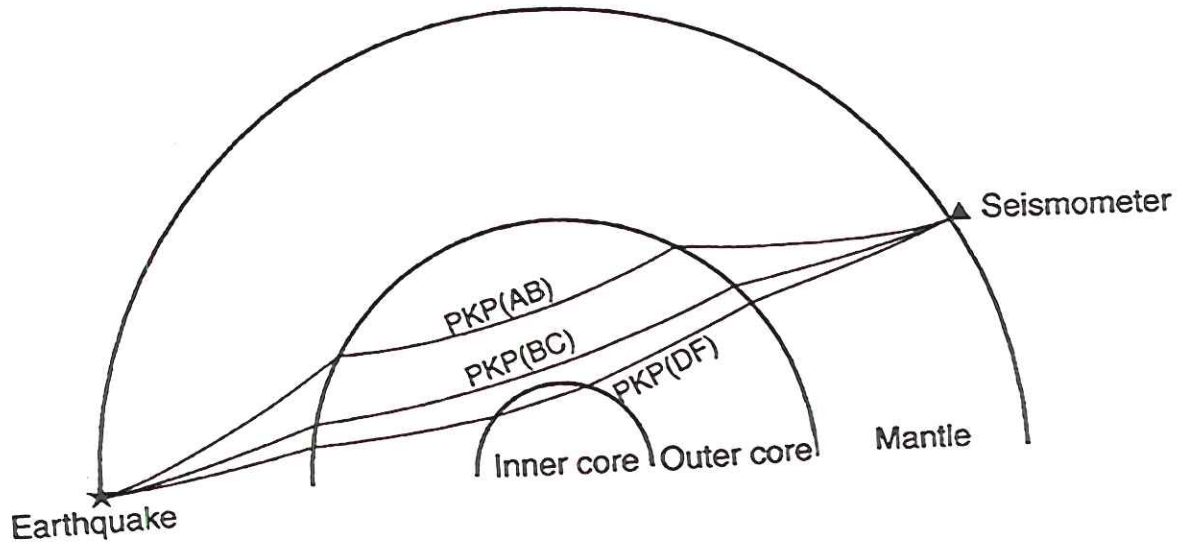

FIG. 1 Ray paths for seismic waves that pass through the Earth's cores.

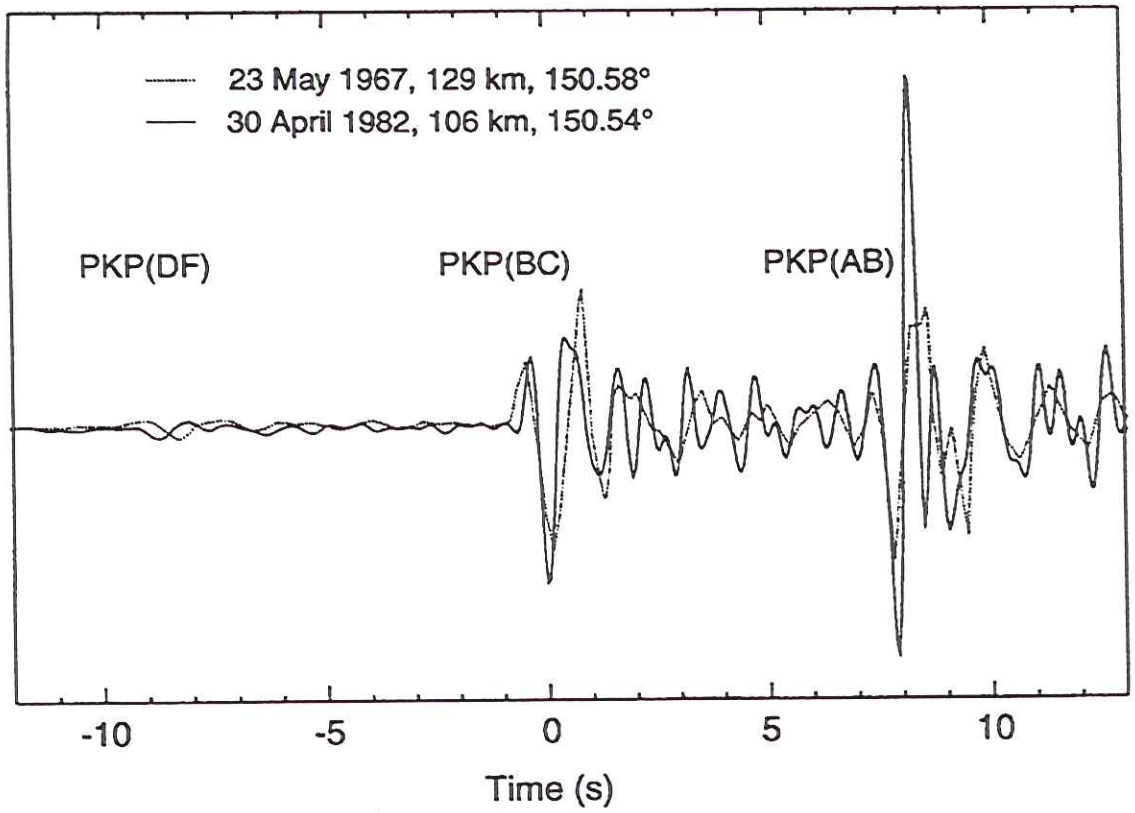

FIG. 2 An overlay of two short-period PKP seismograms from earthquakes that occurred 15 years apart at almost the same location in South Sandwich Islands, as recorded at College, Alaska (COL). Event locations in this study are taken from the Earthquake Data Reports of the US Geological Survey.

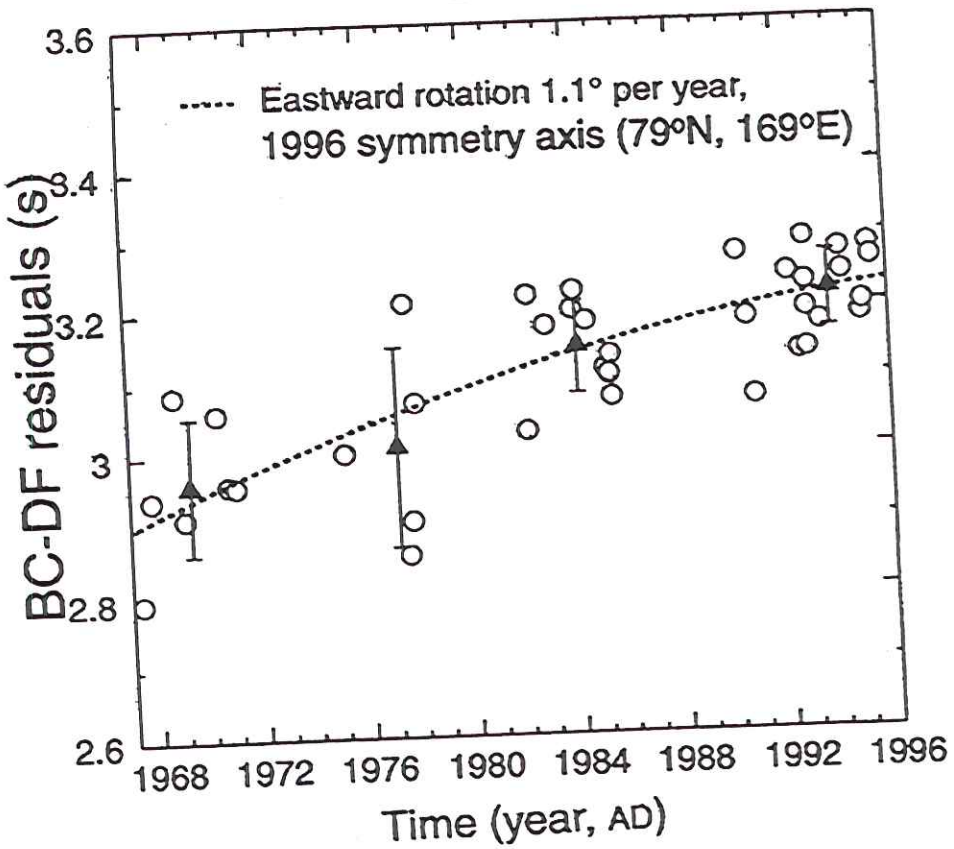

FIG. 5 Residuals for BC – DF times for South Sandwich Islands to COL paths as a function of earthquake time of occurrence. The observed residuals are indicated by open circles. The mean (filled triangles) and ± one standard deviation (error bar) are shown for the residuals over about four-year periods. The predicted times (dashed curve) are based on our best estimate of inner-core rotation about a north–south axis.

nature
INTERNATIONAL WEEKLY JOURNAL OF SCIENCE
Volume 382 No. 6588 18 July 1996 $10.00

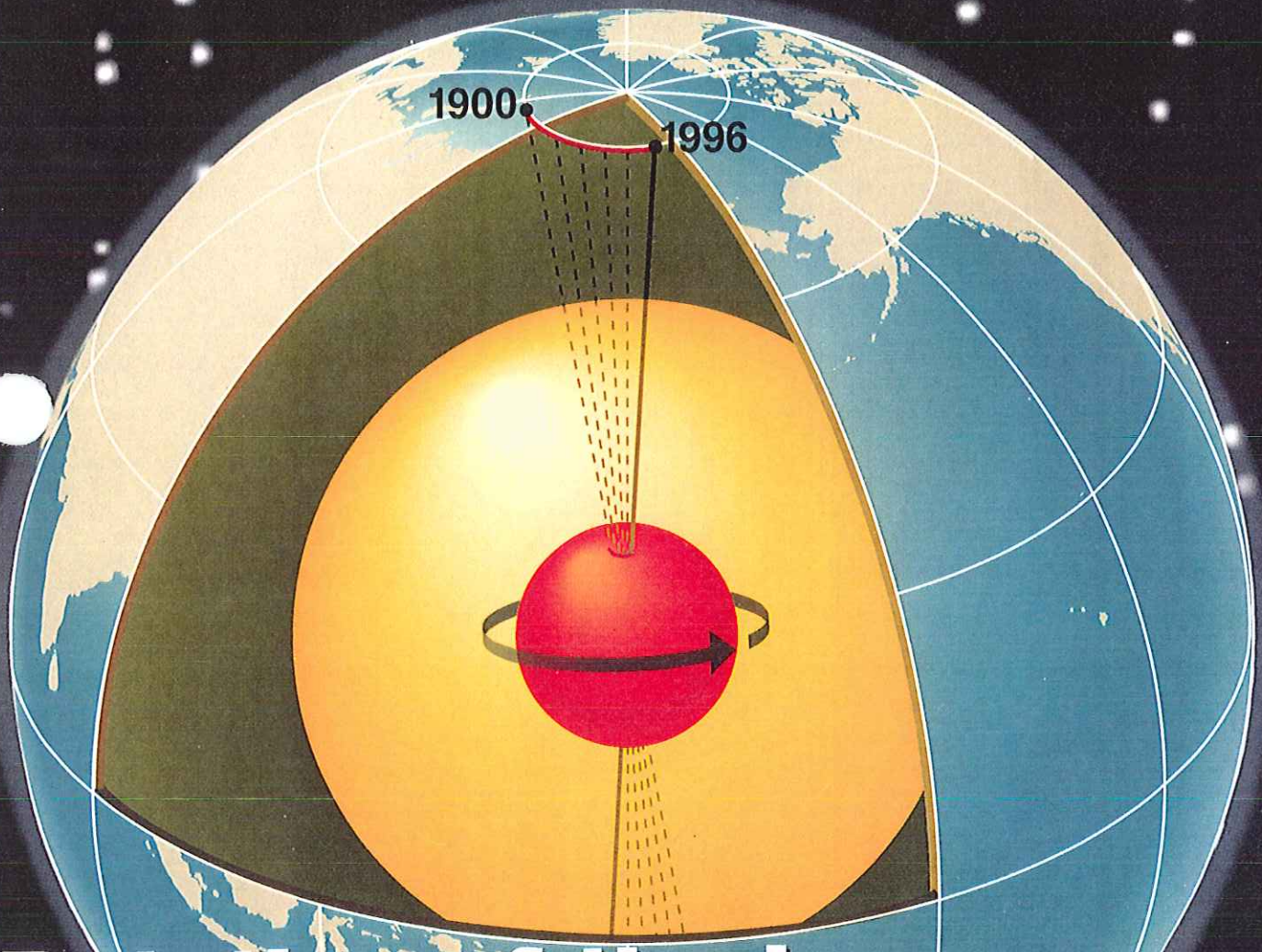

Rotation of the inner core

Nicotine addiction: The smoking gun

Magnetic superconductors

The Wingless receptor

nature

INTERNATIONAL WEEKLY JOURNAL OF SCIENCE

Volume 382 No. 6588 18 July 1996 $10.00

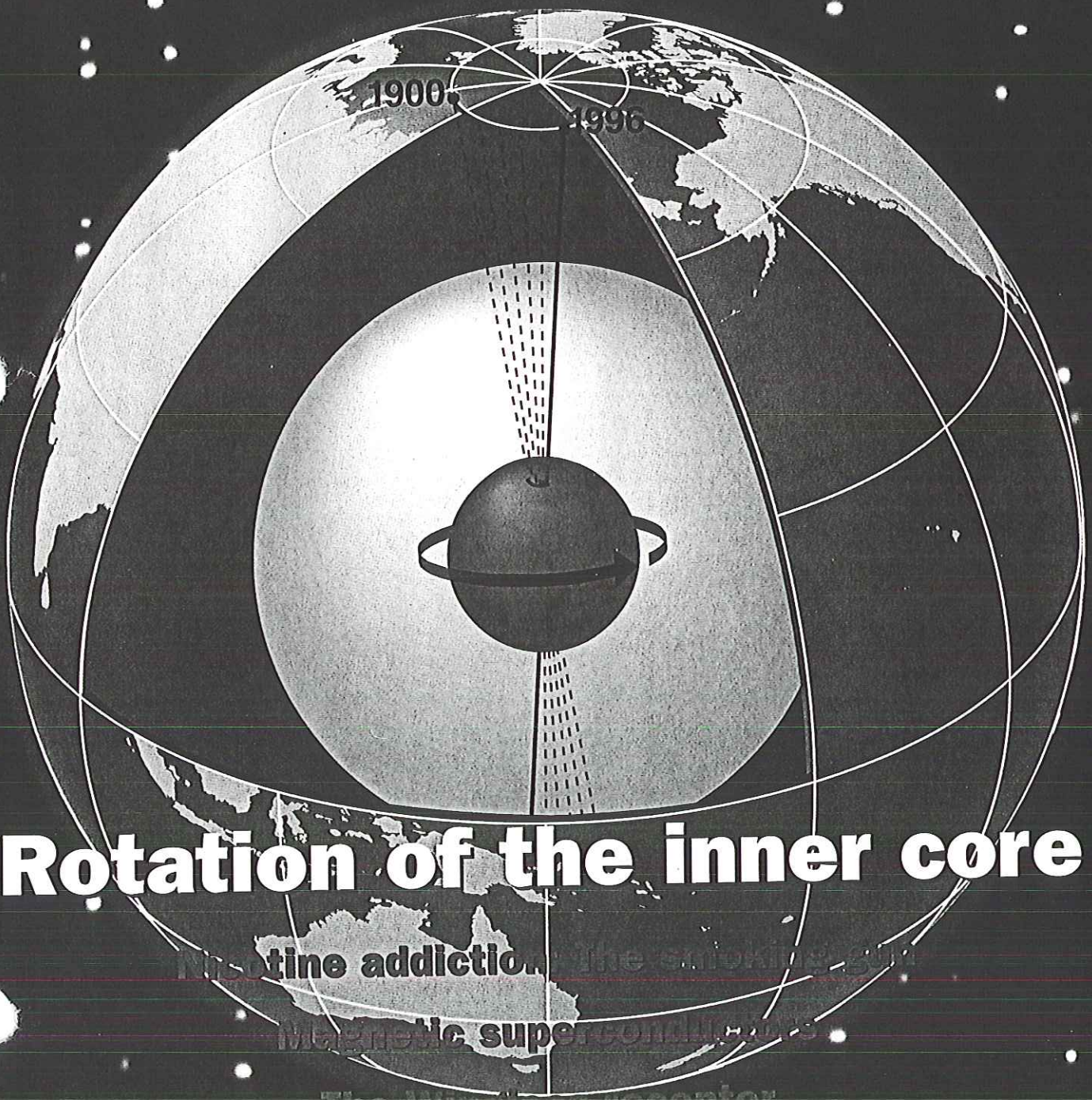

Rotation of the inner core

Nicotine addiction

Magnetic superconductors

The Wingless receptor

always
skipped this
— lack of time

GEO 225 Week 5 Lecture #1

Earthquakes & Earth Structure — continued

So far we have talked only about of the three parameters that can be inferred by seismology.

What about the density $\rho(r)$.

This is determined by observing the free oscillations of the Earth excited by large earthquakes.

The Earth in effect rings like a large bell.

Each note or frequency has a characteristic shape or geometry of the associated vibration.

Analogous to the fundamental and higher overtones of a violin or piano string:

The vibrations of the Earth — a 3D object — are more complicated.

The simplest mode is the fundamental radial mode ${}_0S_0$

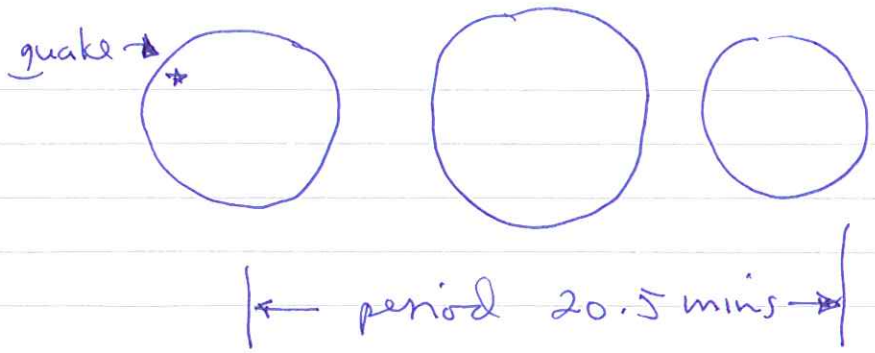

whole ⊕ breathes in and out

This mode has radial overtones, e.g.

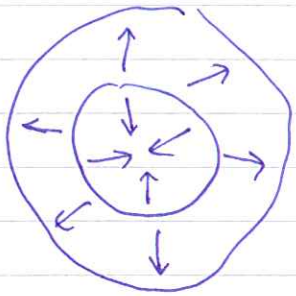

interior points moving inward while surface moving outward and vice versa

period 10.2 mins

Other modes change the shape of the Earth. The gravest such oscillation is the so-called football mode

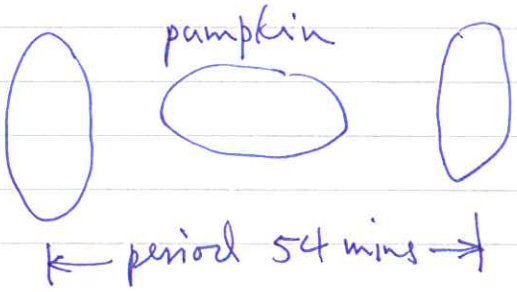

These are also modes involving no radial displacement — pure shear

e.g. $_0T_2$

period 44 minutes

An earthquake excites all of these oscillations — some more strongly than others.

It is as if one were to sit on the keyboard of a piano and listen to the result — one would hear all the notes at once.

There is a standard procedure for unravelling the constituent frequencies — known as Fourier analysis

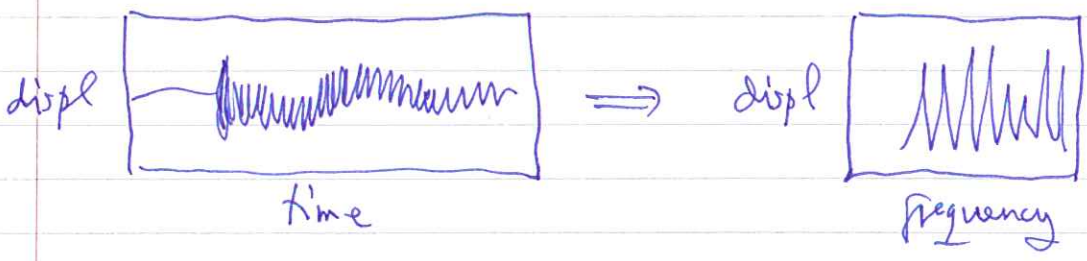

Each peak in the spectrum corresponds to an oscillation.

Approximately 600 frequencies have been measured and identified.

The frequency of $_0S_0$, for example, is

extremely precise: ${}_0S_0$:

$T = 1227.500 \pm$ [redacted] 0.006 seconds

There is very little damping associated with this almost purely compressional oscillation. Visible for weeks after a large 'quake.

The frequencies of the Earth's modes depend upon the density $\rho(r)$.

Of course, they depend on $\alpha(r)$ and $\beta(r)$ too.

Earth-model refinements are obtained by fitting the measured frequencies and body-wave travel times, simultaneously.

Box 6.1 Vibrations of Strings and Spheres

The figure below shows the modes of vibration of a string. The string moves from the position shown in black to the position shown in gray, and back again. The nodes are the points that do not move.

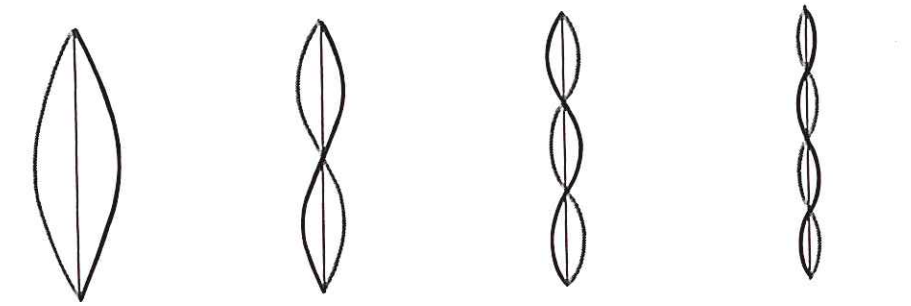

Fundamental First overtone Second overtone Third overtone

This figure shows the surface view of spheroidal vibrations of a sphere. Points at which the black and gray lines intersect are nodal lines in the surface of the sphere.

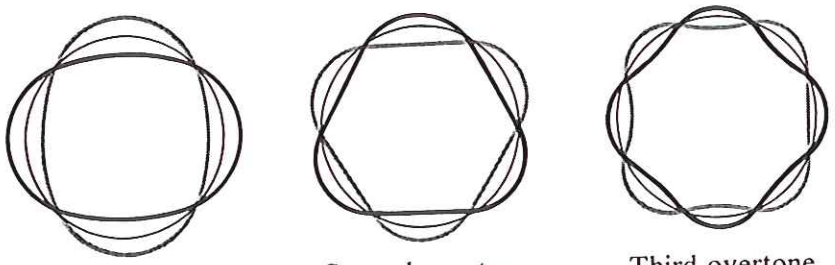

Fundamental mode Second overtone Third overtone

This figure depicts the interior view of the radial modes of vibration of a sphere. The wavy line indicates the variation in displacement with depth in a homogeneous sphere. In the Earth, the displacements are complicated by the liquid core.

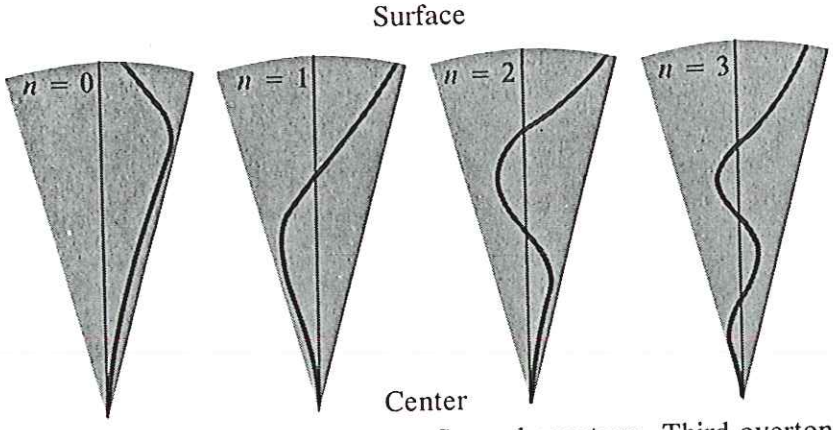

Fundamental First overtone Second overtone Third overtone

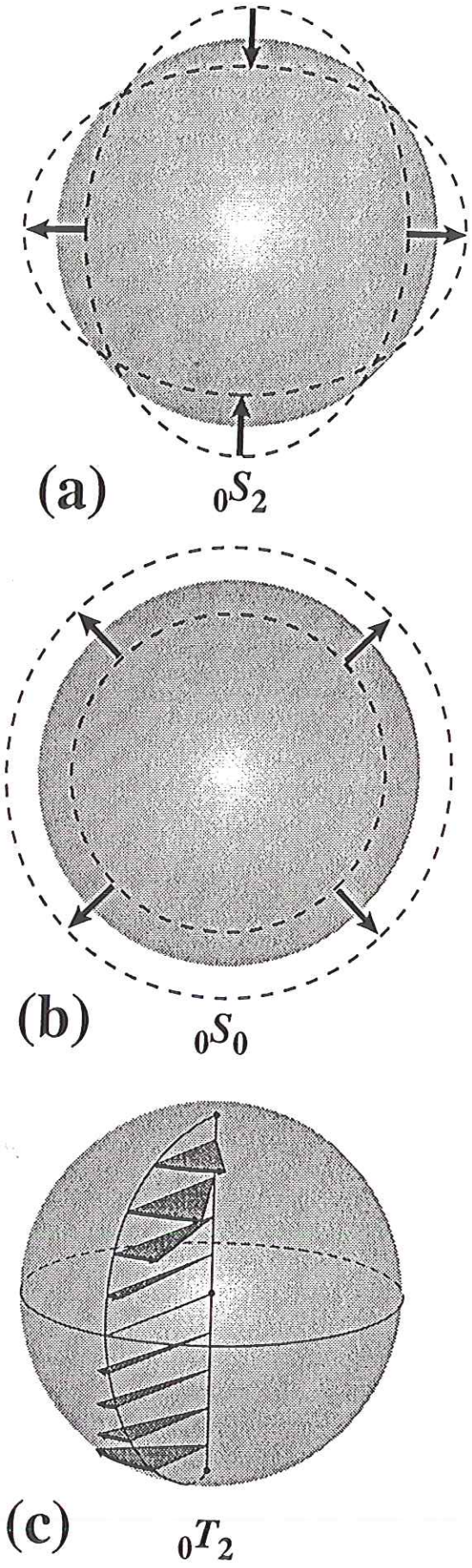

fundamentals

Fig. 1. Illustrations of the displacement fields of various modes of oscillation. a) $_0S_2$, the "football" mode of the Earth, b) $_0S_0$, the "breathing" mode of the Earth, and c) the toroidal mode $_0T_2$.

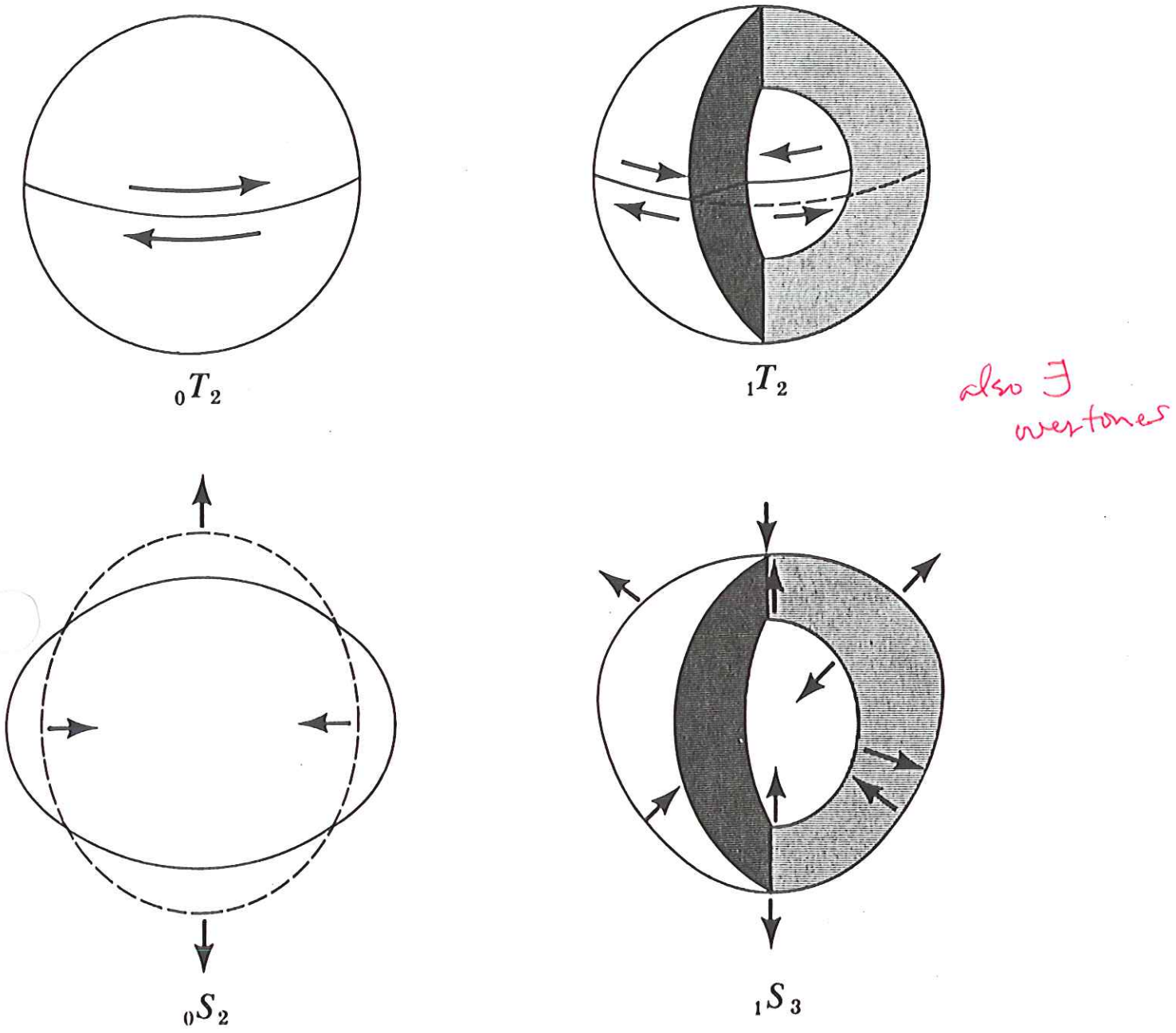

also ∃ overtones

Figure 6.3 Representation of the modes ${}_0T_2$, ${}_1T_2$, ${}_0S_2$, and ${}_1S_3$.

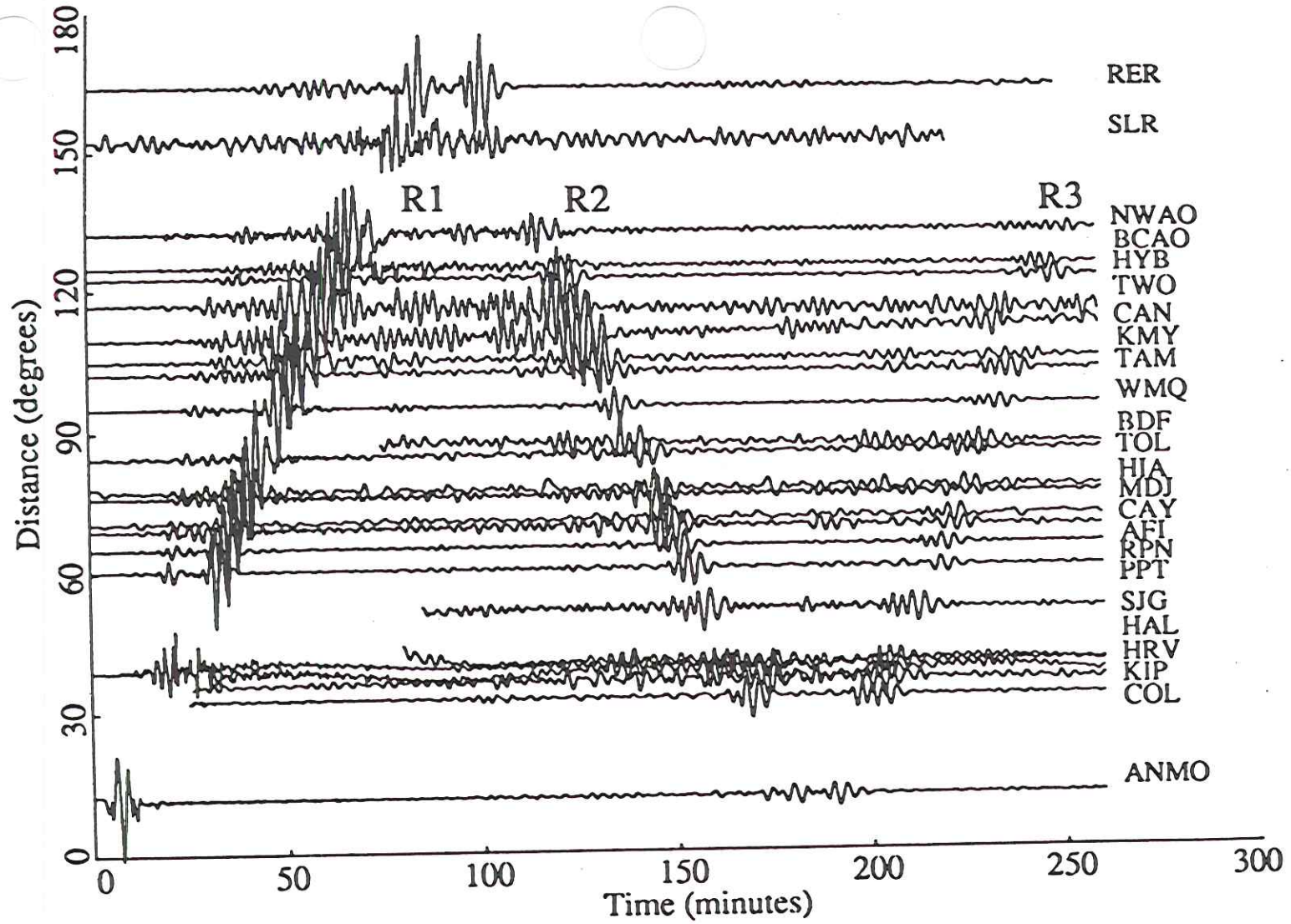

FIGURE 1.7 Long-period Rayleigh waves produced by the 1989 Loma Prieta earthquake as recorded at globally distributed digital seismometers of three global networks (GEOSCOPE, International Deployment of Accelerometers, Global Seismic Network). The vertical-component traces are filtered to include only periods longer than 125 s. The vertical axis is the angular distance along the surface from the California source, and time is from the earthquake origin time. R_1 and R_2 are Rayleigh waves traveling along the minor and major arcs of the great circle from source to station, respectively; R_3 is the next passage of the R_1 wave after circling the entire globe. (From Velasco *et al.*, 1993.)

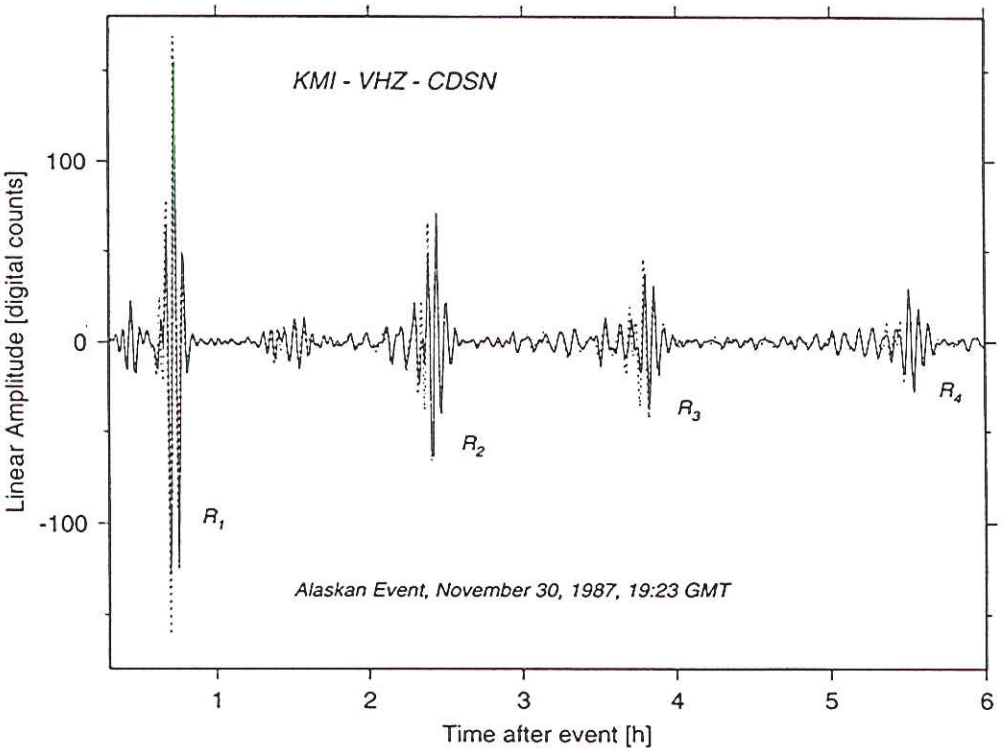

Fig. 2. Comparison of a synthetic seismogram with data for a vertical-component, long-period recording (VHZ) from a station of the Chinese Digital Seismic Network at Kunming (KMI). The dotted line is the synthetic made by mode summation and includes all modes with frequencies less then 8 mHz. The large wave packets labelled R_1–R_4 are Rayleigh wave surface waves. R_1 has travelled the minor arc from the source to receiver while R_2 has travelled in the opposite direction. The travel time to complete a full orbit is about 3 hours (R_3 is the same as R_1 but after one complete orbit).

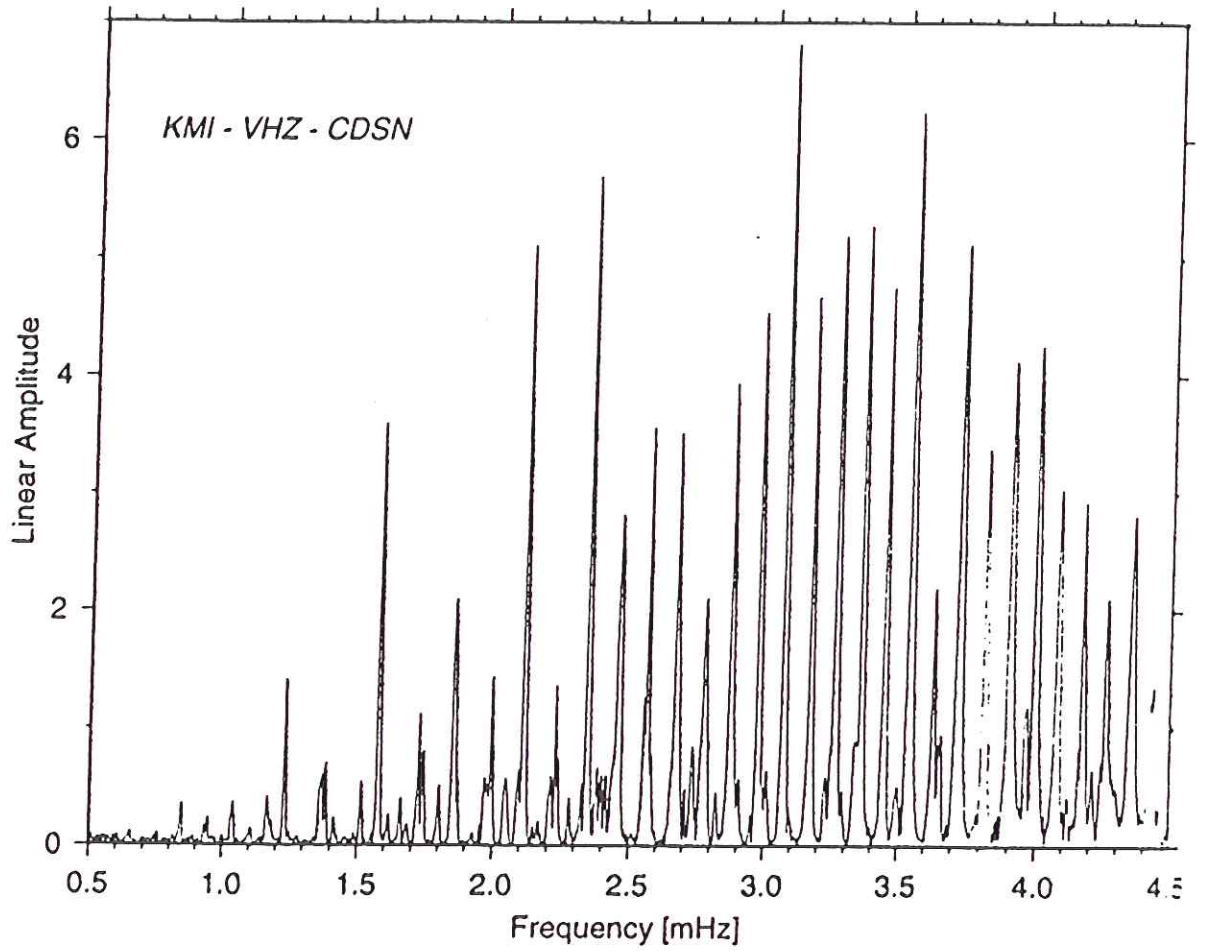

Fig. 3. Fourier amplitude spectrum of 60 hours of the recording shown in Figure 2. The record was Hanning-tapered to reduce spectral leakage effects. The spectrum (which is proportional to ground acceleration) is dominated by large peaks which are roughly uniformly spaced with a separation of about 0.1 mHz. These peaks correspond to fundamental spheroidal modes which compose the large amplitude Rayleigh wave packets seen in Figure 2.

a

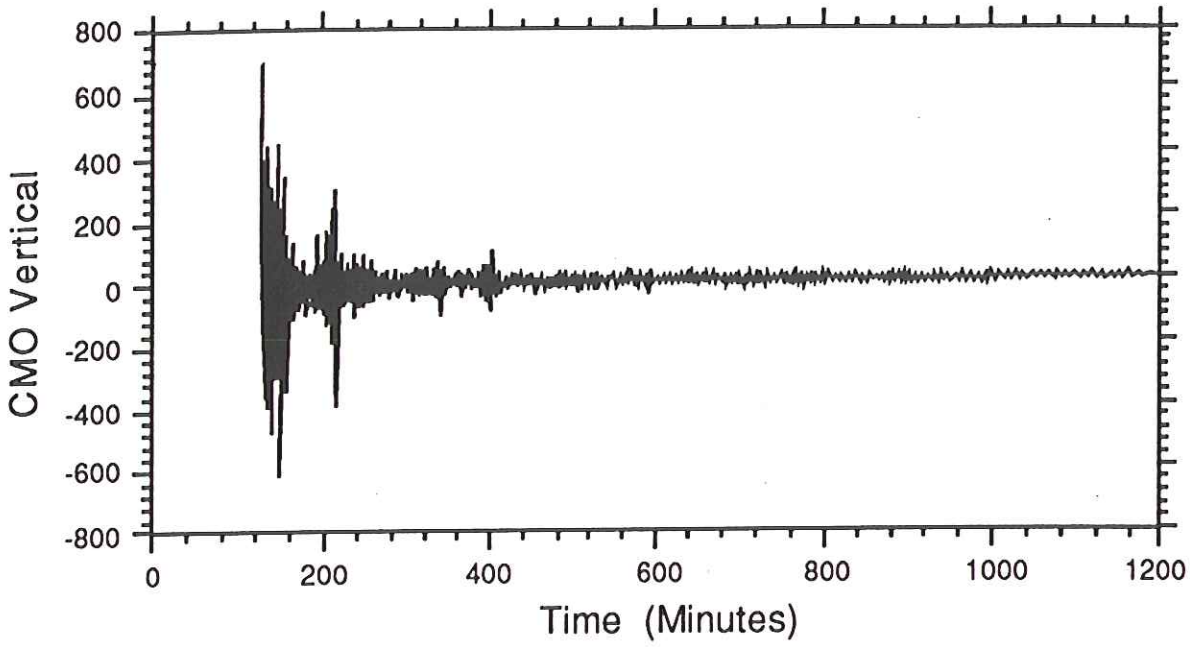
CMO Vertical
800
600
400
200
0
-200
-400
-600
-800
0
200
400
600
800
1000
1200
Time (Minutes)

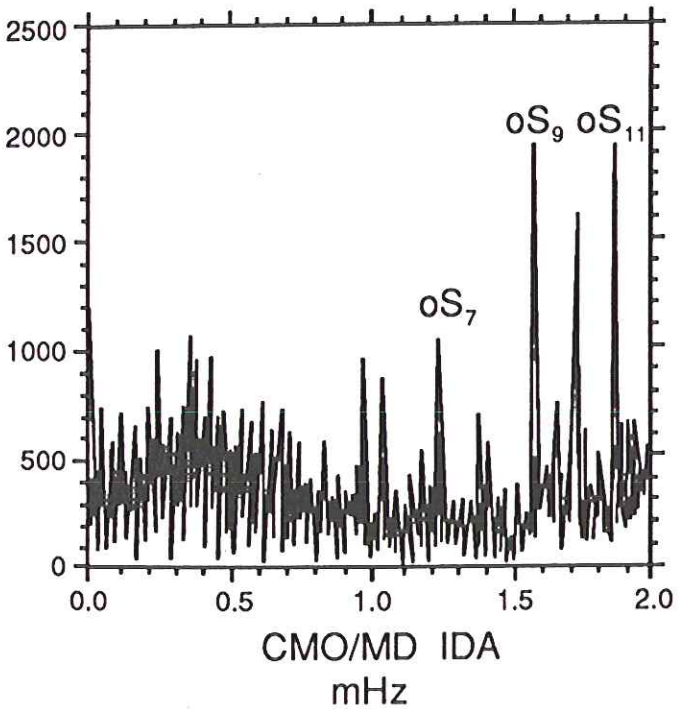
2500
2000
1500
1000
500
0
oS7
oS9
oS11
0.0
0.5
1.0
1.5
2.0
CMO/MD IDA
mHz

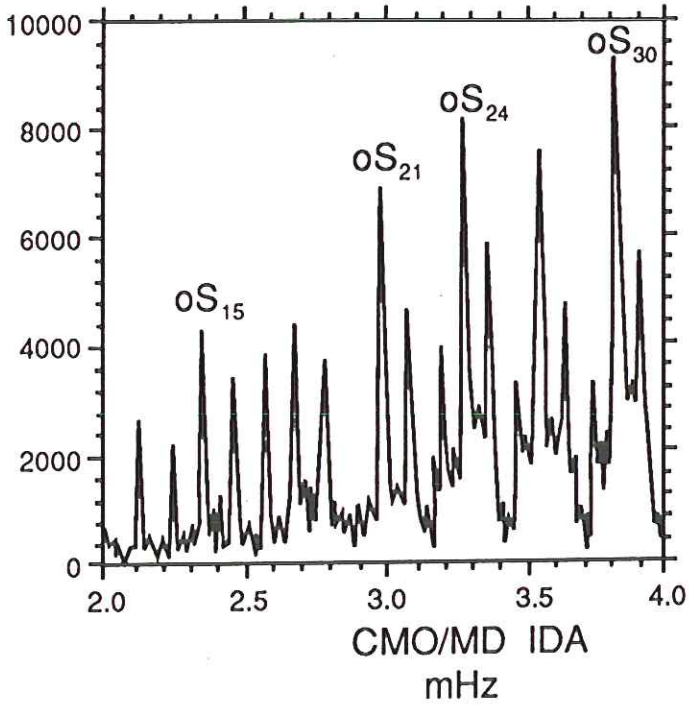
10000
8000
6000
4000
2000
0
oS15
oS21
oS24
oS30
2.0
2.5
3.0
3.5
4.0
CMO/MD IDA
mHz

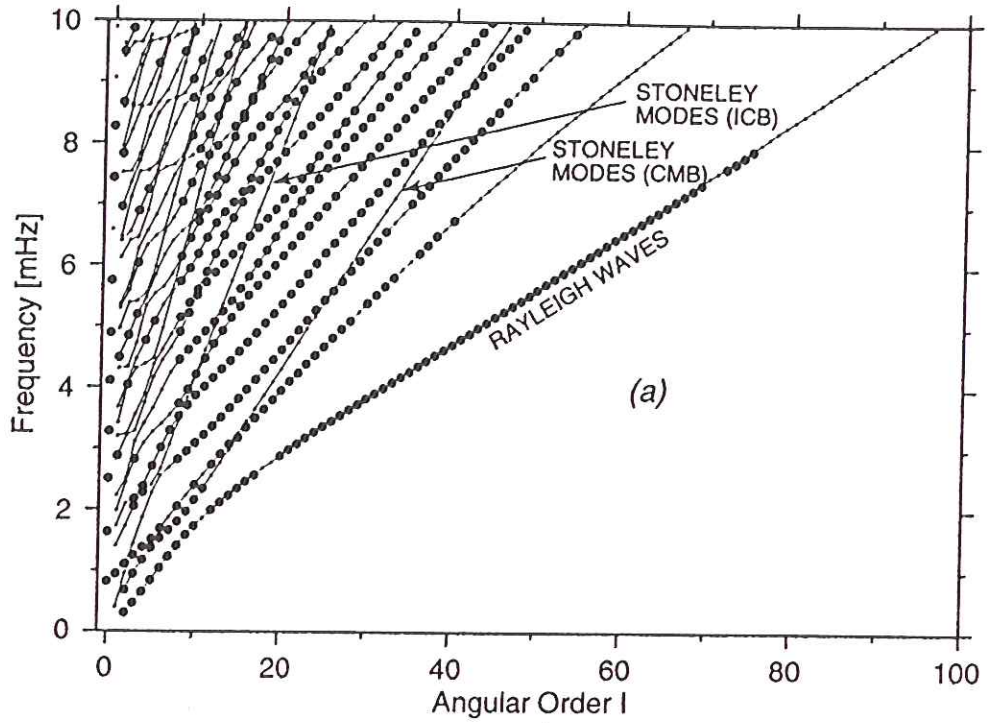
STONELEY
MODES (ICB)
STONELEY
MODES (CMB)
RAYLEIGH WAVES
(a)
Frequency [mHz]
Angular Order l
0
2
4
6
8
10
0
20
40
60
80
100

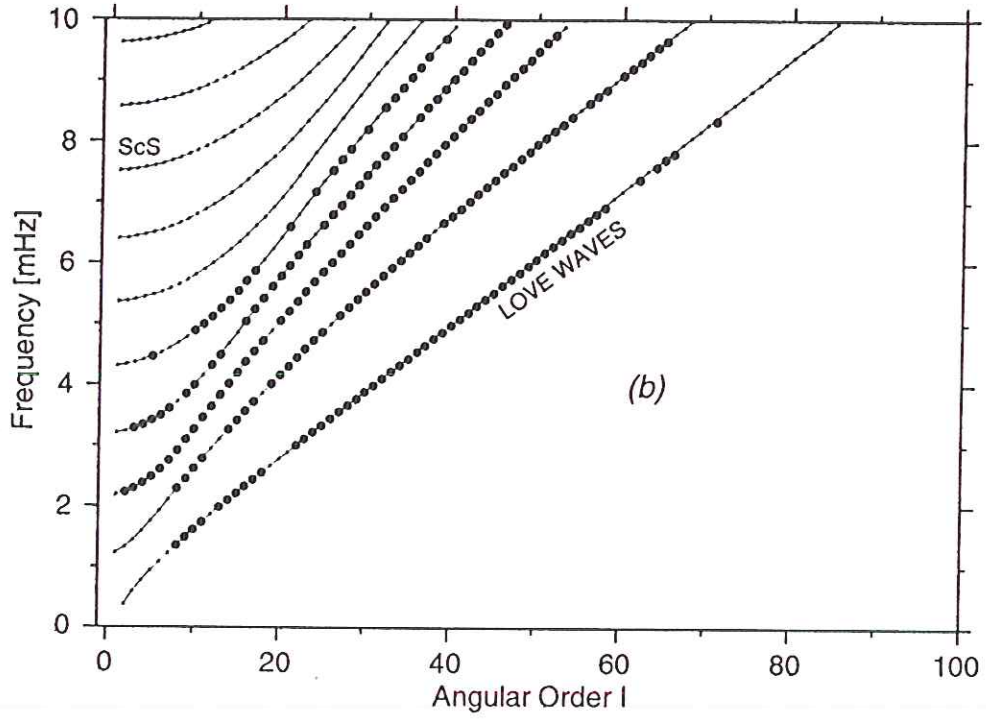
ScS
LOVE WAVES
(b)
Frequency [mHz]
Angular Order l
0
2
4
6
8
10
0
20
40
60
80
100

Earthquakes : we shall consider a number of essentially journalistic questions :

(1) what are they ?

(2) where and when are they ?

(3) how big are they ? or better — how do we measure their size ?

(4) how many are there ? ↑ how many of a given size per year

Press et al chapter 19

Prior to 100 years ago there were a number of proposed causative mechanisms, including motion of subterranean melts, etc.

Now we know that all earthquakes are due to slip on faults.

brittle faults in crust or lithosphere

The 1906 San Francisco earthquake contributed significantly to our understanding of earthquake mechanics.

Devastated city — most damage caused by fire, not by ground shaking.

Clear evidence of faulting — offset roads fences, etc.

Investigated by H.F. Reid — retriangulated many previously surveyed benchmarks

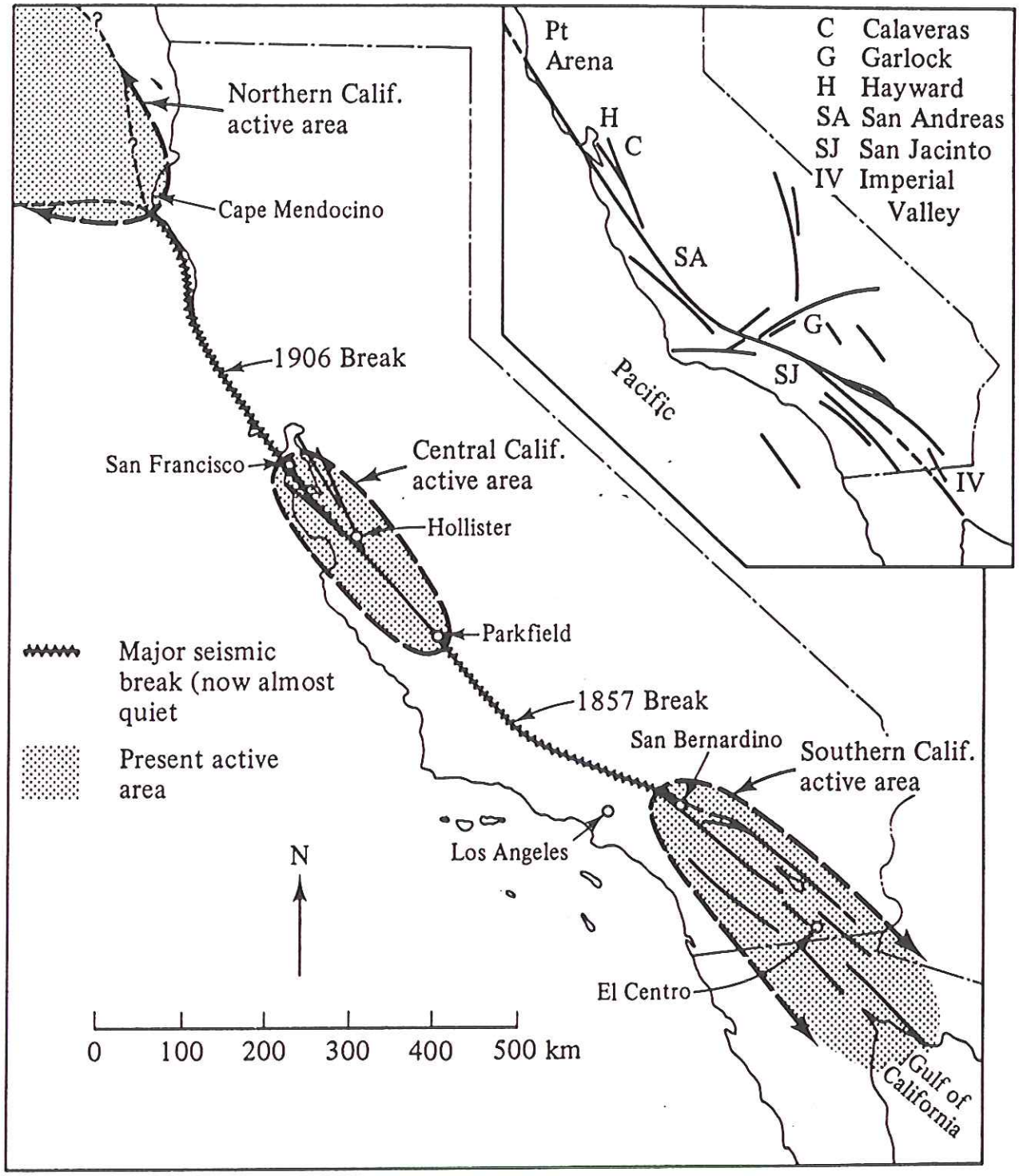

Fig. 7.1. Areas of contrasting seismic behaviour along the San Andreas fault zone in California. (After Allen, 1968.)

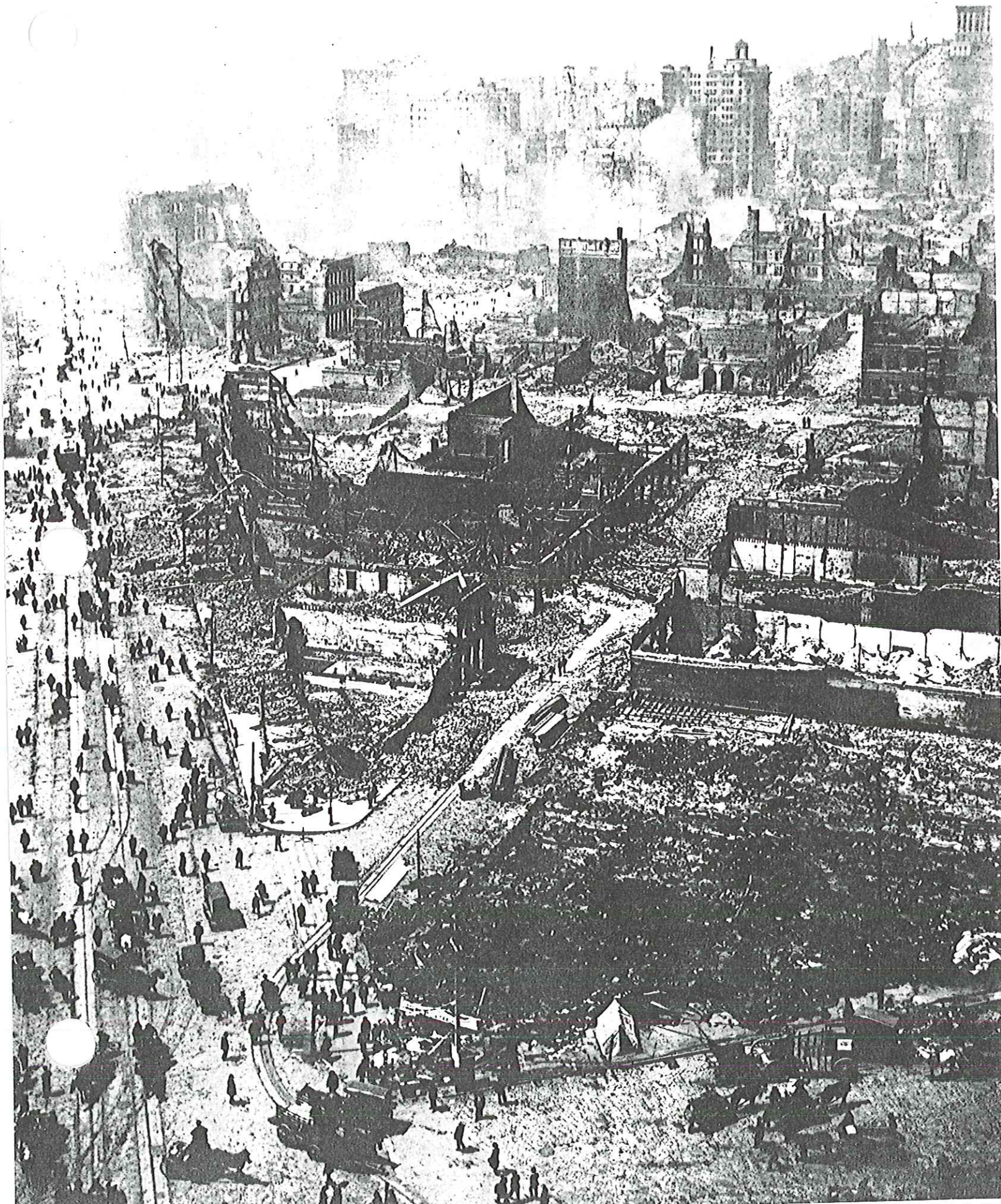


ILLINOIS

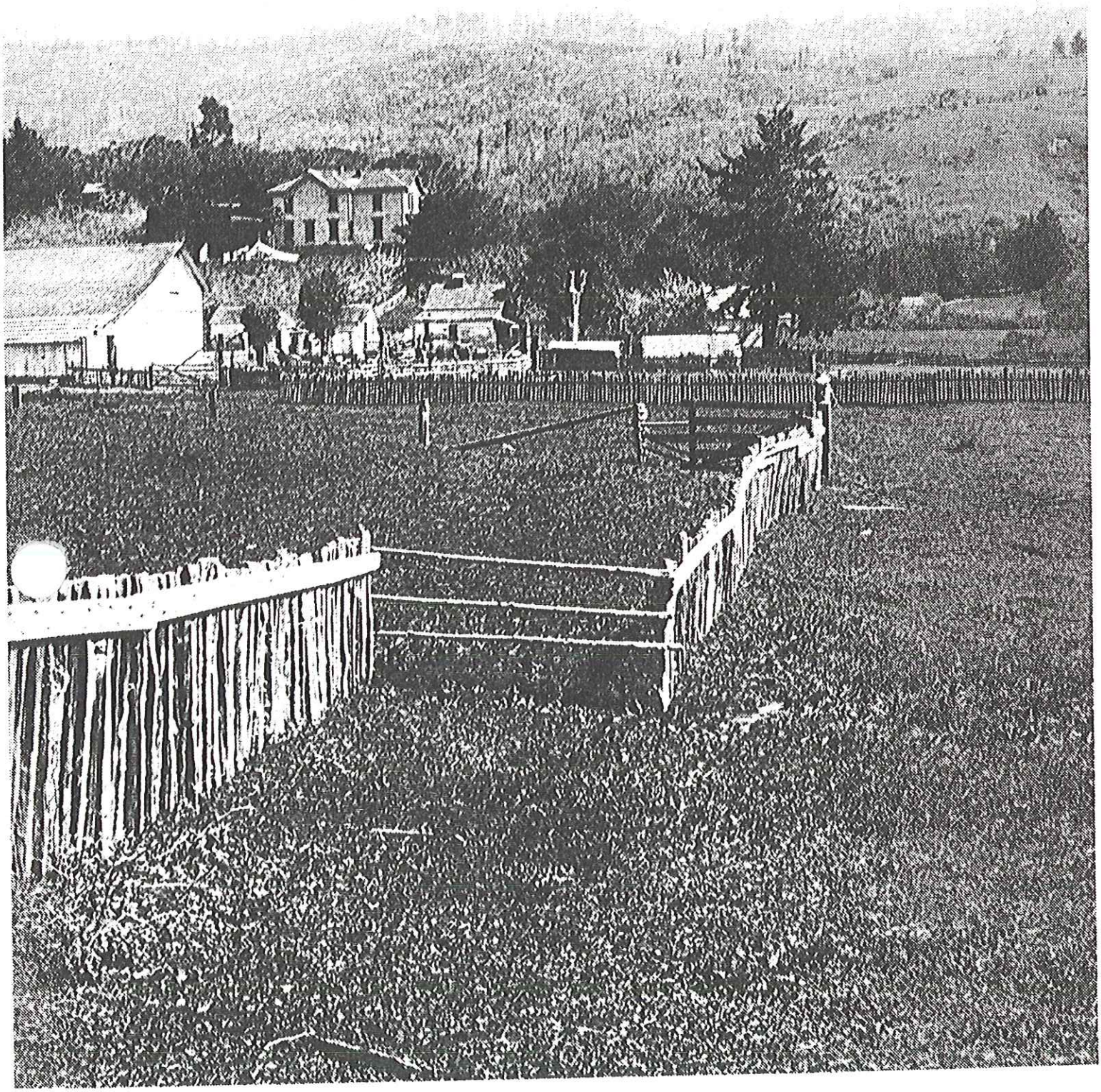

ıre 19-9
The earthquake of 1906 was caused by slip along the San Andreas fault. The offset fence shown here shows a slip of nearly 3 m. Scene is near Bolinas, California. [Photo by G. K. Gilbert; courtesy of R. E. Wallace, U. S. Geological Survey.]

Figure 6.4 Right-lateral horizontal movement of the San Andreas fault in the 1906 earthquake across the old Sir Francis Drake Highway north of San Francisco, at the southern end of Tomales Bay, California. The offset was 6.5 meters (20 feet). [Photo by G. K. Gilbert; courtesy of USGS.]

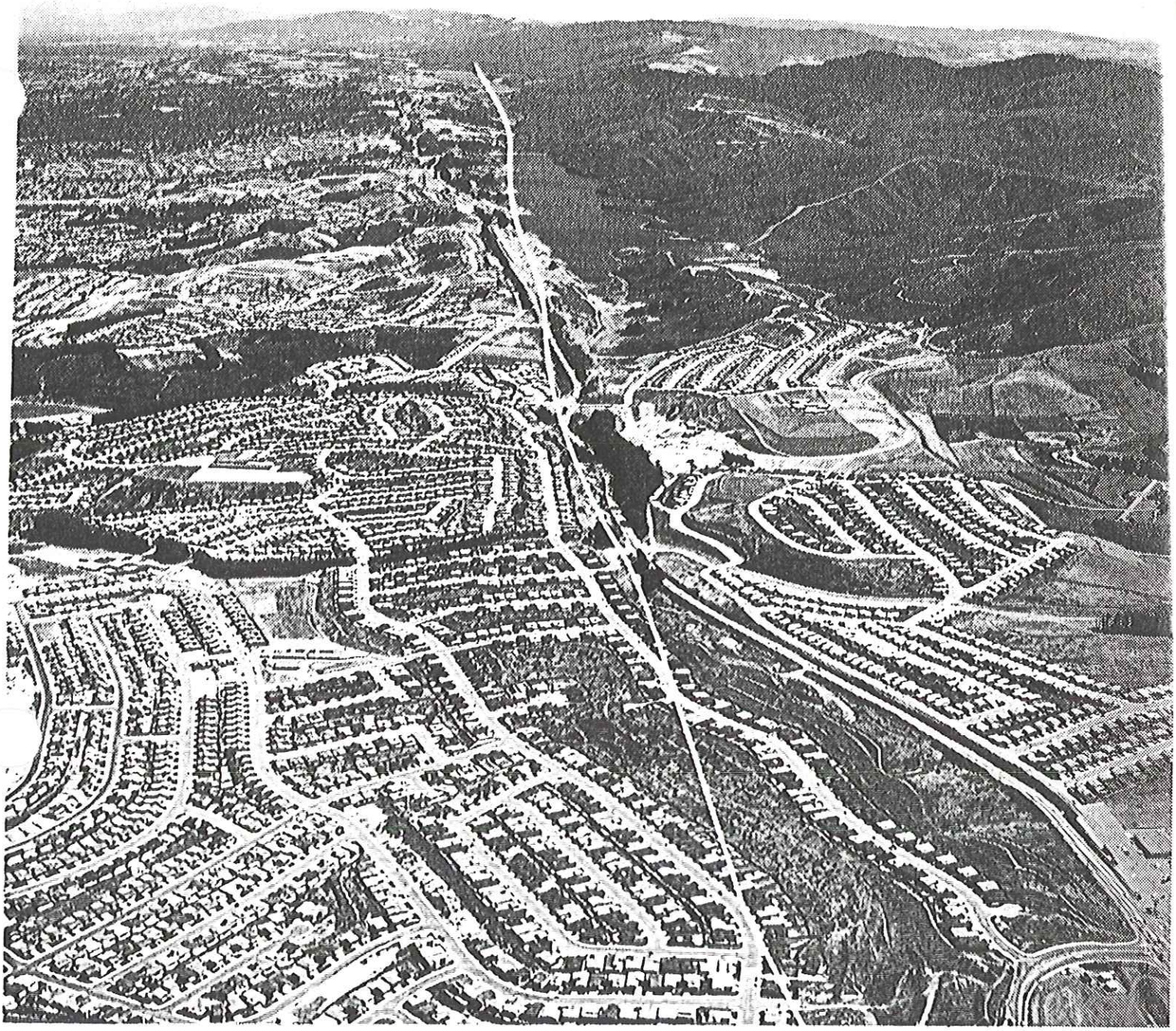

Figure 19-27
Housing tracts constructed within the San Andreas fault zone, San Francisco peninsula. The solid line indicates the approximate fault trace, along which ground ruptured and slipped about 2 m during the earthquake of 1906. [Photo by R. E. Wallace, U. S. Geological Survey.]

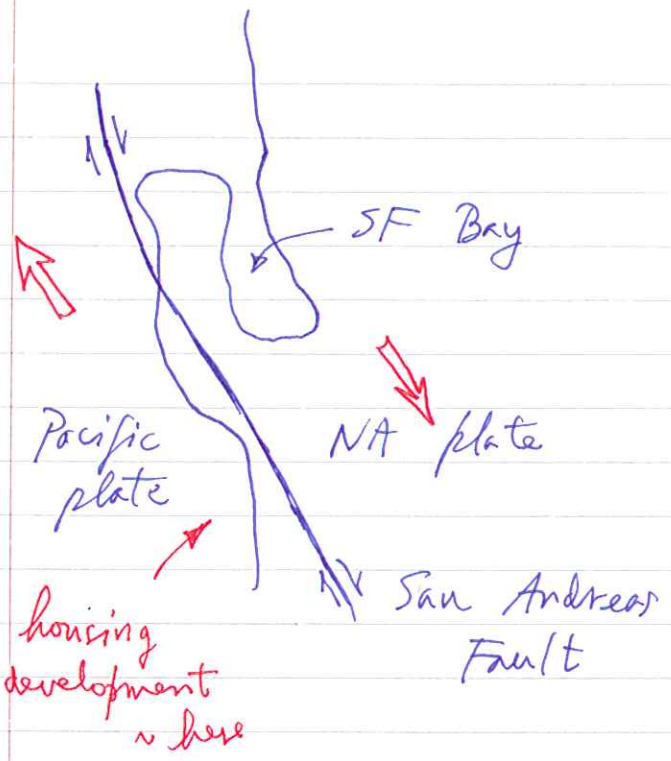

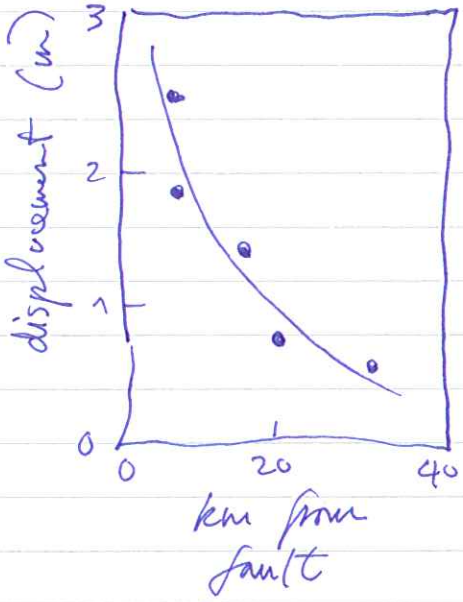

This an inverse picture of elastic strain released by the 'quake

Consider an imaginary straight fence long before 'quake.

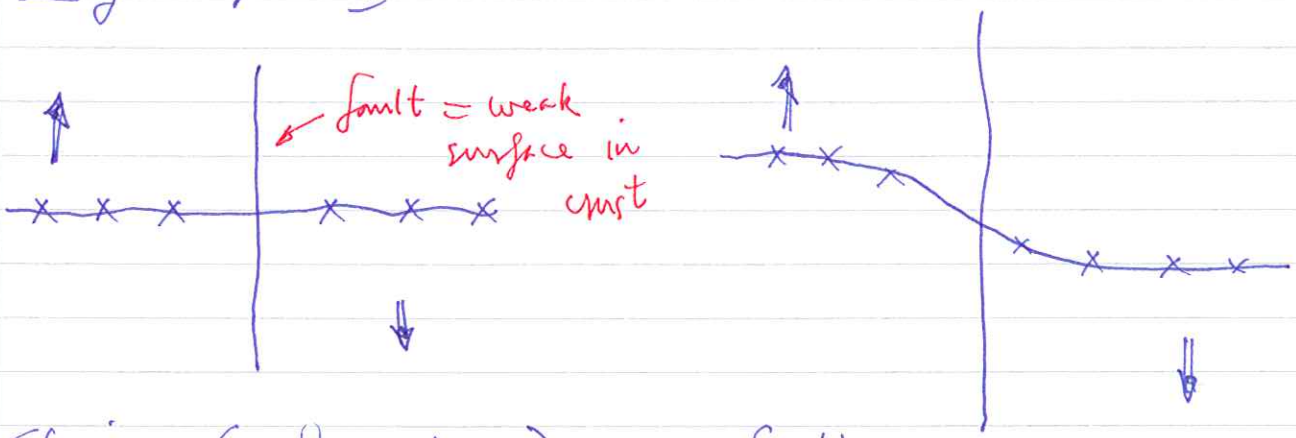

Strain (and stress) on fault builds up on (locked) fault as plate motion. Then failure occurs when the strength of the fault is exceeded

also called stress drop

$\Delta\sigma$ (force / unit area) N/m^2

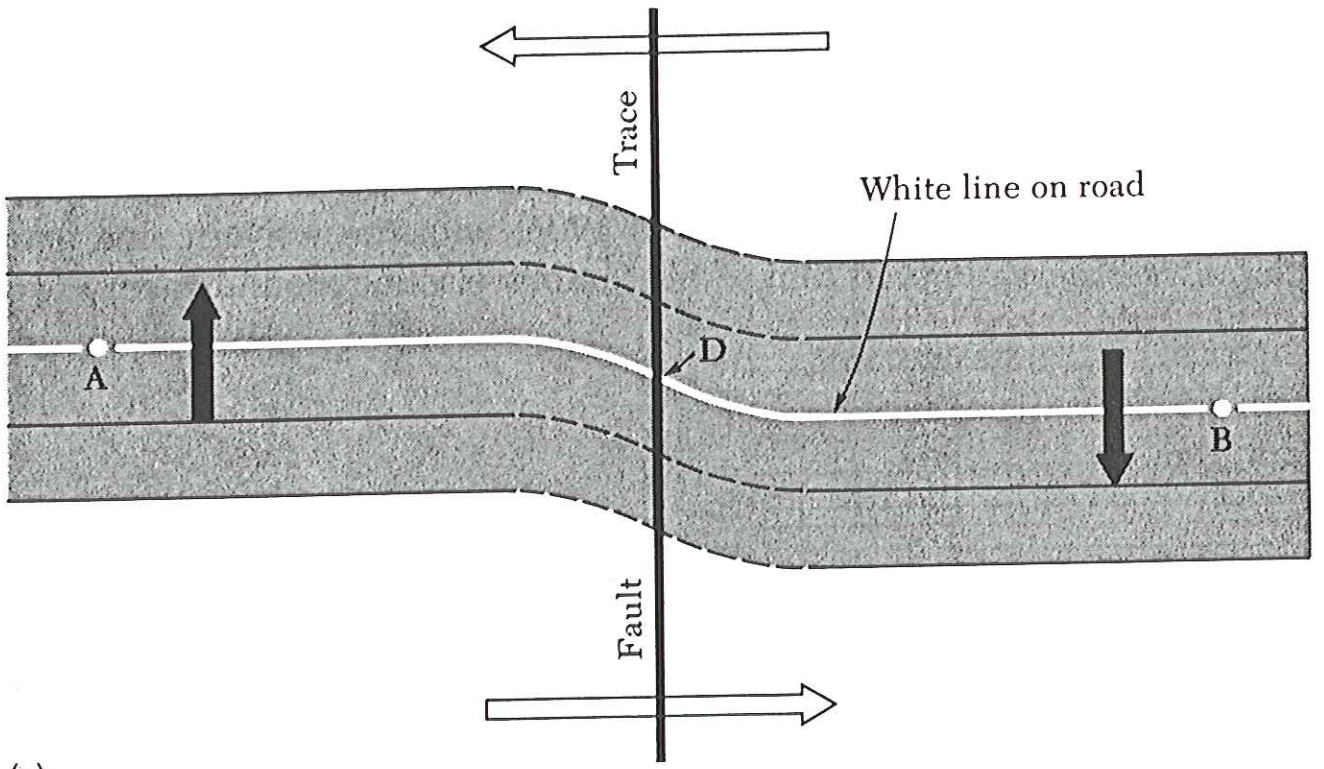

(a)

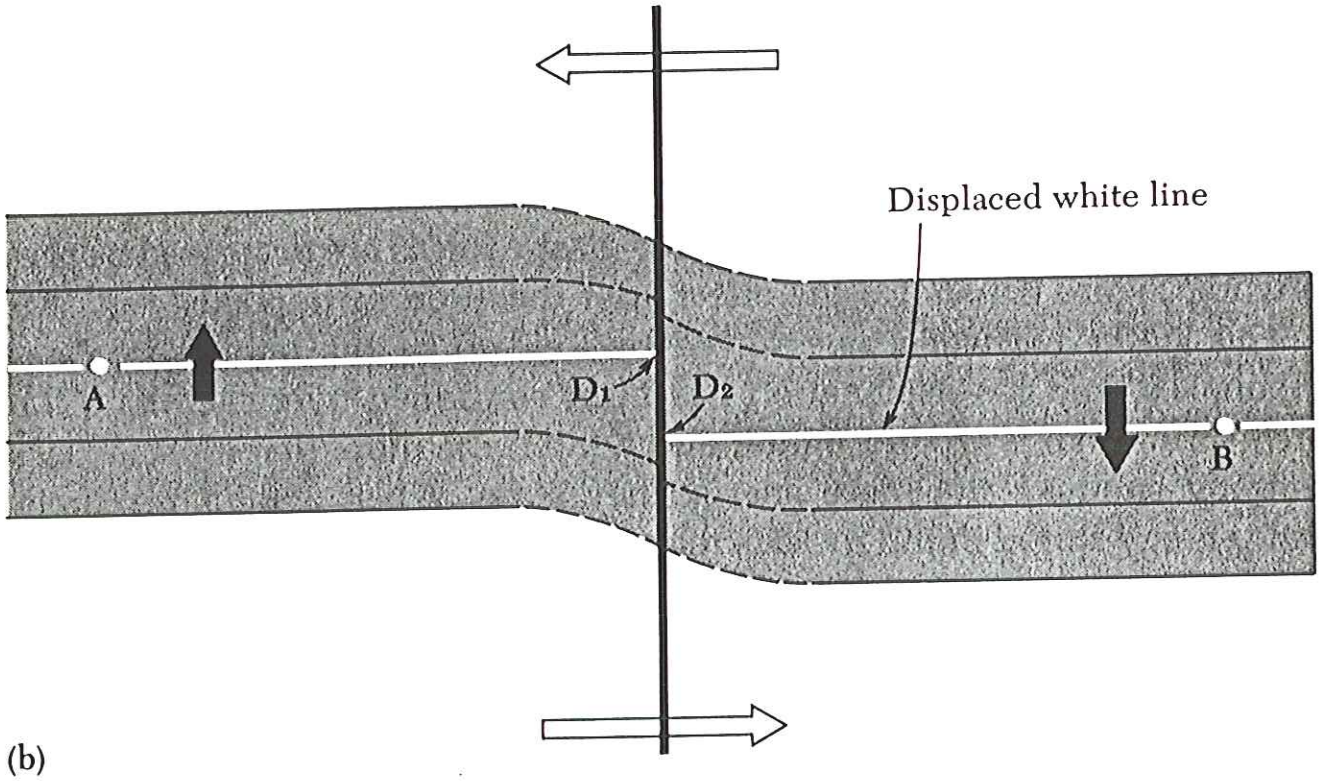

(b)

Figure 6.3 A bird's-eye view of marker lines drawn along a road AB, which crosses a fault trace at the ground surface. (a) In response to the action of tectonic forces, points A and B move in opposite directions, bending the lines across the fault. (b) Rupture occurs D, and strained rocks on each side of the fault spring back to D_1 and D_2. [From Bruce A. Bolt, *Nuclear Explosions and Earthquakes: The Parted Veil* (San Francisco: W. H. Freeman and Company, Copyright © 1976).]

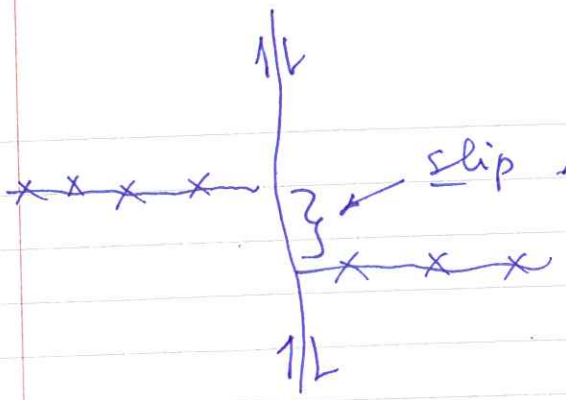

A straight fence built just before the quake would look like

to illustrate: flip the transparency

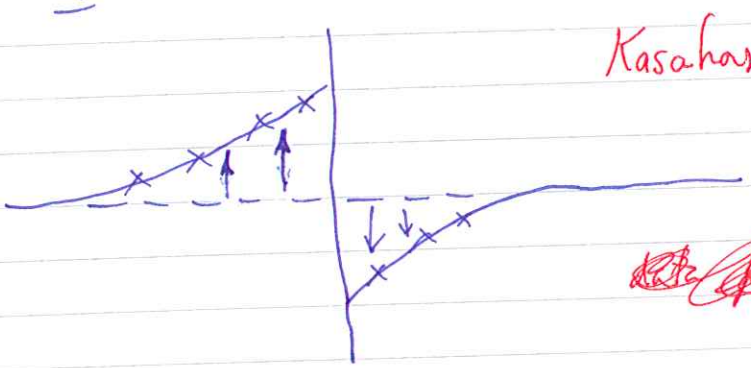

Kasahara's plot flips this around—

The slippage relieves or releases the shear stress $\Delta\sigma$ on the fault

Mathematical model — relieve shear stress σ down to depth h on an ∞ly long strike-slip fault.

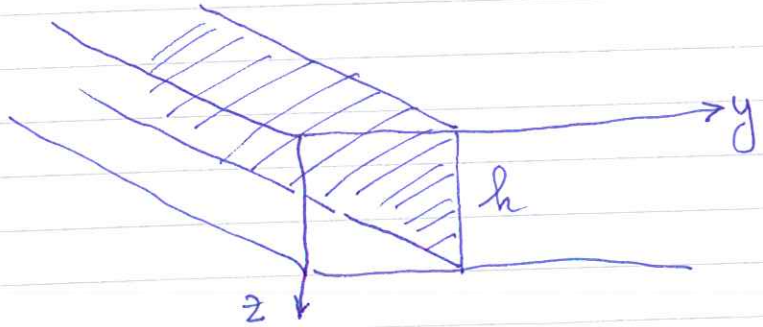

Slip on fault is given by

Σ Actually half the slip — each side moves by same amount

each side

fcn of depth

$s(z) = \frac{\Delta\sigma}{\mu}\sqrt{h^2 - z^2}$

half-slip

μ ← rigidity

proportional to stress release

other side does this

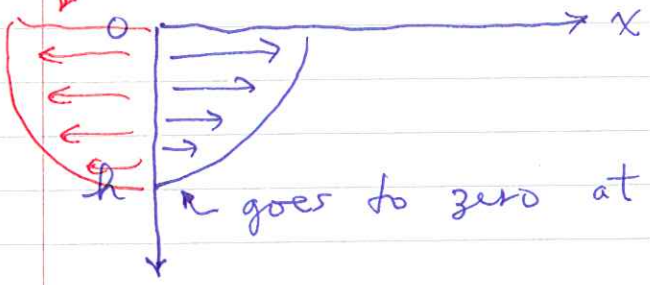

h goes to zero at bottom of fault

on surface of ⊕ ($z = 0$)

$\text{slip} = \Delta s = 2\left(\frac{\Delta\sigma}{\mu}\right)h$

As a function of distance away from fault, on surface of ⊕

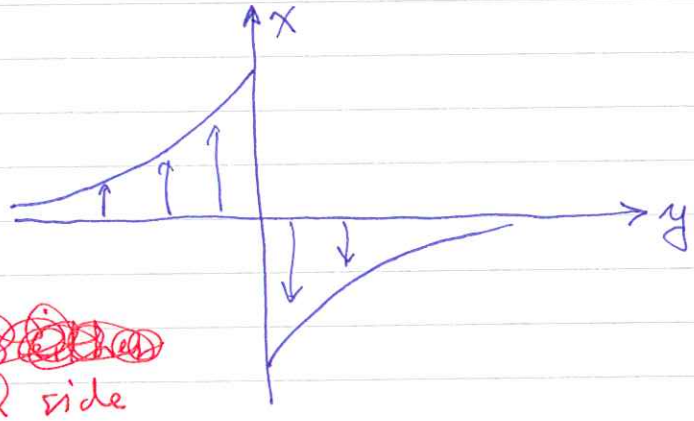

each side

$$s(y) = \frac{\Delta\sigma}{\mu}\left[\sqrt{h^2 + y^2} - y\right] \quad *$$

On fault: $\text{slip} = \Delta s = 2\left(\frac{\Delta\sigma}{\mu}\right)h$

Can fit a function of form * to survey data. Find for SF quake

$\Delta s = 5$ meters

$h \cong 6$ km (Kasahara gives $D = 6$ km)

Implied stress drop (strength of San Andreas fault)

$$\Delta\sigma = \frac{\mu \Delta s}{2h} = \frac{3 \cdot 10^{10}\ \text{Pa} \times 5\ \text{m}}{2 \times 6 \cdot 10^{3}\ \text{m}}$$

(crustal rigidity)

$= 10^7$ Pa $= 10$ MPa $= 100$ bars

(1 bar ≈ 1 atm)

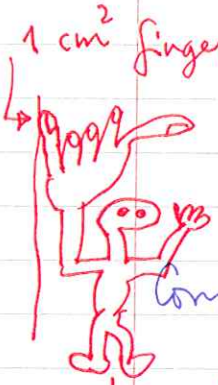

Comparison — glue your palm to the wall and hang on it instead:

$$\frac{100\ \text{kg} \times 10\ \text{m/s}^2}{10^{-4}\ \text{m}^2} = 10^7\ \text{Pa}$$

glue one finger to the wall then stress is same

10 cm × 10 cm palm size

1 cm × 1 cm finger size

100 × your weight

You can exert it with your fingers

Would have to tie an anchor weight around your ankles.

So 100 bars is more stress than you can exert with your hands but still ⇒ faults are very weak.

In general $\Delta\sigma = 10-100$ bars for all crustal quakes

Two other examples (Tango or Gornura eq. in Japan 1927) and 1940 Imperial Valley — offset orange grove. Both strike slip.

Also Fairview Peak, Nevada (1954) Normal fault — displaced outhouse

$\Delta s = 3$ m.

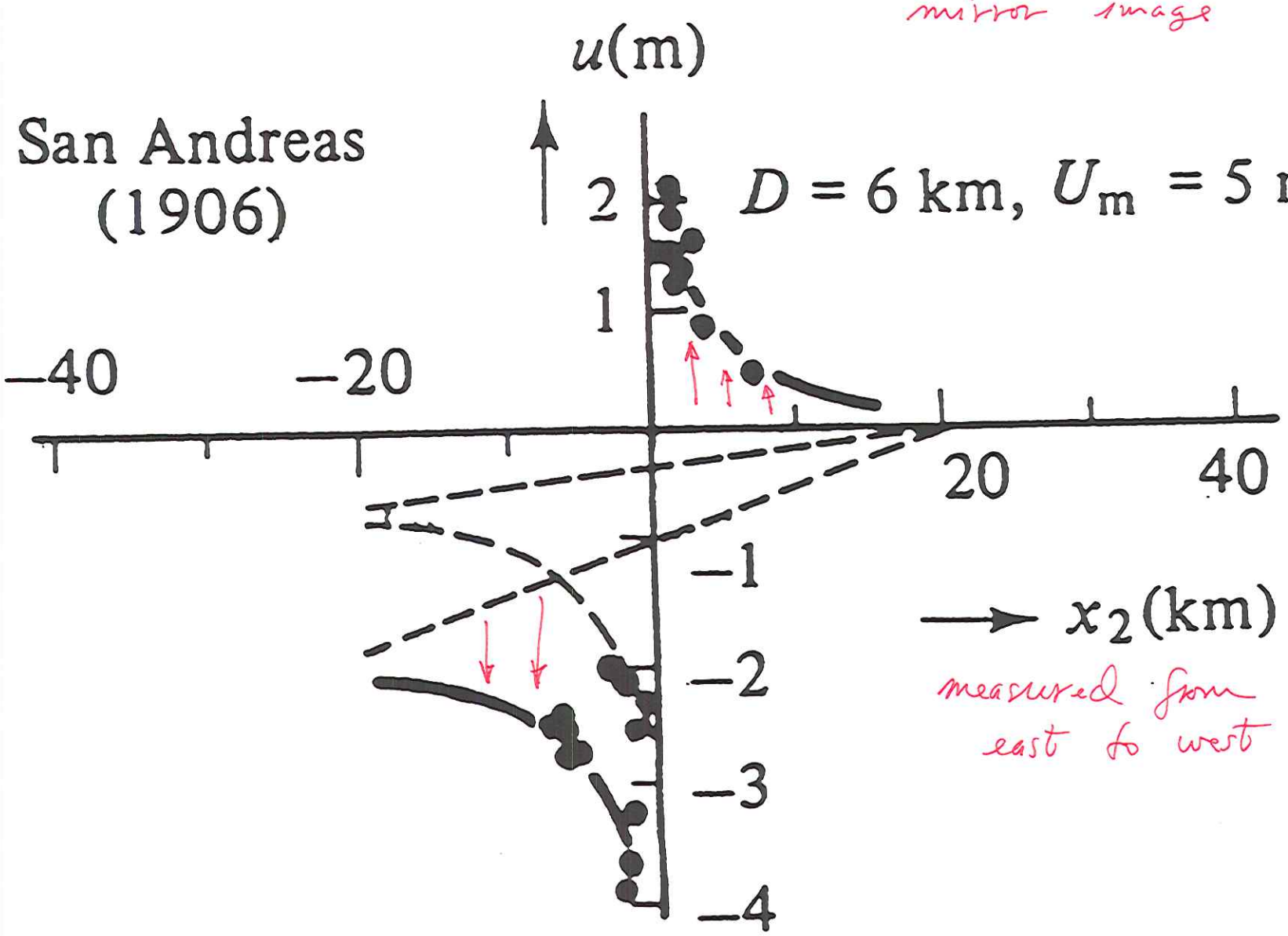
mirror image
u(m)
San Andreas
(1906)
D = 6 km, U_m = 5 m
2
1
−40
−20
20
40
−1
−2
−3
−4
x_2(km)
measured from
east to west

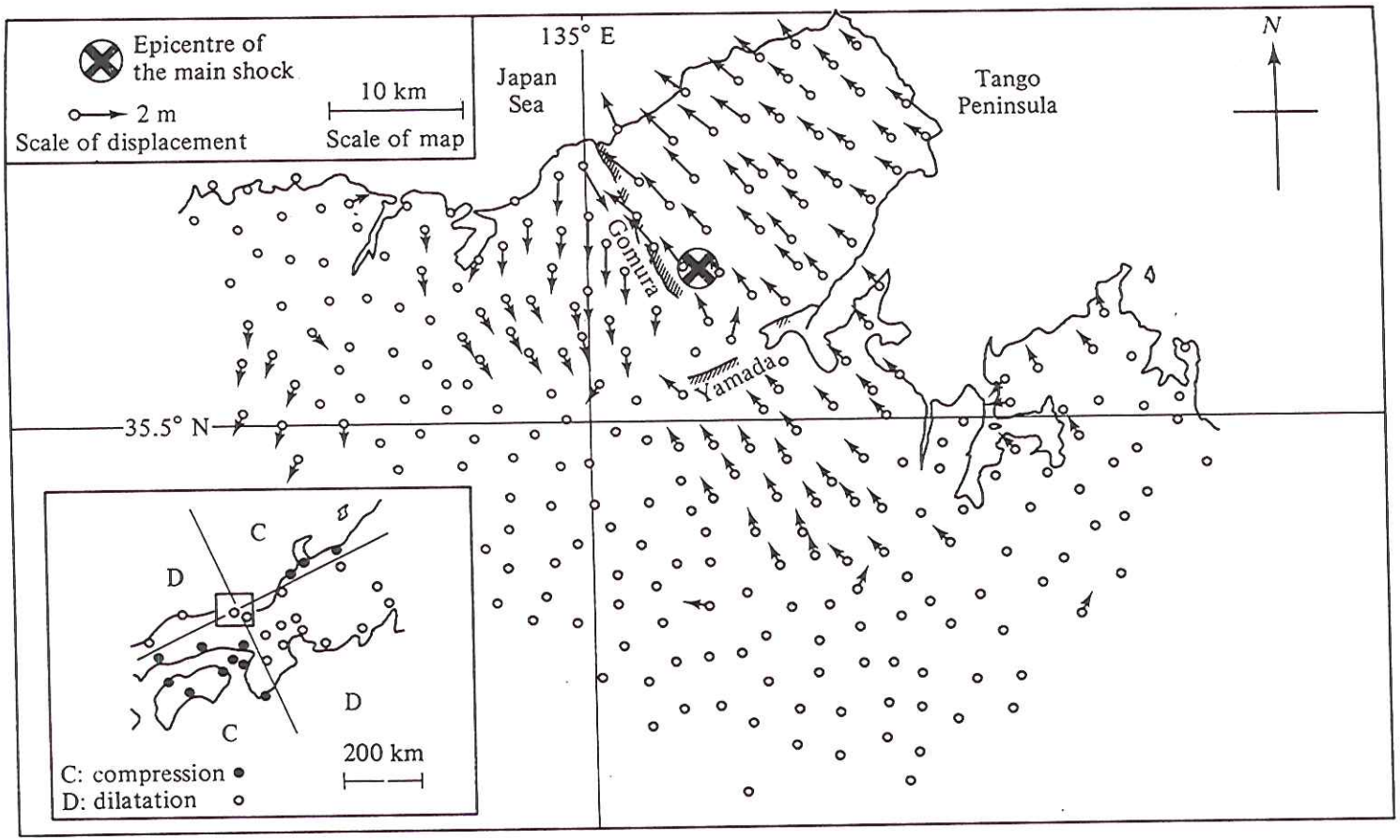

Fig. 4.5. Displacement of triangulation points (Land Survey Department, 1930) in the Tango earthquake of 1927. The distribution of P-wave first motions (Honda, 1932) in the inset shows the radiation pattern. (From Kanamori, 1973. Reproduced, with permission, from the *Annual Review of Earth & Planetary Sciences*, Volume 1. © 1973 by Annual Reviews Inc.)

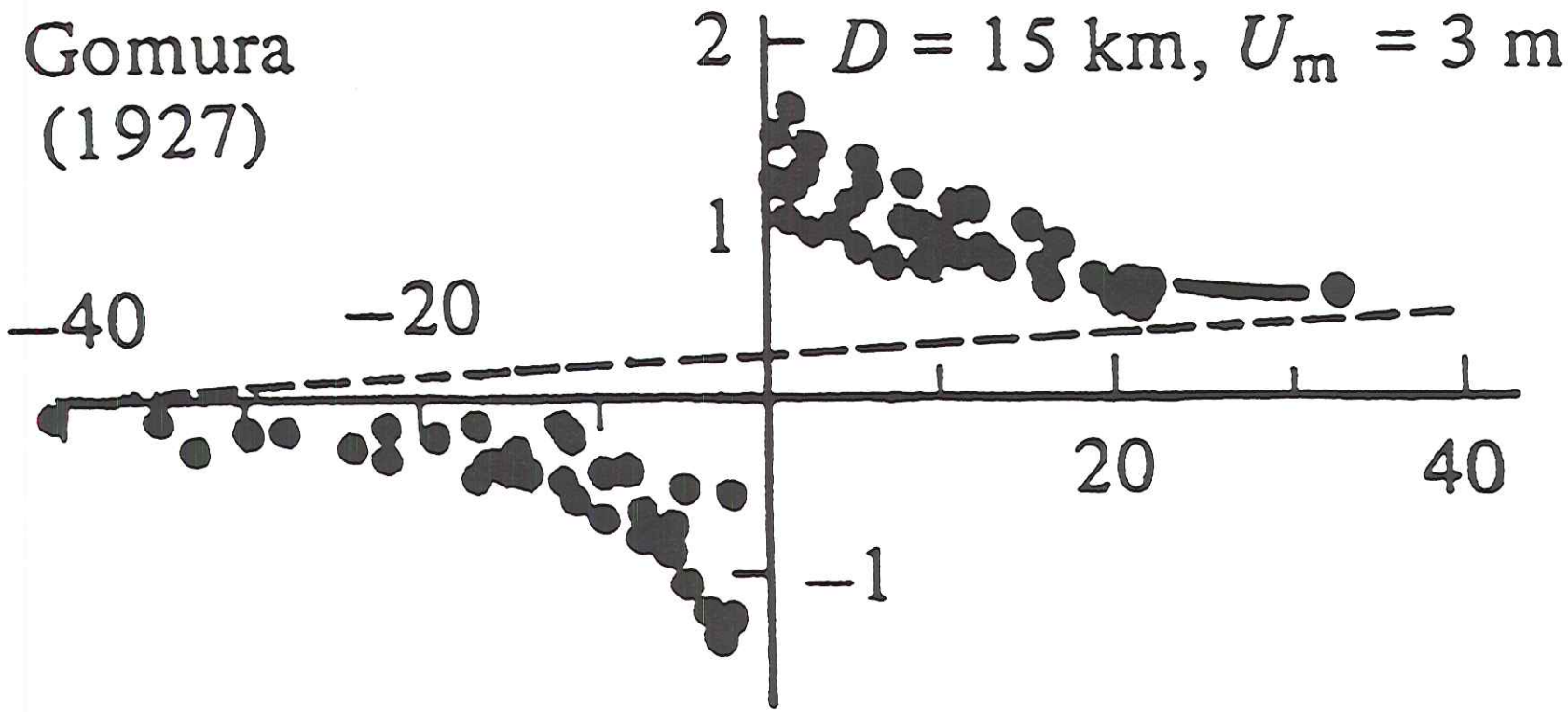
Gomura
(1927)
D = 15 km, U_m = 3 m
2
1
−40
−20
20
40
−1

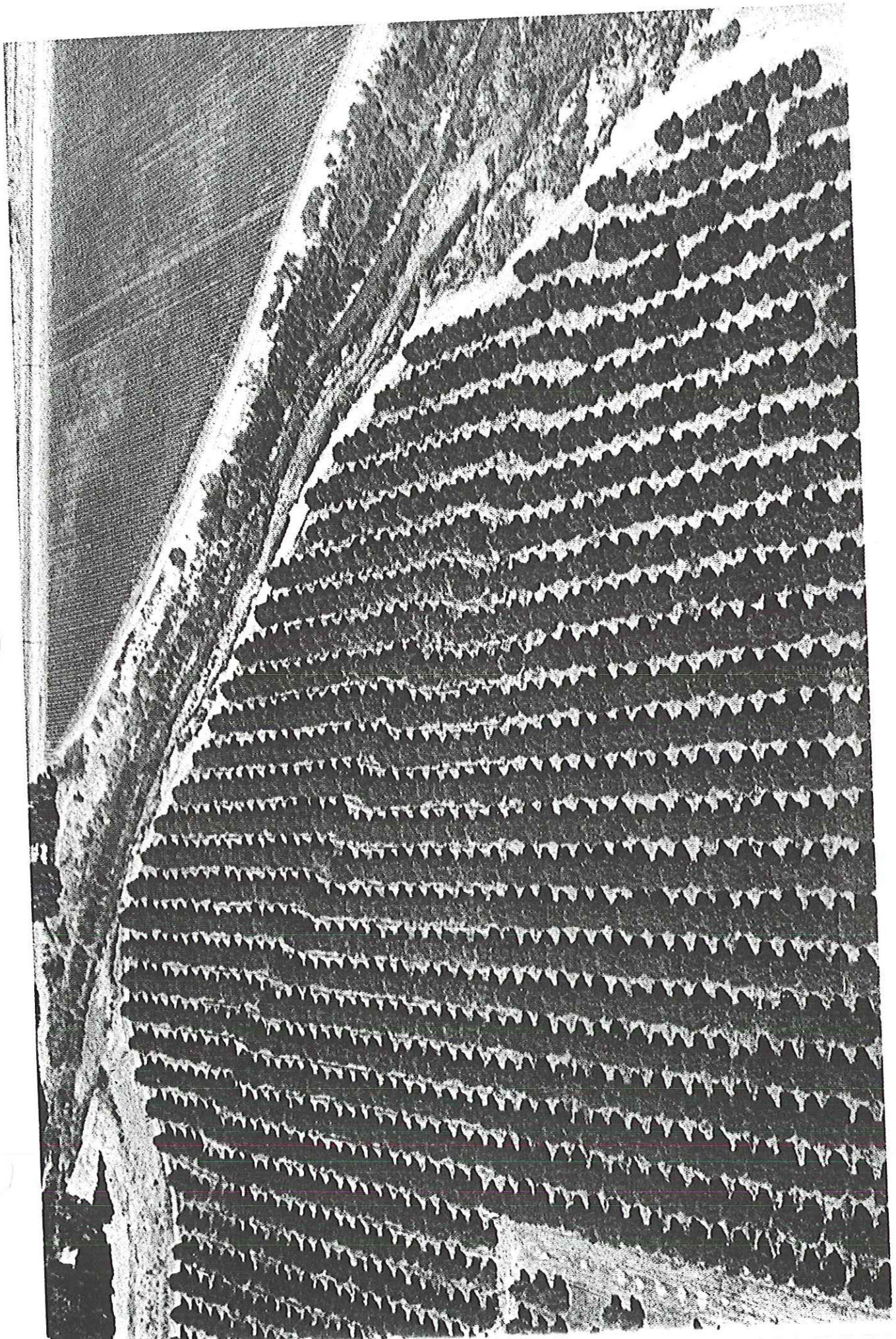

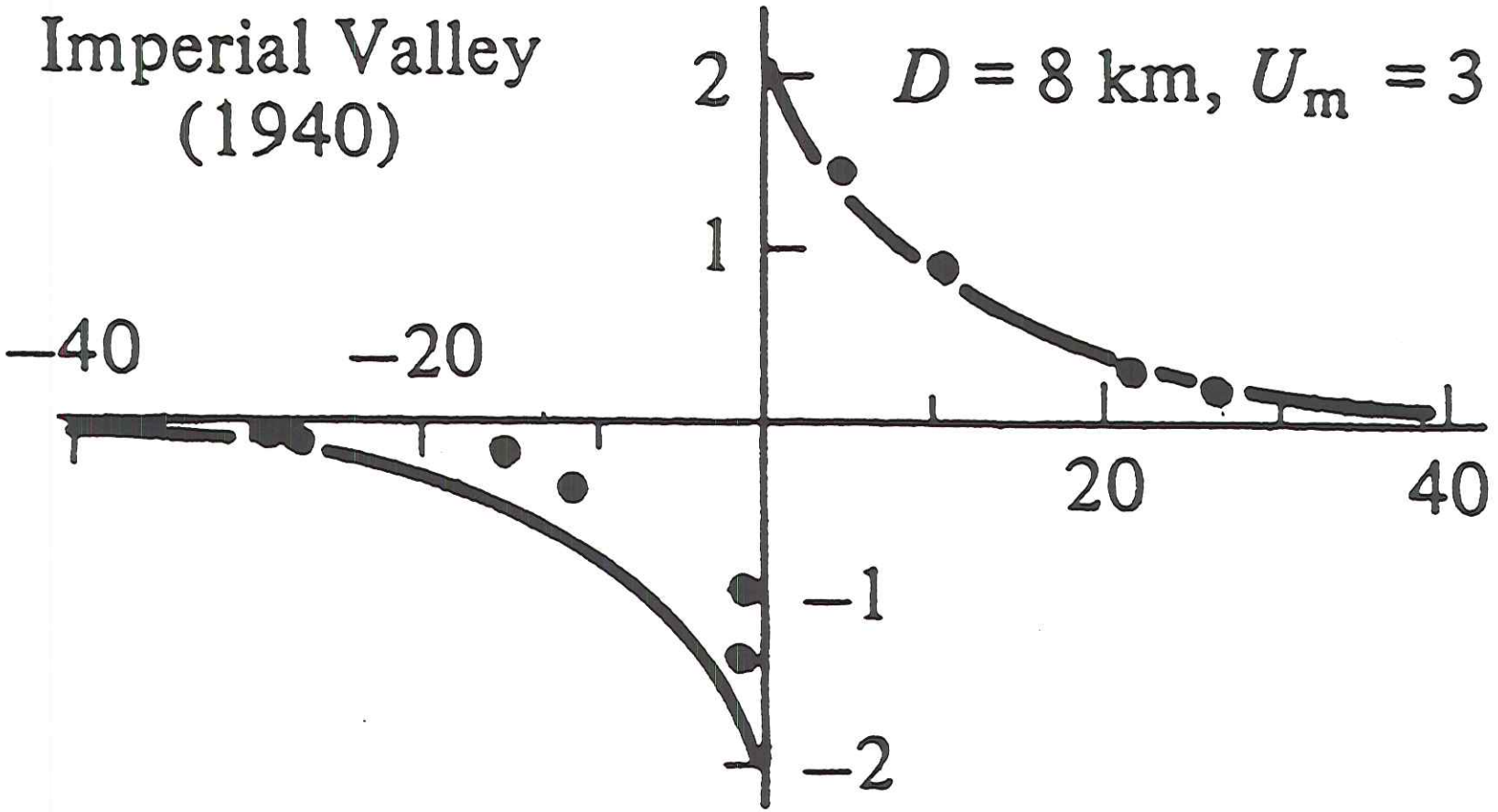
Imperial Valley
(1940)
D = 8 km, U_m = 3
2
1
−40
−20
20
40
−1
−2

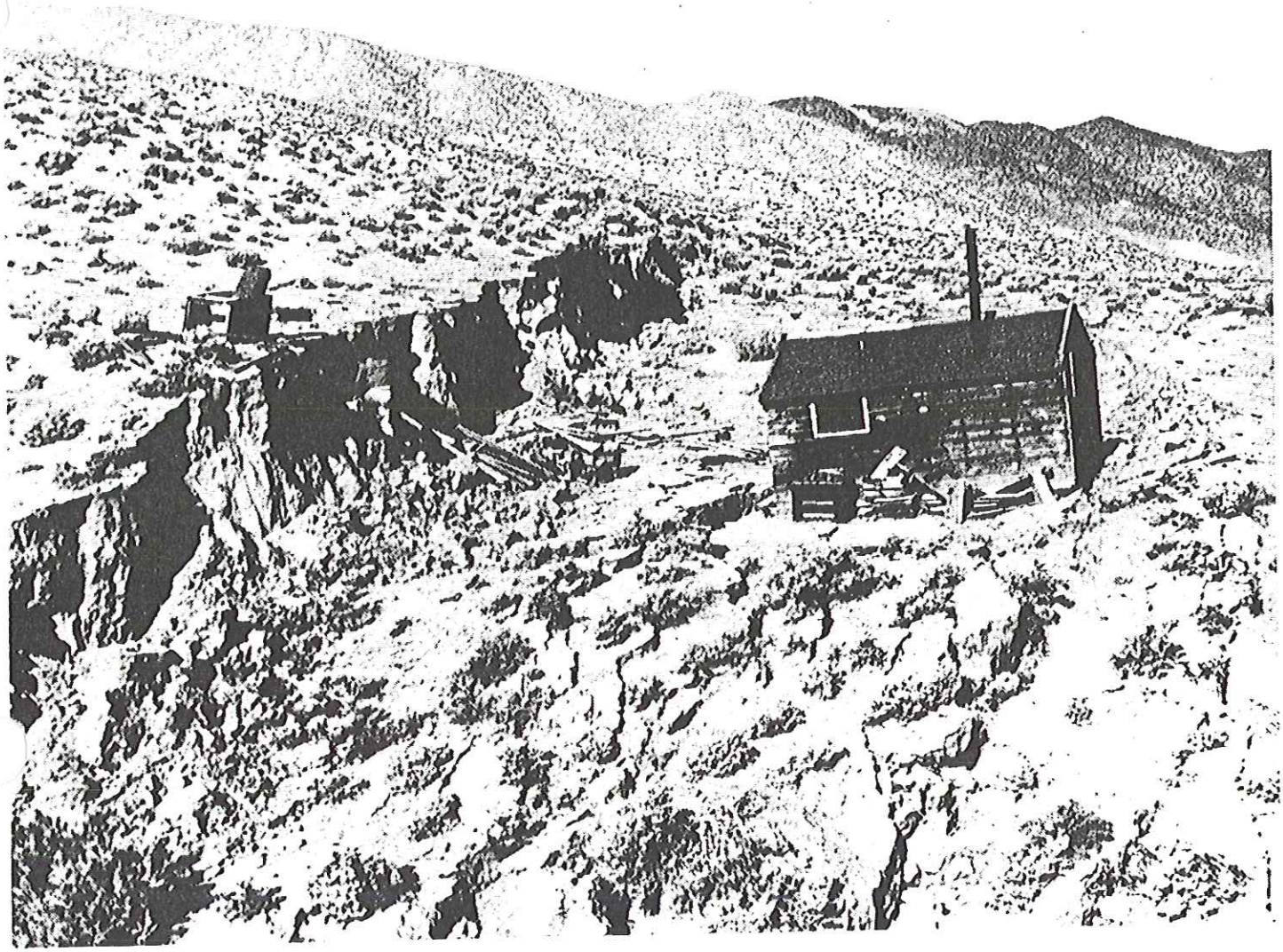

Figure 6.5 A fault scarp in Ixl Canyon, Fairview Mountain, Nevada. [Courtesy of Karl V. Steinbrugge.]

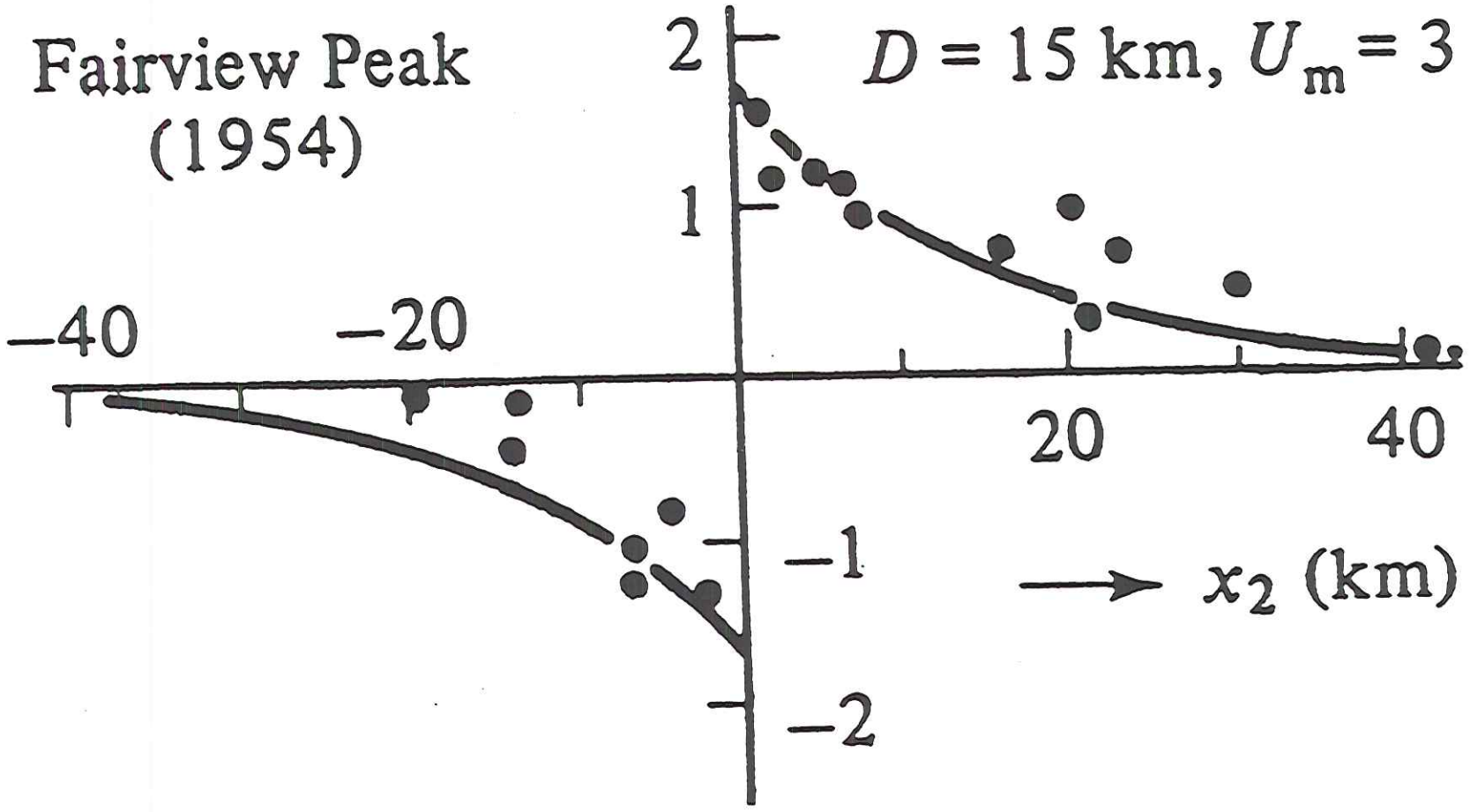
Fairview Peak
(1954)
D = 15 km, U_m = 3
2
1
−40
−20
20
40
−1
−2
x_2 (km)

An important earthquake parameter — best measure of size —

Earthquake moment

$M_0 = \mu A \bar{\Delta s}$ — units Nm (force × dist)

μ ← fault area; $\bar{\Delta s}$ ← average slip

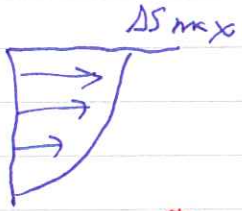

don't give this — just say it's about 4 m

$\bar{\Delta s} = \frac{\pi}{4} \Delta s_{max}$

$M_0 = (3 \cdot 10^{10})(6 \cdot 500) \cdot 10^6 \cdot \frac{\pi}{4} \cdot 5$

length 500 km

$\approx 4 \cdot 10^{20}$ Nm

A major strike-slip event but thrust events can be 2 orders of magnitude bigger.

Energy of earthquakes: elastic energy stored in the vicinity of the fault is radiated away in the form of seismic P and S waves.

The radiated energy is

$E = \frac{1}{2} \Delta\sigma A \bar{\Delta s}$ — measured in Joules (same as Nm)

$$E = \frac{M_0}{0.6 \cdot 10^4} \text{ for SF 1906}$$

For the 1906 SF event:

$$E = \frac{1}{2}(10^{7})(3 \cdot 10^{9}) \cdot 5 \cdot \frac{\pi}{4}$$

actually $6 \cdot 10^{16}$ Joules ← give this

$= 10^{17}$ Joules

≈ about equal to daily US electrical energy consumption

daily US electrical energy consumption $11 \cdot 10^{16}$ Joules

Note that in general

$\Delta\sigma = 1\text{–}10$ MPa, say 3 average

$$E = \left(\frac{\Delta\sigma}{2\mu}\right) M_0$$

$$\approx \frac{3 \cdot 10^{6} \text{ Pa}}{2 \cdot 3 \cdot 10^{10}} M_0 \approx \frac{M_0}{2 \cdot 10^4}$$

Hiroshima 14 kT $= 14 \cdot 10^{12}$ cal $= 6 \cdot 10^{13}$ J

Hiroshima 14 kT $= 6 \cdot 10^{13}$ J

Pinatubo 10^{20} J into mostly atmosphere

$$E \approx \frac{M_0}{2 \cdot 10^4}$$

Estimate of earthquake energy given moment.

1906 SF is

- ≈1000× Hiroshima
- ≈ US daily electrical energy consumption
- ≈ $\frac{1}{1000}$ × Pinatubo

[illegible] energy would the 1906 SF Quake keep a 100 kw light bulb burning?

1 kW hr = 3 MJ

100 kW hr = $3.6 \cdot 10^8$ J

$\frac{10^{17}}{3.6 \cdot 10^8} \approx 3 \cdot 10^8$ hrs ≈ $3 \cdot 10^4$ years

Need to go slowly over this since the circular patch confuses people.

Long skinny ribbon:
1906 · San Francisco
← 500 km →
↓ ~10 km deep
x

In general, the larger a slipped patch, the larger the slip.

Model — uniform stress drop on a circular patch on a fault

strike slip $\bar{\Delta s} = \frac{\pi}{8}\left(\frac{\Delta\sigma}{\mu}\right) h$

$$\bar{\Delta s} = \frac{16}{7\pi}\left(\frac{\Delta\sigma}{\mu}\right) a$$

for only strike-slip fault model $\bar{\Delta s} = \frac{\pi}{2}\left(\frac{\Delta\sigma}{\mu}\right) h$

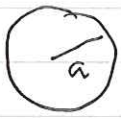

radius a

stress drop $\Delta\sigma$

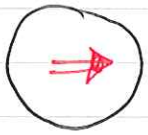

slip $\bar{\Delta s}$

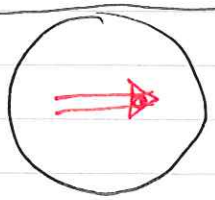

twice as much slip

twice as big in radius (4× in area)

model for small crustal quakes without surface faulting

$$M_0 = \mu A \bar{\Delta s} = \frac{16}{7}\Delta\sigma\, a^3 \qquad (A = \pi a^2)$$

$$M_0 = \frac{16}{7\pi^{3/2}}\Delta\sigma\, A^{3/2}$$

$$M_0 = 0.4\,\Delta\sigma\, A^{3/2}$$

uniform stress drop $\Delta\sigma$ on a circular fault ($A = \pi \times \text{radius}^2$)

$$\log M_0 = \underbrace{\log(0.4\,\Delta\sigma)}_{\approx \text{constant}} + \frac{3}{2}\log A$$

Show Fig 9.25

$\Rightarrow \quad \Delta\sigma = 10 - 100$ bars

Average $\Delta\sigma = 30$ bars $= 3$ MPa

$$\log_{10} M_0 = 5 + \frac{3}{2} \log_{10} A$$

$$E = \left(\frac{\Delta\sigma}{2\mu}\right) M_0 = \frac{3 \cdot 10^6 \text{ Pa}}{(2)(3 \cdot 10^{10} \text{ Pa})}$$

$$E \approx \frac{M_0}{2 \cdot 10^4}$$

Give $E \approx \frac{M_0}{0.6 \cdot 10^4}$ for 1906 SF

Then discuss circular crack model

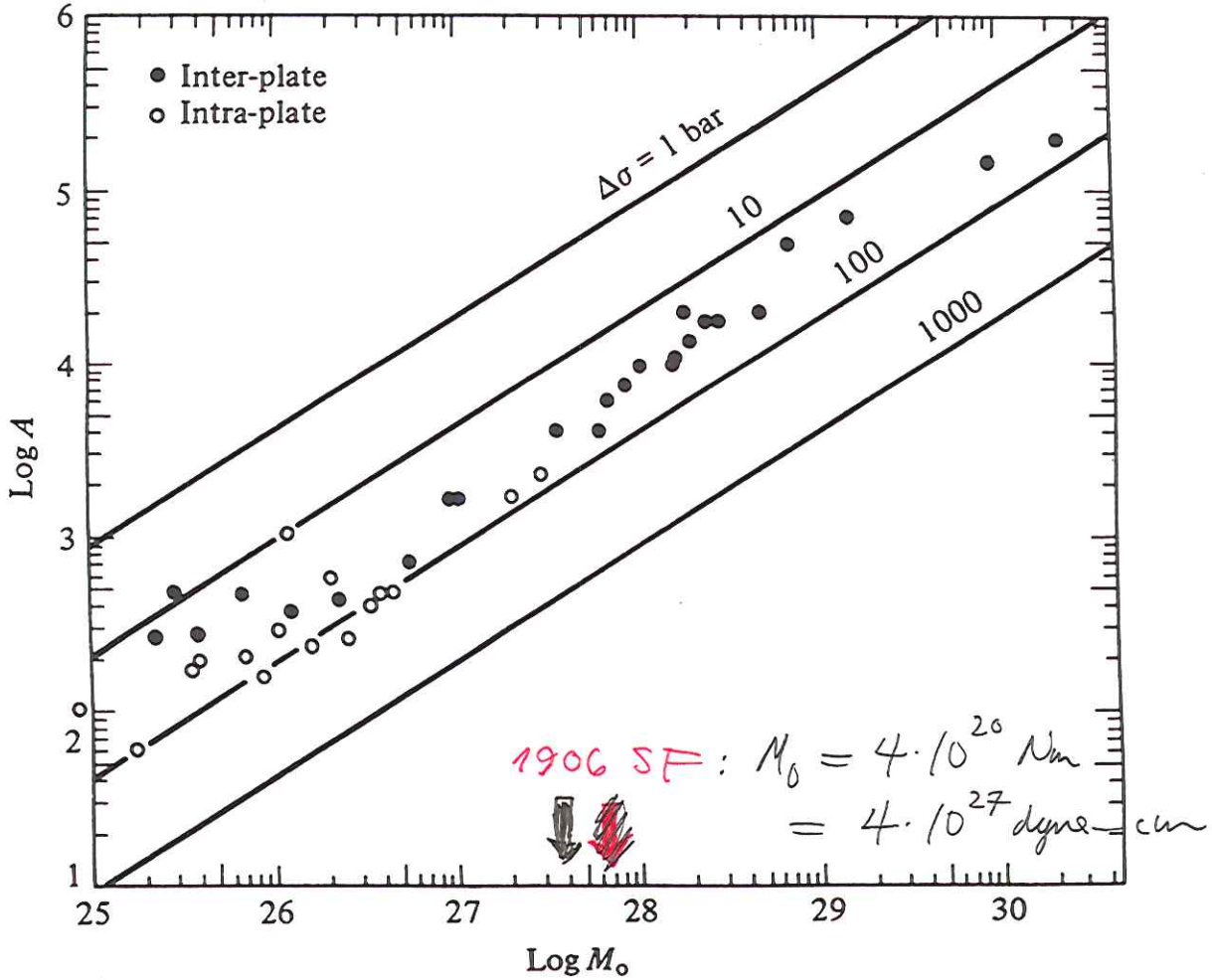

FIGURE 9.25 Area versus moment for inter- and intraplate earthquakes. Note that the interplate earthquakes show little scatter about a stress drop of 30 bars. The intraplate earthquakes have stress drops of ~100 bars. (Modified from Kanamori and Anderson, 1975.)

Another question — suppose the 10^{17} J of energy could be harnessed. For how long would it supply the electrical energy needs of SF?

$$\left(3 \cdot 10^{19} \frac{\text{J}}{\text{year}}\right) \times \frac{1}{300} \approx 10^{17} \frac{\text{J}}{\text{yr}}$$

- $3 \cdot 10^{19}$ J/year: US electrical energy consumption
- 1/300: fraction of US people in SF (~ 1 million)
- 10^{17} J/yr: i.e. for about one year.

One other measure of size — most common in popular media — the earthquake magnitude.

Based on an older empirical scale — developed and refined by C.F. Richter.

Modern moment magnitude simply defined by

$$\log_{10} M_0 = 1.5\, M + 9.1$$

give this → or $$M = \frac{2}{3} \log_{10} M_0 - 6.1$$

For 1906 SF: $M = 7.7$

SEPT 11, 2001

collapsed in ~10 s
speed upon impact ~120 mph

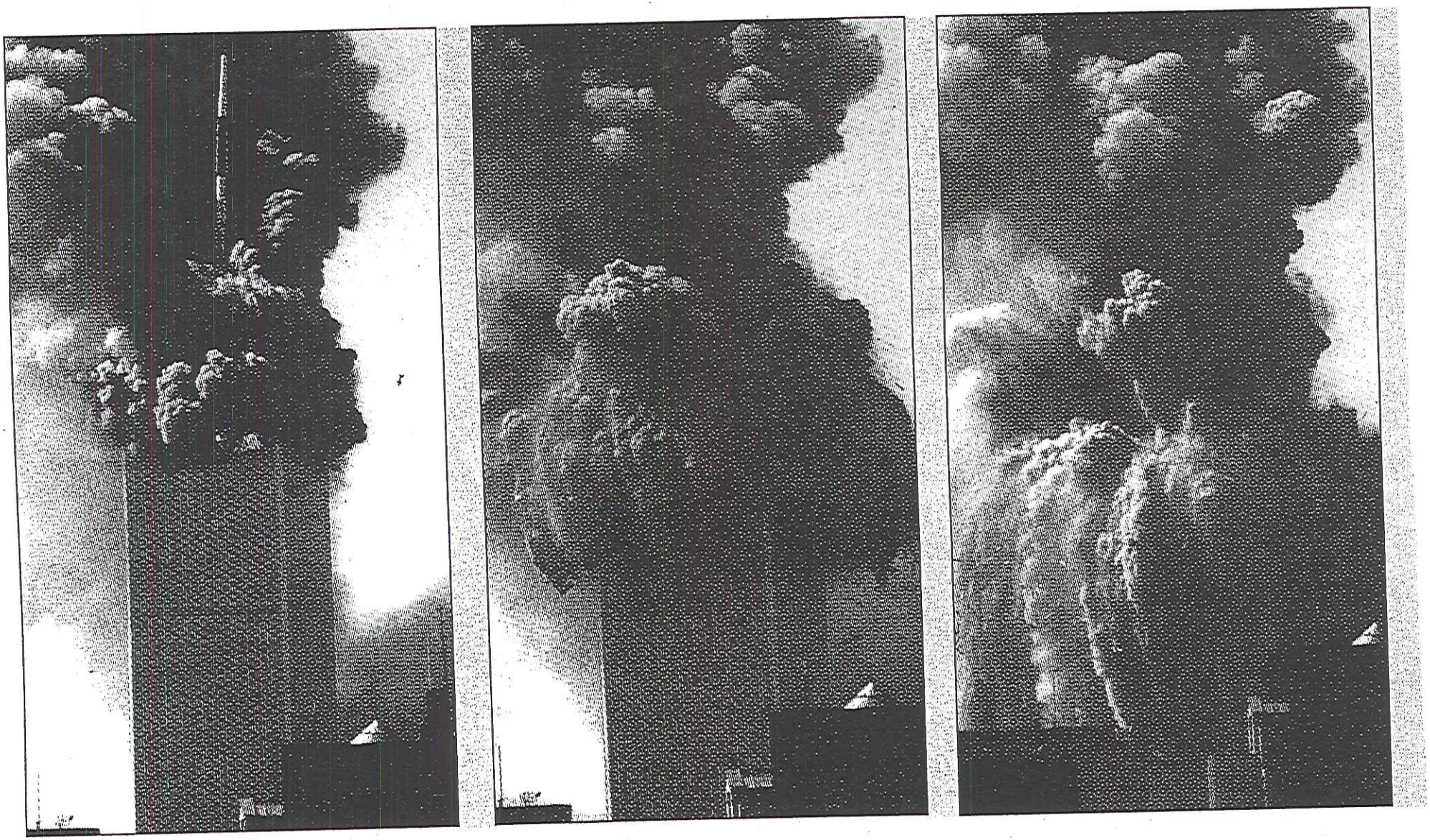

The towers were designed to survive a collision with the smaller airliners used in the 1970s, and the beams were covered with a fire-resistant material. But jet fuel fires are usually fought with special foam, experts note, not the water delivered by most building sprinkler systems. An investigative team organized by the American Society of Civil Engineers will begin its work once rescue operations cease, with its report due early next year.

Some 40 kilometers away, scientists at the Lamont-Doherty Earth Observatory in Palisades, New York, recorded the event on their seismometers (above). The 2.3-magnitude seismic shock was similar to the force from an earthquake that jostled Manhattan in January.

–DAVID MALAKOFF

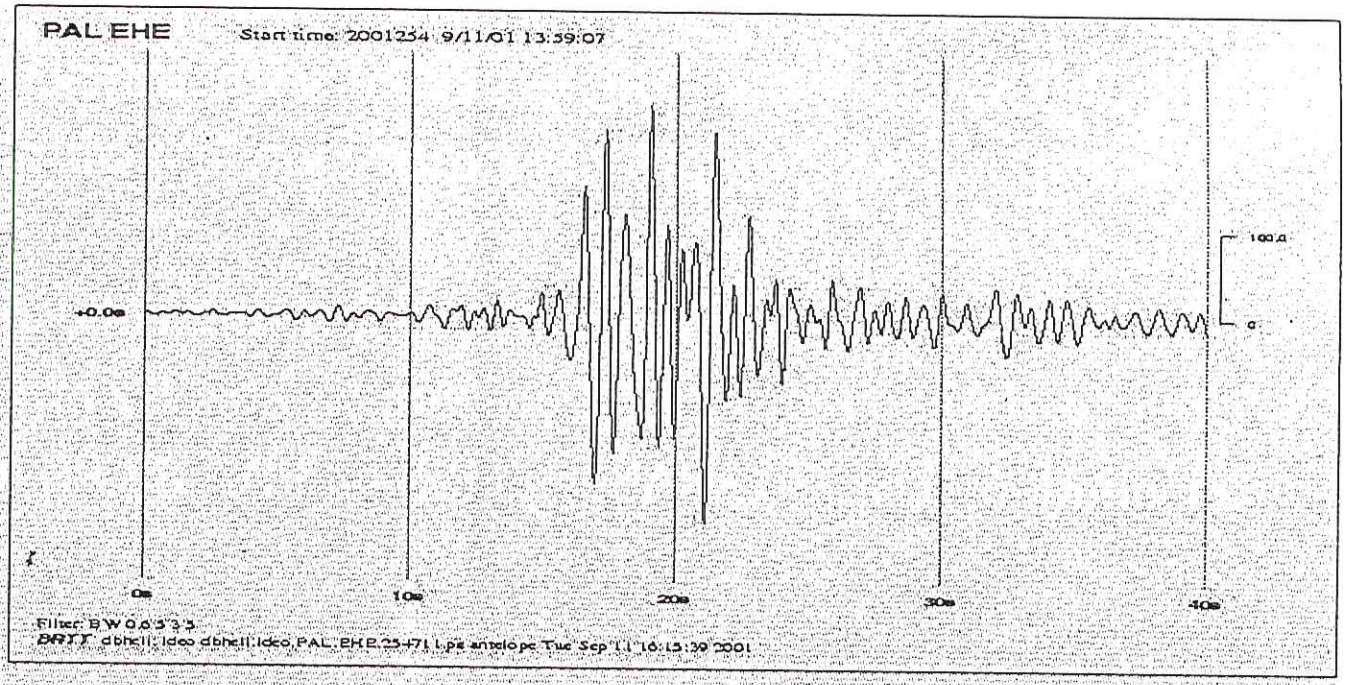

WTC collapse 9/11/01

mgh energy $\approx 10^{11}$ Joules

energy of M=2 quake

$$\log_{10} E = 1.5\,M + 4.8$$

$$E_{seismic} \approx 10^{8} \text{ Joules}$$

only $\sim \frac{1}{1000}$ of energy $\Rightarrow$ ground motion

remaining $\frac{999}{1000}$ into reduction of WTC into dust

Will do this in lab

Empirically, the magnitude originally defined by $M = \log_{10}(A/T) + f(\Delta, h)$

A = displ. amplitude, T period, h depth, Δ corrects for wave spreading etc.

Given $E = \frac{M_0}{2 \cdot 10^4}$ and

$\log M_0 = 1.5\,M + 9.1$ we find

$$\log E = 1.5\,M + 4.8$$

homework problem #5

How much more energy does a $M=8$ quake release than $M=7$?

	M	E in Joules	M_0 (N m)
Hiroshima → 14 kT	6	$6.3 \cdot 10^{13}$	$1 \cdot 10^{18}$
	7	$2 \cdot 10^{15}$	$4 \cdot 10^{19}$
1906 SF →	8	$6.3 \cdot 10^{16}$	$1 \cdot 10^{21}$
	9	$2 \cdot 10^{18}$	$4 \cdot 10^{22}$

Go up by $M=1$: $10^{1.5} = 31.6$ times as much energy

Go up by $M=2$: $10^3 = 1000$ times as much

Earthquake statistics: how many earthquakes are there of a given magnitude per year?

For any region of the Earth and any long enough time period, the empirical observation is the same

Known as the Gutenberg – Richter magnitude – frequency law

N = # of quakes of magnitude $\geq M$

$$\log_{10} N = a - bM \qquad b \approx 1$$

$b = 1 \Rightarrow$ # of $M \geq 7$ is 10 times # of $M \geq 8$, etc.

a depends on size of region & time interval.

Corresponding moment – frequency law is

$$\log_{10} N = a - b\left(\tfrac{2}{3}\log_{10} M_0 - 6.1\right)$$

or with $b = 1$:

$$\log N + \tfrac{2}{3}\log M_0 = a + 6.1$$

$$N M_0^{2/3} = 10^{a+6.1}$$

$$N = 10^{a+6.1} M_0^{-2/3}$$

with $b \equiv 1$

Show Göran Ekström's plot of Harvard CMT data since 1977.

The # must be per year

ONE PAGE SUMMARY OF FORMULAE

Summary

$\Delta\sigma = 10 - 100$ bars
$= 1 - 10$ MPa

Say $\Delta\sigma = 3$ MPa

$$M_0 = \mu A \bar{\Delta s} = \mu \pi a^2 \bar{\Delta s}$$

$$\bar{\Delta s} = \frac{16}{7\pi}\left(\frac{\Delta\sigma}{\mu}\right) a$$

$$M_0 = \frac{16}{7} \Delta\sigma\, a^3 = 0.4\, \Delta\sigma\, A^{3/2}$$

$$E = \frac{M_0}{2 \cdot 10^4}$$

$$M = \frac{2}{3} \log_{10} M_0 - 6.1 \quad \text{or}$$

$$\log_{10} M_0 = 1.5 M + 9.1$$

$$\log_{10} E = 1.5 M + 4.8$$

worldwide Gutenberg - Richter

$$\log_{10} N = 8.2 - M$$

$$\text{or} \quad N = 2 \cdot 10^{14} M_0^{-2/3}$$

$\log_{10} N = 8.2 - M$ or $N = 2 \cdot 10^{14} M_0^{-2/3}$

Find for shallow quakes world wide

$$\log_{10} N \simeq 8.2 - M \quad \text{or} \quad N = 2 \cdot 10^{14} M_0^{-2/3}$$

worldwide

M	M_0 (N m)	N (# per year)
9	$4 \cdot 10^{22}$	0.16
8	$1 \cdot 10^{21}$	1.6
7	$4 \cdot 10^{19}$	16
6	$1 \cdot 10^{18}$	160
5	$4 \cdot 10^{16}$	1600
4	$1 \cdot 10^{15}$	16,000

magnitude of monitoring problem → about 40/day worldwide $M \geq 4$

$M \geq 7$

Show # per year / from Kanamori & Lay

Some years up to 40 (1906 in fact)
Some years < 10.

Also show # fatalities / year due to earthquakes: mean 15,000 / year

Tangshan, China 1976 ($M = 7.7$)
250,000 fatalities

Most lives lost in populated third-world countries with lots of unreinforced masonry or stone structures.

NB – it's the relative cumulative probability – need to merge 3 datasets Parkfield a particularly active region in California, e.g.

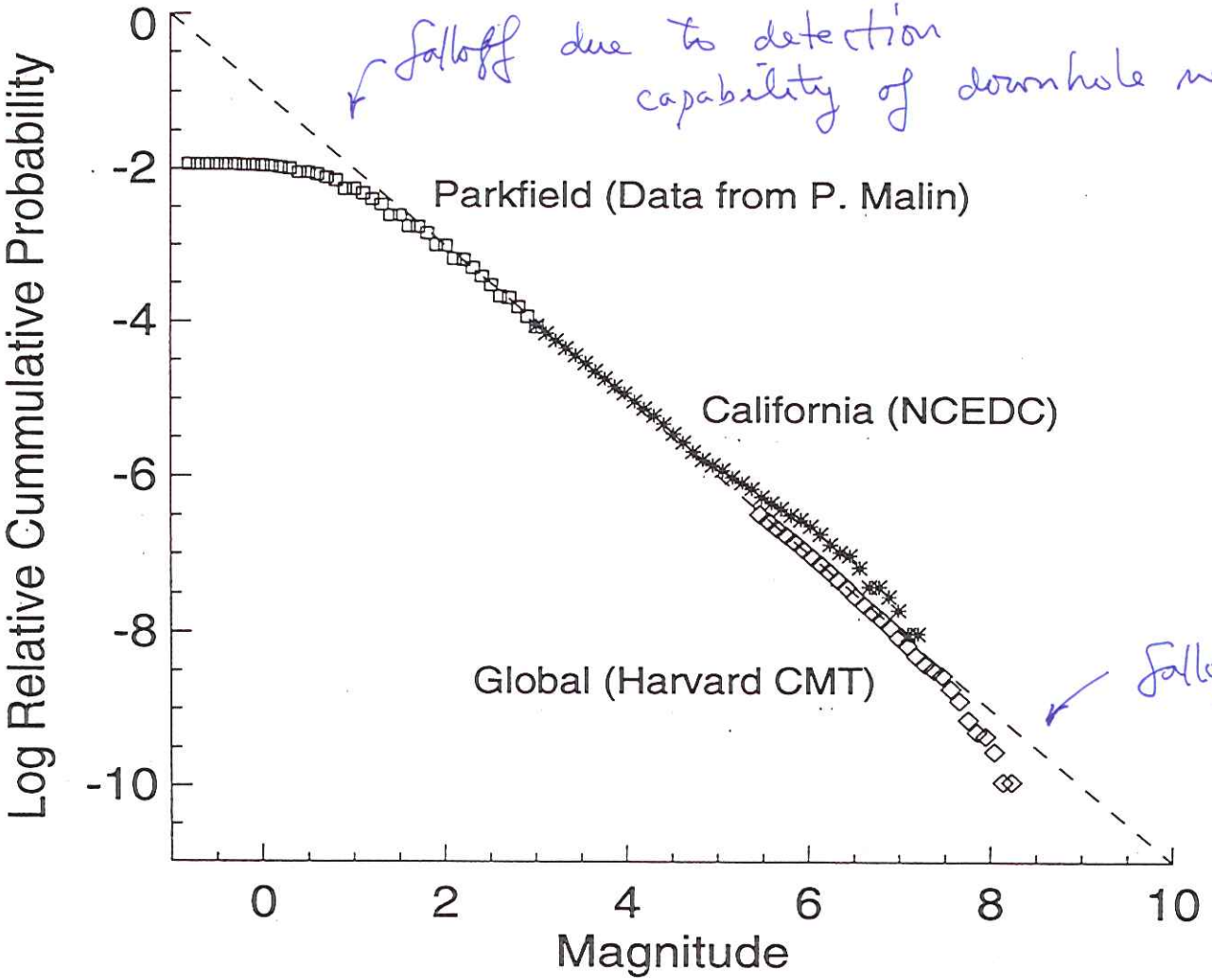

falloff due to detection capability of downhole network

falloff due to insufficiently long data base

$$\log_{10} E = 1.5M + 4.8$$ (E in joules)

Let's calculate the energy released by earthquakes per year

M	$N(M+1 \le \text{mag} \le M)$	E (Joules/yr)
8-9	1.4	10^{17}
7-8	14	$3 \cdot 10^{16}$
6-7	140	10^{16}
4-5	1400	$3 \cdot 10^{15}$
3-4	14 000	10^{15}
		⋮

Total $\approx 2 \cdot 10^{17} \frac{J}{yr}$

$= 6 \cdot 10^9$ W

Dominated by the occasional big quake — the little more frequent ones are relatively inconsequential.

actually $6 \cdot 10^9$

This is about 10^{10} W — small in comparison to the total heat flow $3 \cdot 10^{13}$ W

earthquakes $\approx \frac{1}{5000}$ × heat flow

efficiency of $\oplus$ as a heat engine

The largest event every year ($M \approx 8$) accounts for about 50% of the total.

1991 Mt. Pinatubo eruption released $\sim 10^{20}$ Joules 1945 Hiroshima $6 \cdot 10^{13}$ J

Largest earthquake ever recorded:

1960 Chile

subduction zone event: shallow-angle thrust fault

roughly: $\bar{\delta s} = 20$ meters

$A = 200\text{km} \times 1000\text{ km}$
(downdip) (along strike)

bigger since deeper

$M_0 = (5 \cdot 10^{10})(20)(200 \times 1000 \cdot 10^6)$

$= 2 \cdot 10^{23}$ N m

170 times SF

$E = \frac{M_0}{2 \cdot 10^4} = 10^{19}$ Joules — more than 100 times more than 1906 SF

Magnitude $M = 9.5$ — note there is no upper bound on the magnitude

It is not a scale between 1 and 10; in fact, these can even be negative magnitude quakes.

falloff at low moment due to undersampling

# of events per year with seismic moment $\geq M_0$

M_0 in dyne-cm

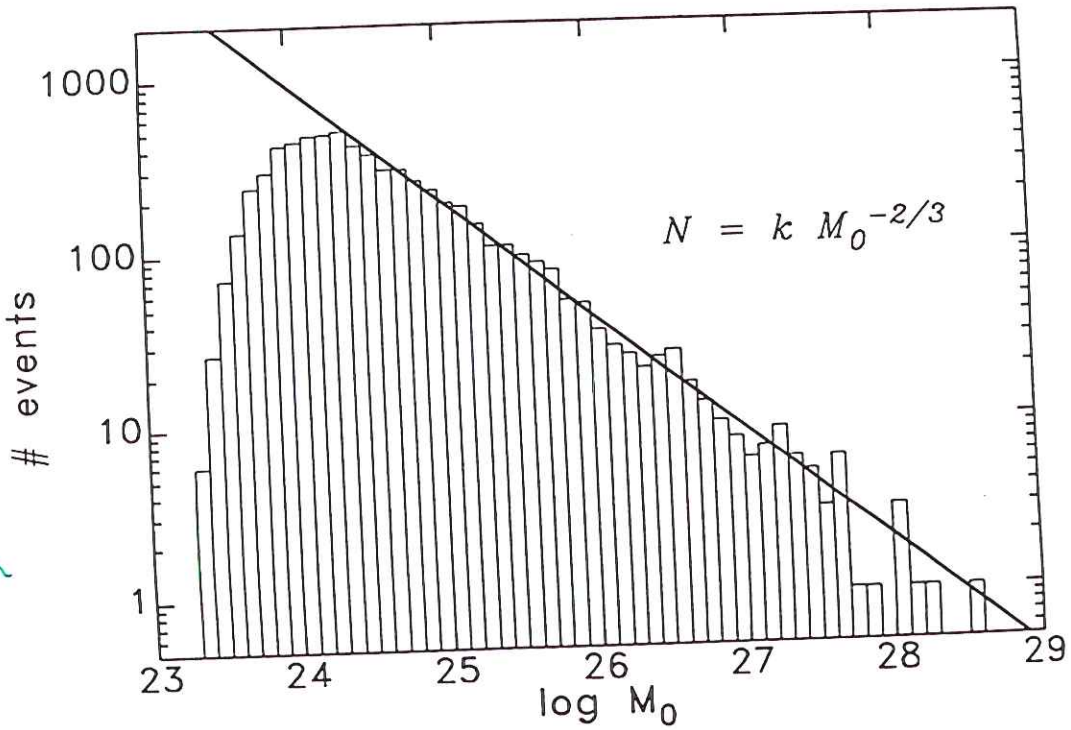

FIGURE 9.30 Number of earthquakes as a function of seismic moment. This is a global data set for shallow events since 1977. (Courtesy of Göran Ekström.)

1 Nm = 10^7 dyne cm

cumulative : magnitude $\geq M$

interval : magnitude in range $(M-0.2, M)$

In both cases number in a 76-year period

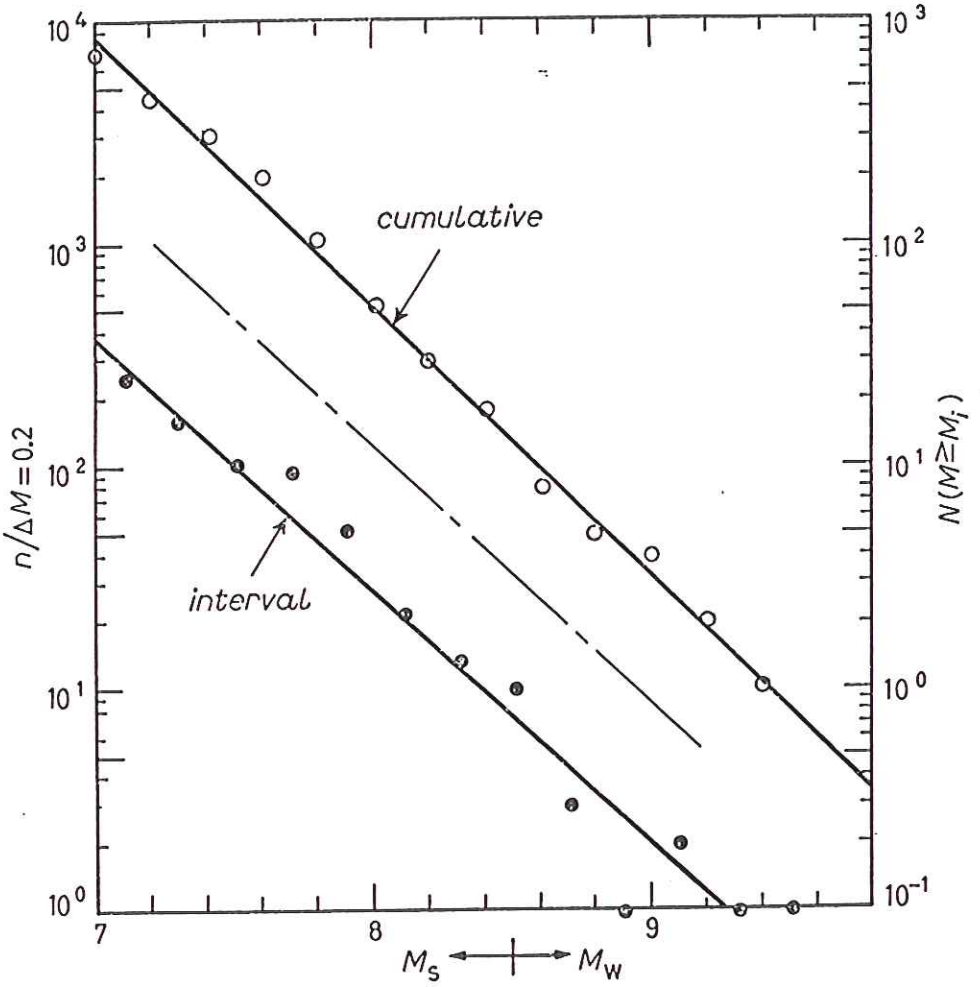

Fig. 1. – The magnitude-frequency relation for the earthquakes in the world during the period from 1904 to 1980. The surface wave magnitude M_S listed in [1] is used for all the events except those with $M_w \geqslant 8.5$ for which M_w is used. The ordinate on the left is for the interval frequency ($\log n = (10.42 \pm 0.57) - (1.13 \pm 0.7)\, M$) ($n_2$ in table II, the number of events per 0.2 magnitude unit for the period 1904 to 1980), and that on the right is for the cumulative frequency ($\log N = (11.41 \pm 0.19) - (1.21 \pm 0.02)\, M$) ($N$ in table II). The straight lines are the least-squares fit for the entire range.

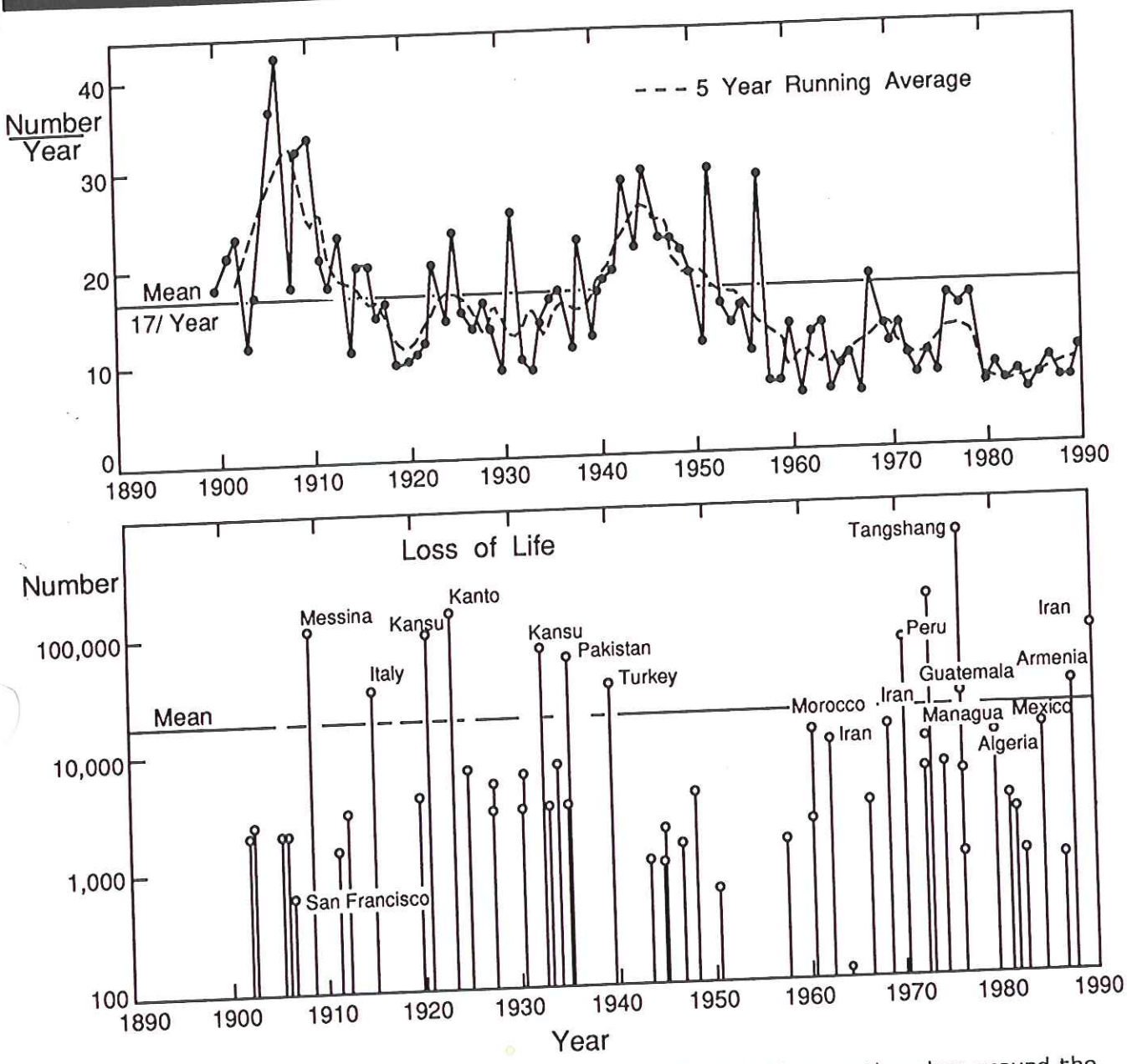

FIGURE 1.10 (Top) The annual number of large ($M_S \geq 7.0$) shallow earthquakes around the world. There are about 17 events of this size annually. (Bottom) The history of earthquake-induced fatalities in this century, with the locations of major events being indicated. Note the poor correlation with the top trace. Even small earthquakes can cause extensive loss of life in regions with poor building construction, or if secondary hazards such as fires or landslides enhance the damage. (Modified from Kanamori, 1977, 1978.)

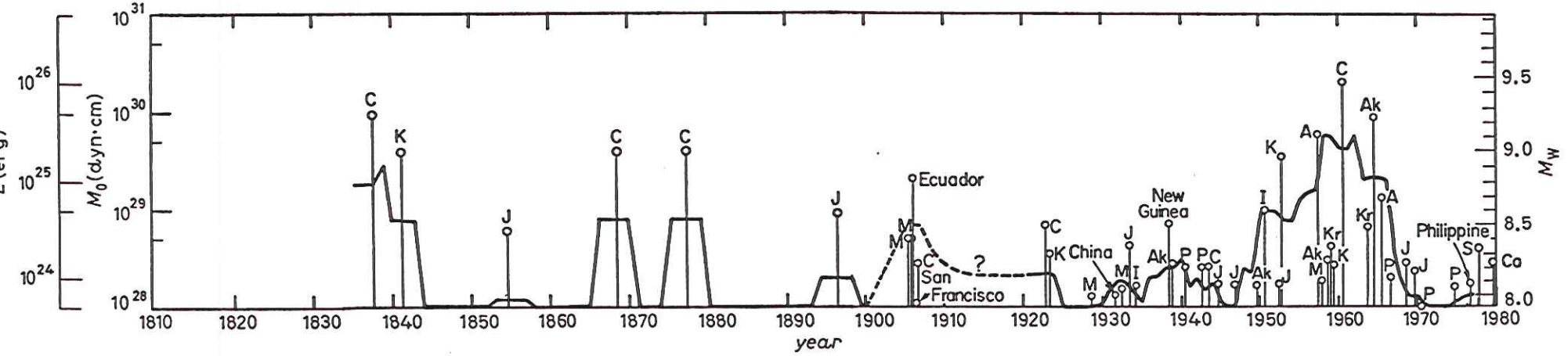

Fig. 4. – The seismic moment M_0, the seismic energy E and the magnitude M_w of great and large earthquakes as a function of time (A, Aleutian; Ak, Alaska; C, Chile; Co, Colombia; I, India; J, Japan; K, Kamchatka; Kr, Kurile; M, Mongolia; P, Peru; S, Sumbawa). The solid curve shows unlagged 5-year running average (in erg per year) taken at the center of the interval (modified from [2]). For the period from 1835 to 1900, tsunami magnitude M_t [1] is used to estimate M_0, E and M_w.

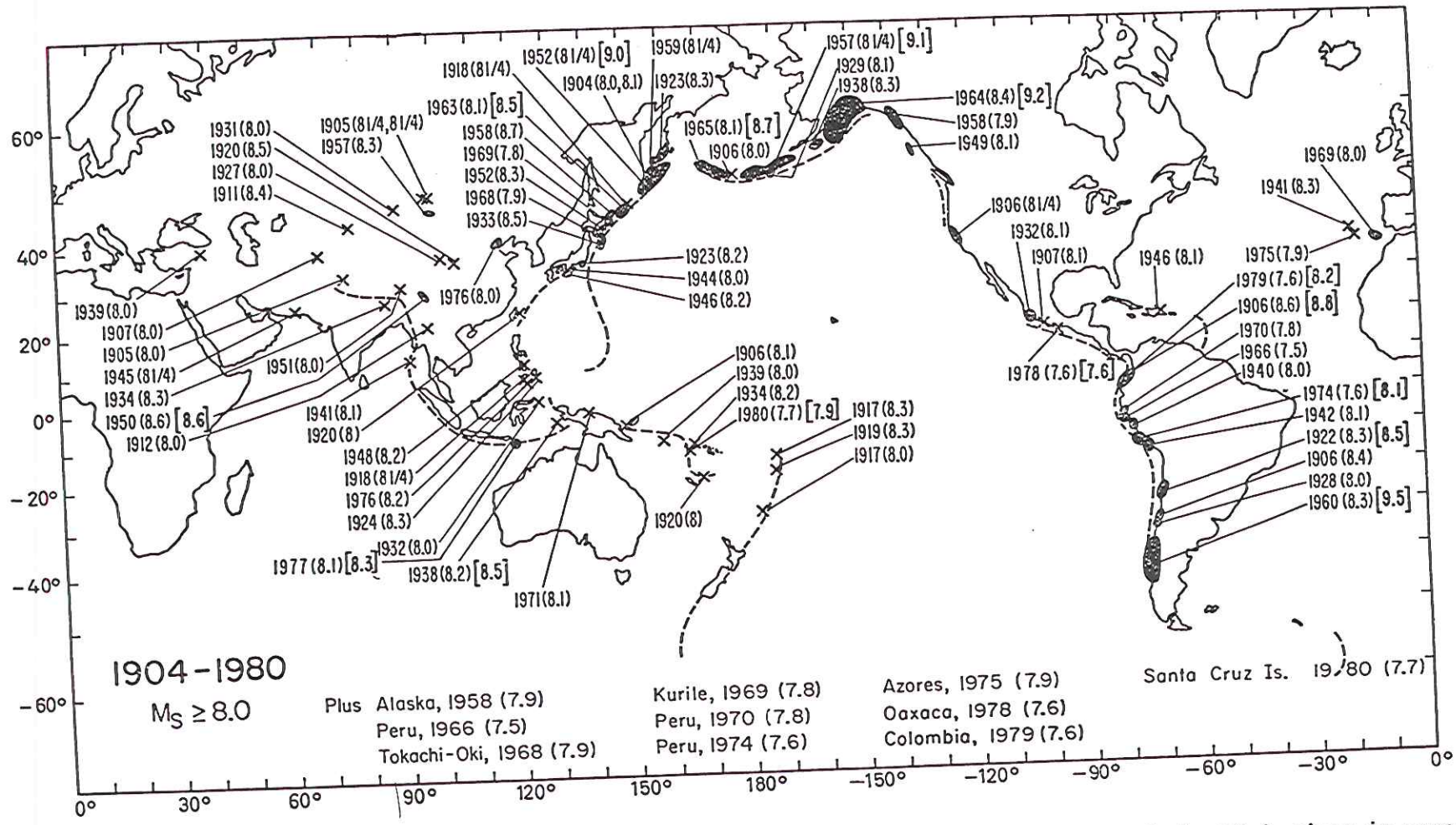

Fig. 2. – Great and large earthquakes for the period from 1904 to 1980. The surface wave magnitude M_S is given in parentheses and M_w is given in brackets for some earthquakes, including the ten largest earthquakes. Major rupture zones are indicated by dark zones. This figure is modified from that in [2], and the magnitude values differ slightly from those listed in table I.

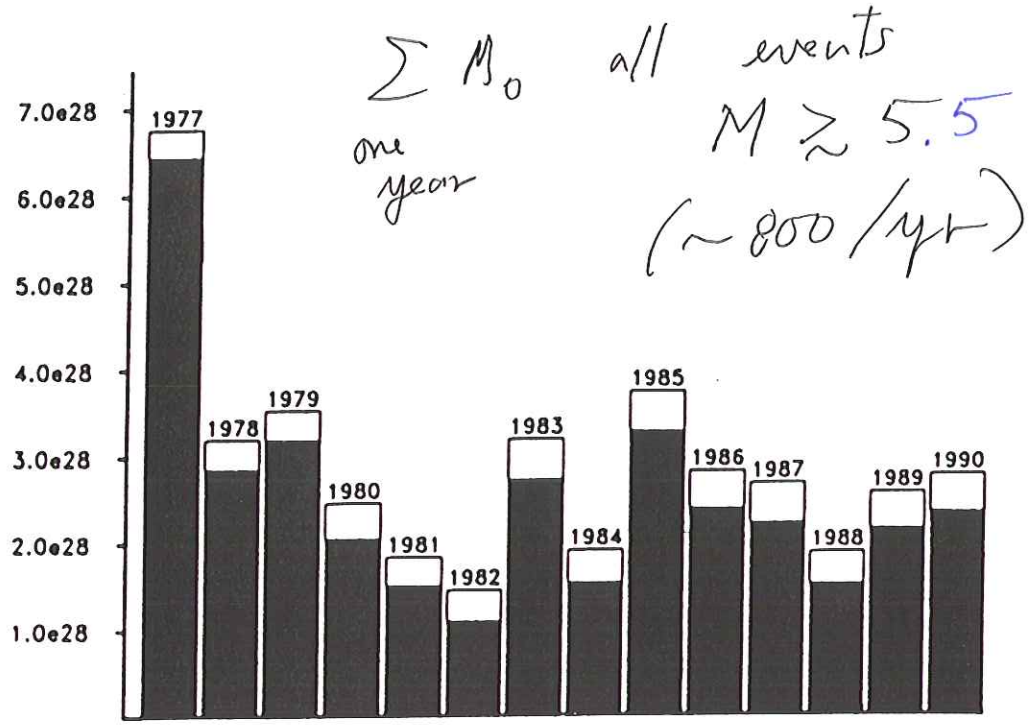

FIGURE 1.15 Top: The source mechanism for all earthquakes with $M_W \geq 6.5$ in 1989. The e and stereographic projection of the *P*-wave radiation pattern for each event are shown, with the size of the projections scaling with relative moment of the source. The dark areas represent compression (away from the source) motions; the white areas indicate dilatational (toward the source) motions. These source mechanisms are fully described in Chapter 8, but here they can be taken to indicate the direction of faulting associated with each source. Bottom: The annual cumulative seismic moment release from all significant seismic events, which is about 800 events per year. The darker portion of each bar indicates the contribution from just the $M_W \geq 6.5$ events, demonstrating that the small number of large events (about 20/yr) dominates. (From Dziewonski *et al.*, 1990, 1991.)

TABLE II. – *Frequency-magnitude relation, 1904-1980 (data from* [1]).

Interval				Cumulative		
$\leqslant M_S <$		n_1 (a)	n_2 (b)	$M_S \geqslant$	N_1 (c)	N_2 (d)
7.0	7.2	252	252	7.0	720	720
7.2	7.4	162	162	7.2	468	468
7.4	7.6	104	104	7.4	306	306
7.6	7.8	97	97	7.6	202	202
7.8	8.0	52	52	7.8	105	105
8.0	8.2	25	22	8.0	53	53
8.2	8.4	17	13	8.2	28	31
8.4	8.6	8	10	8.4	11	18
8.6	8.8	3	3	8.6	3	8
8.8	9.0		1	8.8		5
9.0	9.2		2	9.0		4
9.2	9.4		1	9.2		2
9.4	9.6		1	9.4		1

(*a*) n_1 is the number of events within the magnitude range of 0.2 for the period 1904 to 1980.
(*b*) Same as (*a*) with M_S replaced by M_w for the ten largest events with $M_w \geqslant 8.5$ listed below.
(*c*) N_1 is the total number of events larger than the given M_S for the period 1904 to 1980.
(*d*) Same as (*c*) with M_S replaced by M_w for the ten largest events with $M_w \geqslant 8.5$ listed below.
1960 Chile ($M_S = 8.5$; $M_w = 9.5$), 1964 Alaska (8.4; 9.2), 1957 Aleutian Is. (8.1; 9.1), 1952 Kamchatka (8.2; 9.0), 1906 Colombia (8.6; 8.8), 1965 Aleutian Is. (8.2; 8.7), 1950 Assam (8.6; 8.6), 1938 Banda Sea (8.2; 8.5), 1963 Kurile Is. (8.1; 8.5), 1922 Chile (8.3; 8.5).

TABLE III. – *World's worst earthquakes* [12] (*1900-1979*).

Date	Region	Latitude	Longitude	M_S	Lives lost
27.07.1976	Tangshan	39.5	117.9	7.9	240 000
16.12.1920	Kansu	36.5	105.7	8.6	200 000
1.09.1923	Kanto	35.3	139.5	8.2	99 331
31.05.1970	Peru	— 9.1	—78.8	7.6	66 794
28.12.1908	Messina	38.3	15.6	7.2	58 000
22.05.1927	Tsinghai	37.6	102.6	7.9	40 912
26.12.1939	Turkey	39.7	39.5	7.8	32 700
13.01.1915	Italy	42.1	13.4	6.9	32 610
25.01.1939	Chile	—36.2	—72.2	7.8	28 000
30.05.1935	Pakistan	29.5	66.7	7.6	25 000
4.02.1976	Guatemala	15.3	—89.1	7.5	23 000
10.05.1974	Szechwan	28.2	104.0	6.8	20 000
5.10.1948	Iran	38.0	58.3	7.3	19 800
4.04.1905	E. Kashmir	33.0	76.0	8.1	19 000
16.09.1978	Iran	33.2	57.4	7.2	15 000
21.01.1917	Bali Is.	— 8.0	115.4		(15 000)
1.09.1962	Iran	35.6	49.9	6.9	12 225
31.08.1968	Iran	34.0	59.0	7.1	12 100
21.10.1907	Afghanistan	38.0	69.0	7.7	12 000
29.02.1960	Morocco	30.4	— 9.6	5.9	12 000
15.01.1934	Nepal/India	26.5	86.5	8.3	10 700
25.08.1933	Szechwan	32.0	103.7	7.5	10 000
13.02.1918	Yunnan	23.5	117.0	7.4	10 000

The values of M_S are from [1] whenever available.

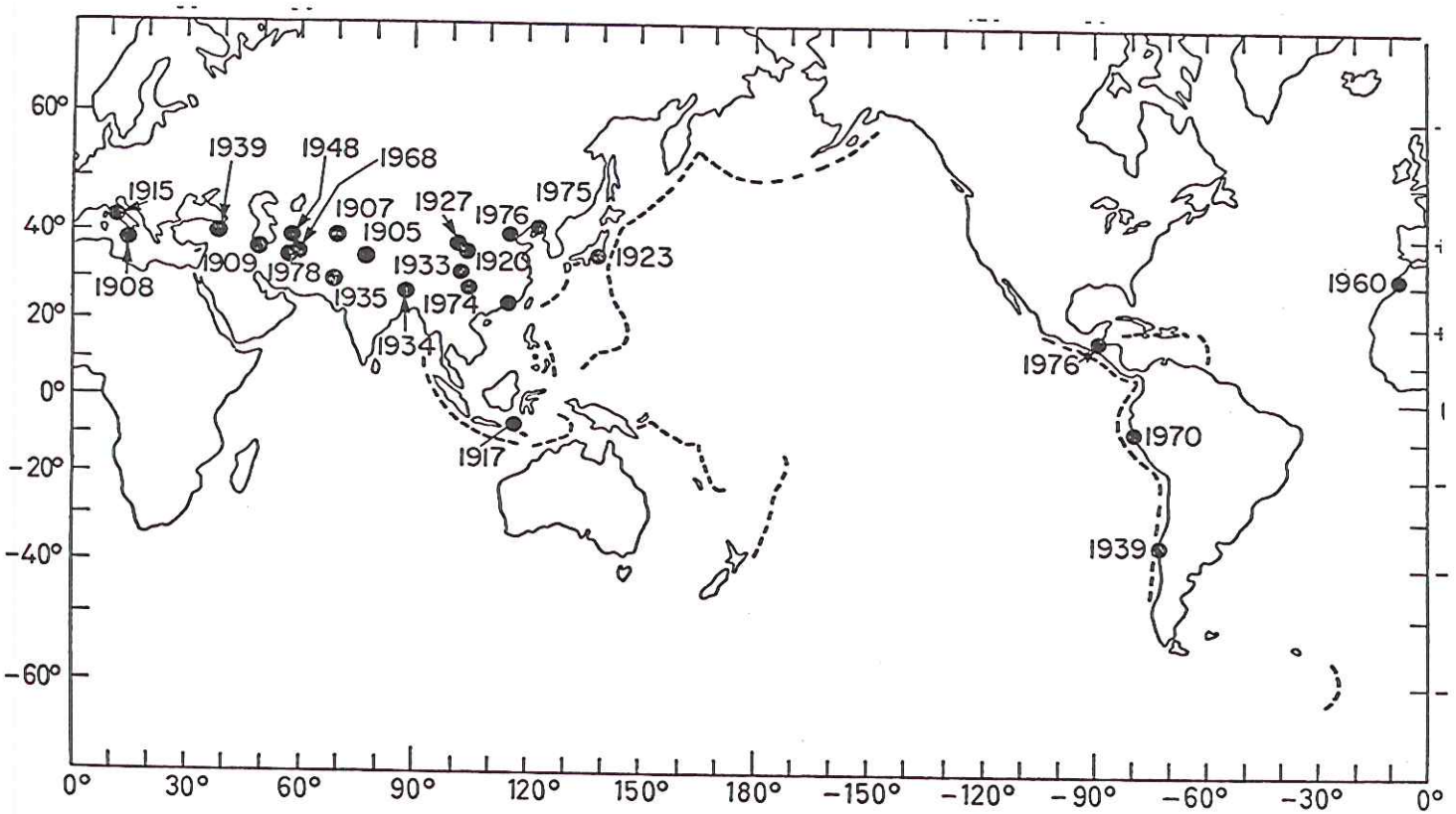

Fig. 6. – Locations of destructive earthquakes listed in table III.

century shown in fig. 4 are obtained from tsunami data [1] and are somewhat incomplete; however, it is probably true that during the period from 1835 to 1900 there is no peak comparable to that for the period 1952 to 1965. It is clear that the global seismic activity is very nonuniform in time at least on a

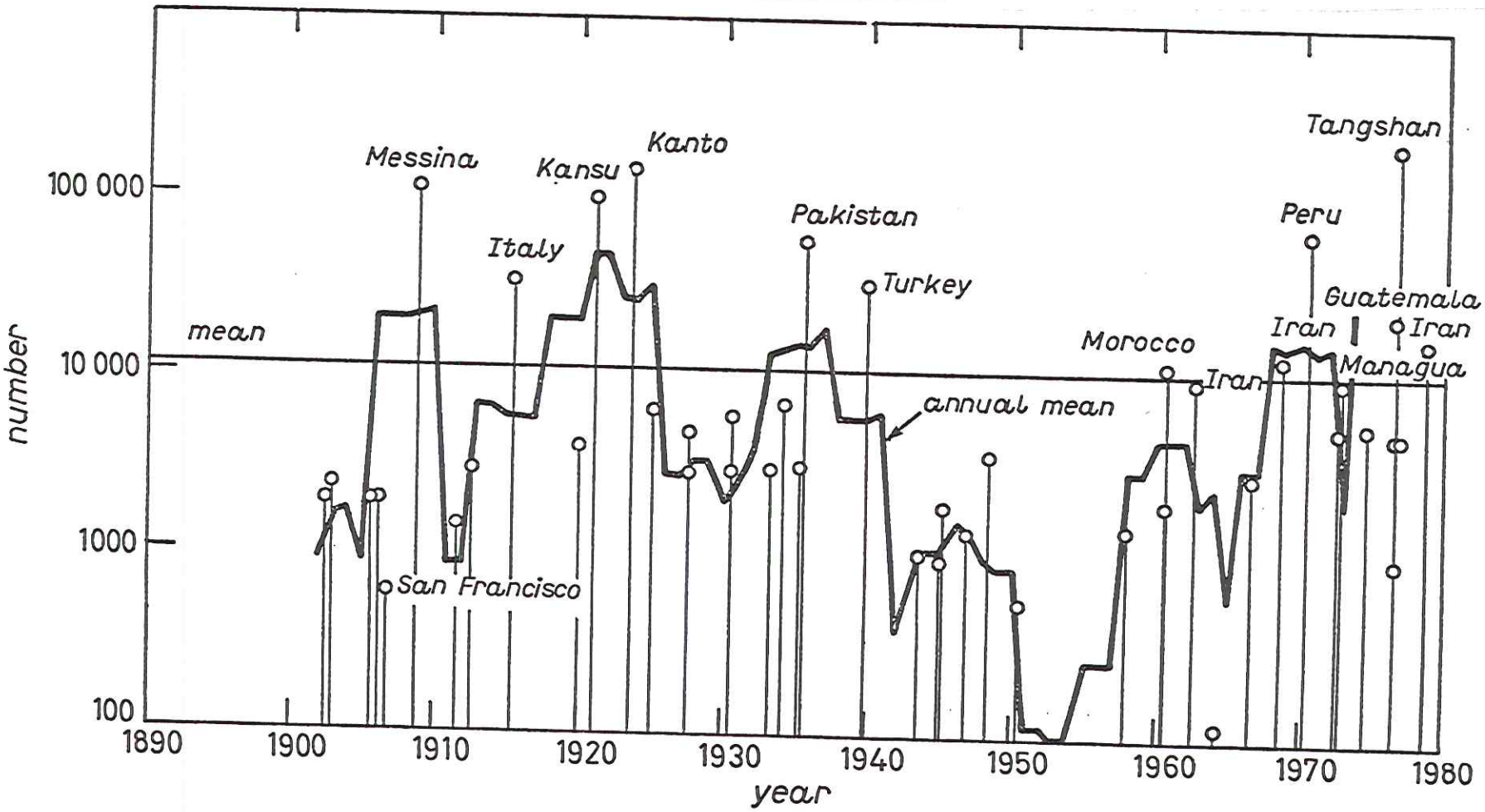

Fig. 7. – Loss of life caused by major destructive earthquakes. The vertical bars are for the individual event and the solid curve shows the annual average (unlagged 5-year running average). This figure is modified from fig. 1 in [13], and the numbers differ slightly from those in table III.

Death toll from earthquakes

A headline in the news section of the March issue of *Geotimes*, "High death toll from 1997 earthquakes," implies that the global death toll from earthquakes in 1997 (3,000) was unusually high. In fact, the 1997 death toll was one-fifth the annual rate averaged over the past century. The annual fatality rate fluctuates erratically when all fatal earthquakes are considered because damaging earthquakes occur in areas with different densities of population.

By excluding rare devastating events from the catalog, a smooth increase in the number of global fatalities from earthquakes is evident (see figure). For example, if events with fewer than 5,000 deaths per earthquake are considered, the fatality rate averages 2,000 — plus or minus 300 per year. But, for the same period, the fatality rate for earthquakes in which fewer than 30,000 deaths per earthquake occur is 5,900 — plus or minus 500 per year. These numbers are growing slowly at rates that are lower than the rate of global population increase, which may reflect improved building methods in some seismogenic zones.

The global death toll from earthquakes averaged over the past century is dominated by infrequent earthquakes (e.g., Tangshan, 1976), associated with more than 30,000 fatalities. These catastrophic events result in an average mortality-rate of more than 16,000 per year. If rare high-mortality events are ignored, the fatality rate is seen to be linked loosely to global population increase. Regrettably, the rate is likely to rise because damaging earthquakes recur near supercity and megacity agglomerations (more than 2 million and 8 million people respectively). These population centers currently host more than 20 percent of the total world population.

Approximately one-third of these future urban populations are located near plate boundaries with known histories of earthquakes of magnitude 7 or greater. Catastrophic events are thus not only more likely, but potentially more devastating than any before.

— Roger Bilham, professor of geology, CIRES and the Department of Geological Sciences, University of Colorado, Boulder, Colo.

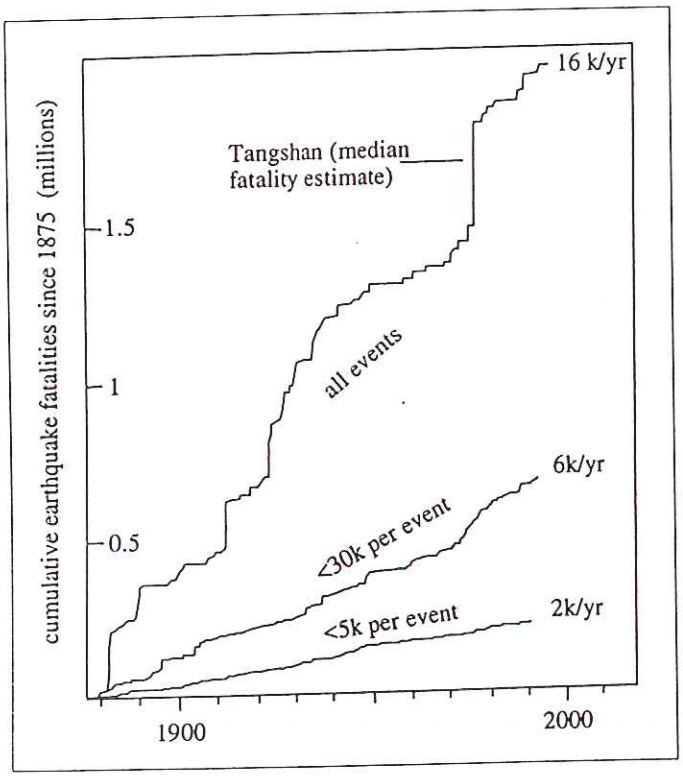

Figure excerpted from "Global Fatalities in the past 2000 years: prognosis for the next 30," by R. Bilham. In *Reduction and Predictability of Natural Disasters*, edited by J. Rundle, F. Klein, and D. Turcotte. Santa Fe Institute Studies in the Sciences of Complexity, Vol. XXV.

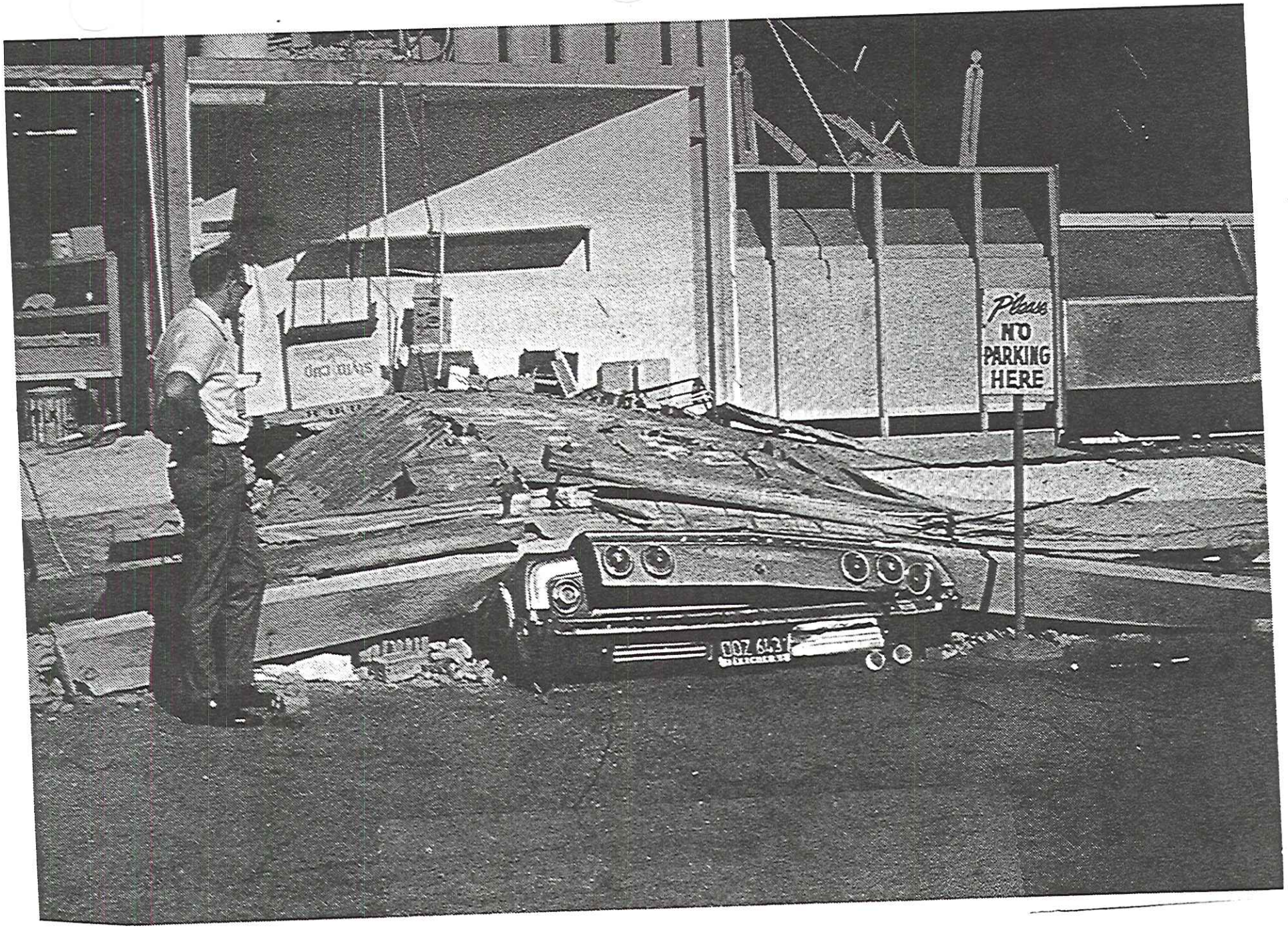
Please
NO
PARKING
HERE

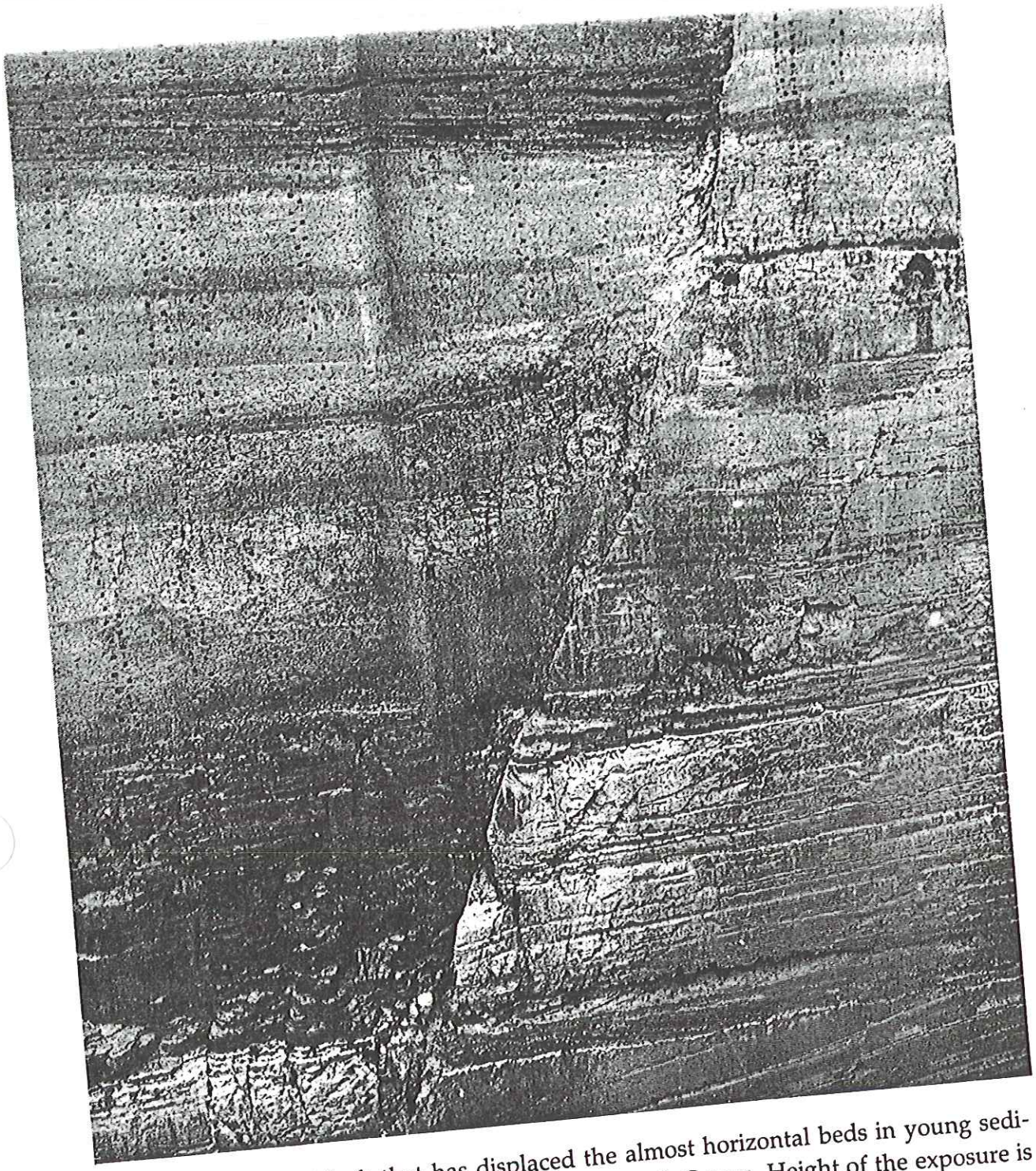

Figure 5.1 Normal fault that has displaced the almost horizontal beds in young sedimentary rocks on the north side of the Corinth Canal, Greece. Height of the exposure is about 70 meters, and the total offset along the fault amounts to more than 10 meters. [Courtesy of L. Weiss.] Major earthquakes, often with tsunamis, occurred in the Corinth region in 227 B.C., 551 A.D., and 1858, 1928, and on February 24, 1981. In the most recent earthquake, surface fault rupture was observed for a length of about 5 kilometers with vertical slip of up to 0.7 meters.

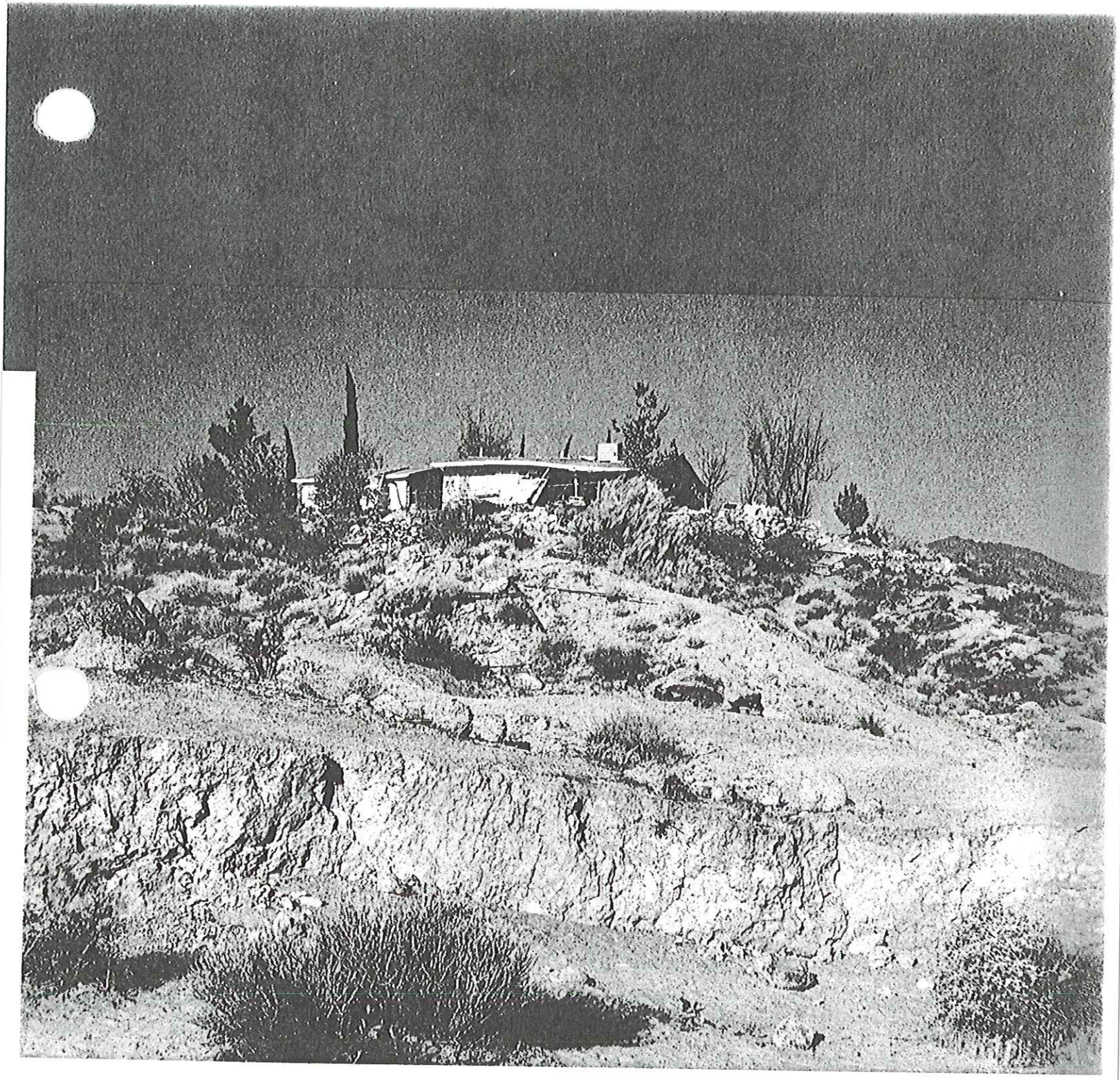

Fresh scarp on Johnson Valley fault below a damaged house after the June 28, 1992 earthquake in Mojave Desert, California. [Courtesy of E. Keller.]